Study on
Dispersion-Managed High-Speed WDM Transmission Technologies in Optical Submarine Cable Systems

光海底ケーブルシステムにおける 分散マネージメント高速 WDM 伝送技術 に関する研究

February 2014

Keiji TANAKA

田中 啓仁

Study on
Dispersion-Managed High-Speed
WDM Transmission Technologies
in Optical Submarine Cable Systems

光海底ケーブルシステムにおける
分散マネージメント高速 WDM 伝送技術
に関する研究

February 2014

Waseda University

Graduate School of Fundamental Science and Engineering

Keiji TANAKA

田中 啓仁

Contents

Chapter 1

Introduction

1-1 Background and objectives

Optical submarine cable systems have been crucially important infrastructures to provide high-capacity international transmission links for increasing overseas data traffic. In order to meet insatiable market demands, new cable systems have been developed by breaking through technological bottlenecks for the transmission capacity expansion.

Figure 1-1 shows the capacity growth of the transpacific optical submarine cable systems. Since the first transpacific optical submarine cable (TPC-3) was installed in 1989, the capacity per fiber has been dramatically increasing associated with the technological evolution. In 2010, the capacity per fiber was eventually expanded to 1 Tbit/s, which was more than 1000-fold capacity increase.

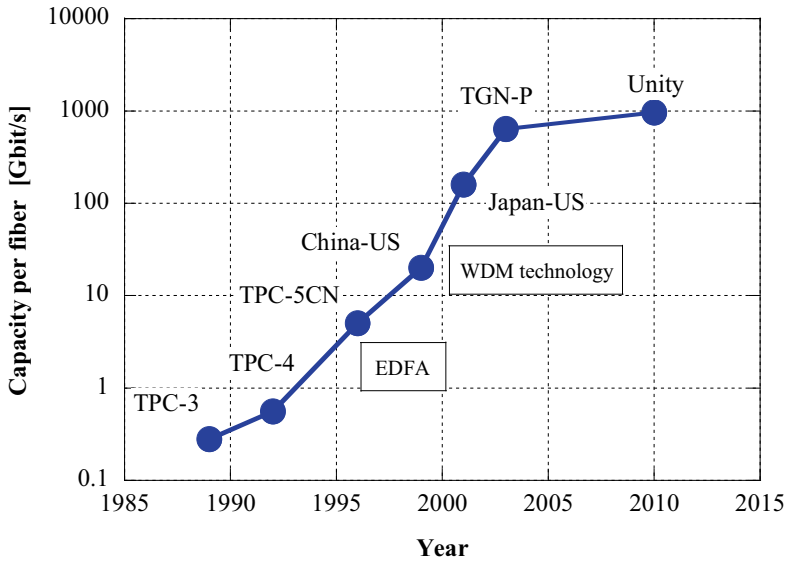

Fig. 1-1 Capacity growth of the transpacific optical submarine cable systems.

Table 1-1 summarizes the installed year, per-fiber capacity, and applied technologies of each cable systems. Among many innovative technologies which were applied to newly developed cable systems, in particular, the advent of the erbium-doped fiber amplifier (EDFA) and wavelength division multiplexing (WDM) accelerated the capacity expansion and technological evolution. EDFAs can facilitate the transmission of lightwave signals over long distances by providing periodic analog amplification rather than digital regeneration. This is the main benefits of EDFA-based optically amplified systems, and it does not require electro-optic regenerators, which include high-speed electronics and restrict the increase of the transmission bit rate due to its complexities and difficulties. Thus, the EDFA-based repeater systems enabled gigabit-capable transmissions, and per-fiber bit rate was increased from 560 Mbit/s to 5 Gbit/s of TPC-5CN [1]. TPC-5CN introduced in 1996 employs a single-channel 5 Gbit/s signal with non-return-to-zero on-off keying (NRZ-OOK) format and dispersion-shifted fiber (DSF)-based transmission line. The DSF is designed such that the zero-dispersion wavelength is shifted to 1.55-μm band, where the fiber exhibits a minimum loss.

EDFAs can amplify optical signals independently of its format and bit rate, and the transparency of the EDFAs made WDM transmission technology to be a practical solution to expand the system capacity [2]. The emergence of WDM transmission technology also contributed to a dramatic increase of the system capacity. The transmission capacity eventually increased to more than 20-fold in the next few years from the installation of TPC5-CN, and the performance of WDM transmissions was enhanced to be applicable to transoceanic distances using low noise 980-nm pumped EDFA chains. In the 2000's, transpacific cable systems with more than 100 Gbit/s per-fiber capacity were commercially introduced, such as Japan-US and PC-1 with the per-fiber capacity of 160 Gbit/s by using 10 Gbit/s-based WDM transmission technologies [3].

Table 1-1 Key technologies applied to submarine cable systems.

System	Year	Per-fiber capacity [Gbit/s]	Signal	Transmission line	
				Span	Repeater
TPC-3	1989	0.28	NRZ (1.3-μm band)	SMF	3R (50-km spacing)
TPC-4	1992	0.56	NRZ (1.55-μm band)	DSF	3R (120-km spacing)
TPC-5CN	1995	5	NRZ	DSF	EDFA (1.48-μm pumped)
China-US	1999	20 (2.5 x 8 WDM)	NRZ (2.5 Gbit/s-based WDM)	NZ-DSF	
Japan-US PC-1	2001	160 (10 x 16 WDM)	RZ (10 Gbit/s-based WDM)	Hybrid LCF + NZ-DSF	EDFA (0.98-μm pumped)
TGN-P	2003	640 (10 x 64 WDM)		Hybrid SMF + SCDCF	
Unity	2010	960 (10 x 96 WDM)	RZ-DPSK (10 Gbit/s-based WDM)		

The transparent property of the EDFA imposes impairments on the transmission performance, while the feature is advantageous in the low system cost and bit-rate free flexibility. As optically amplified repeater systems recover the only amplitude of the signals by nature, all the impairments generated through the transmission accumulate with the distance and cannot be recovered. Amplified spontaneous emission (ASE) noise generated in EDFAs degrades the optical signal-to-noise ratio (SNR), and the interactions between chromatic dispersion and nonlinear effects in optical fibers cause the pulse distortions [4]-[9]. The system should be designed to mitigate the transmission impairments by managing the dispersion and nonlinearities of the transmission line and using suitable modulation formats and schemes.

When the system is operated at the zero-dispersion wavelength of fibers, the signal and the amplifier noise, which are accompanied with wavelengths close to the signal, travel at almost the same velocities. Under these conditions, the signal and noise interact closely over a long distance, and induce undesirable nonlinear phenomena [5]-[7]. Chromatic dispersion making different wavelength components to propagate at different group velocities contributes to suppress the nonlinear effects, and in order to minimize the effects, non-zero dispersion-shifted fiber (NZ-DSF) had been introduced instead of the DSF [10]. The NZ-DSF has a dispersion of -2 to -4 ps/nm/km, in general.

The management of single channel transmission performance is relatively simple. The accumulated dispersion of the DSF or NZ-DSF with a negative dispersion value can be compensated for by standard single-mode fiber (SMF) which has a positive dispersion value of +17 ps/nm/km. This dispersion compensation (i.e. dispersion management) can prevent the generation of the nonlinear effects caused by the interactions between the signal and ASE noise, owing to the short phase-matching lengths and the small end-to-end dispersion. In contrast, the dispersion management in WDM transmissions using a higher-channel bit rate is much more complicated than that of single channel transmissions. For WDM transmissions, the system design factors which should be managed are increased, and we must additionally consider the impact of nonlinear crosstalk among WDM channels and dispersion slope on the transmission performance. These issues make the system design of dispersion management increasingly complicated.

The objective of this thesis is to explore the technologies for the further capacity expansion of a per-fiber capacity of more than 160 Gbit/s and to develop new dispersion-managed high-speed WDM transmission technologies for terabit-capacity submarine cable systems beyond Japan-US and PC-1. The usable bandwidth of long-haul WDM systems is limited by both the inherent bandwidth of the EDFAs and the acceptable dispersion of the channels located at far from zero-dispersion wavelength. The EDFA bandwidth is finite and of the order of 20 nm, and the waveform distortions of the channels whose wavelengths are far from zero-dispersion wavelength are potentially large. It is very challenging to increase the aggregate capacity of WDM systems on the above conditions, and key design issues are the dispersion management of the transmission line to mitigate nonlinear impairments and to resolve the wavelength dependency of dispersion among WDM channels and the technologies to increase the channel packing density, namely spectral efficiency, at the terminals.

For achieving such a high-capacity transmission, dispersion values of all the WDM channels must be managed. Transoceanic submarine cable systems using NZ-DSF-based transmission lines such as PC-1 and Japan-US have a wavelength dependency on the WDM transmission performance, and the transmissible distance and capacity are restricted by the performance of the edge channels located at far from zero-dispersion wavelength. The largely accumulated dispersion at the edge channels severely deteriorates the performance through the interactions with nonlinear effects. This is the main bottleneck for increasing the transmission capacity in the NZ-DSF-based transmission lines, which is caused by the wavelength dependency of the dispersion, namely the dispersion slope over the WDM signal band.

The dispersion management using a SMF-based hybrid span configuration is considered as a candidate to resolve the problems associated with the dispersion slope of the fibers. The hybrid span configuration of a SMF with an enlarged effective core area (A_{eff}) and a slope-compensating dispersion compensation fiber (SC-DCF) attains flat dispersion characteristics all over the WDM channels, and a large absolute dispersion value of 17 ps/nm/km and a large A_{eff} of the SMF contribute to the reduction of nonlinear effects such as four-wave mixing (FWM) and cross-phase modulation (XPM) in WDM systems [5]-[13]. This approach is quite effective for further capacity expansion of more than 160 Gbit/s, and the feasibility of terabit-capacity transoceanic

submarine systems are numerically and experimentally studied in Chapter 3. In fact, the hybrid-span configuration of a SMF and a SC-DCF was applied to the submarine cable systems of TGN-P and Unity which were deployed next to 160 Gbit/s-classed PC-1 and Japan-US in 2003 and 2010, respectively.

The dispersion management for unrepeatered transmission systems is also included in the scope of this thesis. For unrepeatered transmission systems, different dispersion management schemes are required because the profiles of power level over the distance are completely different from those in EDFA-based repeatered systems. Raman amplification and remote-EDFA are usually applied for unrepeatered systems by feeding the pump power for amplifications from both or either side of the terminals [14], [15]. In this application, the dispersion management is one of the most important key design issues to expand the transmissible capacity by suppressing the nonlinear penalty and the accumulated dispersion in optical amplified transmission lines. As the channel bit rate of WDM transmission systems, a higher-channel bit rate of 40 Gbit/s is commercially advantageous over 10 Gbit/s in terms of spectral efficiency and footprint in the terminals. The longest distance of 40 Gbit/s-based WDM unrepeatered transmissions in the previous reports was limited to 250 km [16]. In the research on the 40 Gbit/s-based WDM unrepeatered transmission described in Chapter 4, by optimizing the transmission line configuration composed of SMFs with an A_{eff} of 175 μm^2 and a NZ-DSF and the amplification scheme, the transmission distance over 306 km was successfully demonstrated for the first time.

In addition to dispersion management, several technologies at the optical transmitter and receiver are also explored. Spectral efficiency (i.e. bandwidth efficiency) is another key parameter for the system design to enlarge aggregate capacity in a finite EDFA bandwidth. The technologies for a highly spectral efficient 40 Gbit/s-based WDM transmission are studied in Chapter 5. As the method to achieve a high spectral efficiency, the bandwidth limitation of signal spectrum by using an optical filter before transmission (i.e. pre-filtering) is considered. Detailed studies on the benefits of asymmetric pre-filtering have been reported for return-to-zero (RZ) and carrier-suppressed return-to-zero (CS-RZ) OOK signals [17]-[21]. Regarding differential phase-shift keying (DPSK) signal, which is a promising modulation scheme for high-speed long-haul system applications, no similar study has been reported,

whereas remarkable demonstrations of 40 Gbit/s-based dense WDM (DWDM) transmission have been reported by using symmetrically pre-filtered DPSK signals [22]-[24].

After revealing the impact of inter- and intra-channel interactions on transmission performance in 40 Gbit/s-based DWDM systems using SMF-based transmission spans, the optimum pre-filtering condition for 42.7 Gbit/s CS-RZ DPSK signals is numerically and experimentally investigated by comparing the dispersion and nonlinear tolerances between unfiltered, asymmetrically, and symmetrically filtered CS-RZ DPSK signals. In addition, the feasibility of transoceanic transmission with a spectral efficiency of 0.8 bit/s/Hz is explored through the transmission experiments.

Capacity upgrade is also an important key issue on system design, and the technologies at the terminals of optical transmitter and receiver are also studied. The rapid progress of transmission technologies as shown in Fig.1-1 has shortened the effective lifetime of the existing submarine cable systems because the applied technologies at the time of the deployment became old-fashioned one. Submarine cable systems have an adequate beginning-of-life system margin as they are designed with a 25-year life expectancy. It is desired to utilize the existing infrastructure efficiently by upgrading the capacity in order to extend the system lifetime and recoup the investment. As installed optical fiber spans and amplifiers in submarine cable systems cannot be replaced, the adoption of the terminal upgrade technologies is the only way to enlarge the transmission capacity. These are advanced signal formats and forward error correction (FEC) codes [25]. The trade-offs in the selection of upgrade technologies are cost and performance, and it is important to design the upgrade system in order to satisfy the required quality with the minimum cost.

The possibility of more than 16-fold capacity upgrade is studied in Chapter 6 by citing a domestic submarine cable system of Japan Information Highway (JIH) [26]. JIH submarine cable system has the per-fiber capacity of around 50 Gbit/s using 2.5 Gbit/s-based WDM technologies with 100 GHz-spaced NRZ signals. The possibility of terabit-capacity upgrade is numerically and experimentally explored by using a higher-channel bit rate of 40 Gbit/s signal with RZ or CS-RZ modulation formats and FEC codes in the transmission line designed for a 2.5 Gbit/s-based WDM system.

1-2 Outline of the thesis

This thesis includes seven chapters and three appendixes. Figure 1-2 illustrates the organization of the thesis. Dispersion management technologies are mainly presented in Chapters 2, 3, 4, and 5, and terminal technologies are described in Chapters 5 and 6. Appendixes A, B, and C are attached in the thesis to explain the derivation of the fundamental equation describing optical signal propagation, modulation formants, and FEC technologies supplementarily.

In this chapter, Chapter 1, the evolution of optical submarine cable systems is described with the accompanied technologies. Then, after reviewing the key system design issues for the capacity expansion of WDM transmission systems, the objective of the thesis work is mentioned.

In Chapter 2, system design considerations are presented for optical fiber communications. Firstly, fundamental concept of system design is explained based on the nonlinear Schrödinger equation, which governs the behavior of optical pulse propagation in fibers. From the model equation, the conditions and concept for system design are analytically discussed on transmission loss compensation, dispersion management, and nonlinearity mitigation. In addition, the methods for the system design are presented: analytical method to estimate accumulated nonlinearities over a single fiber span, numerical method to fully analyze the model equation to simulate the transmission performance, and experimental method using recirculating loop technique. Finally, the meaning of the Q-factor which is the key index to evaluate the transmission performance of digital communication systems is explained.

In Chapter 3, the dispersion management for transoceanic submarine cable systems is described. After reviewing two different dispersion management schemes using DSF- and SMF-based span configurations, the transmission performances of the two configurations are numerically and experimentally compared. The results obtained by these studies show that the SMF-based span configuration is more beneficial than the DSF-based one, and a successful 320 Gbit/s (32 x 10.7 Gbit/s) WDM transmission over 7,280 km is presented. In addition, the potential of dispersion-flattened fiber-based systems is discussed through a 400 Gbit/s (20 x 20 Gbit/s) soliton-based WDM

transmission experiment.

In Chapter 4, the dispersion management for unrepeatered transmission systems is described. Firstly, dispersion-managed transmission line configuration for Raman amplification is studied to alleviate the transmission impairments and to extend the transmissible distance by increasing the amplification gain. Then, as the result of the optimization, a successful result of a 40 Gbit/s-based terabit-capacity unrepeatered transmission over 306 km is presented.

In Chapter 5, the technologies for a highly spectral efficient 40 Gbit/s-based WDM transmission are discussed. Firstly, the impact of nonlinear crosstalk on conventional RZ signal format is experimentally explored in 50 GHz-spaced 40 Gbit/s DWDM systems to clarify the transmissible distance and induced transmission penalties. Next, the optical pre-filtering scheme is described as a practical solution to reduce the linear crosstalk for achieving a highly spectral efficient transmission, and a 50 GHz-spaced 40 Gbit/s x 25 WDM transmission over 480 km is presented by using bandwidth-limited RZ signals. Finally, pre-filtering conditions for different signal formats are numerically and experimentally investigated for achieving a spectral efficiency of 0.8 bit/s/Hz. As the results of the optimization studies for pre-filtering conditions including 9,000 km WDM transmission experiments, the feasibility of transoceanic transmission with a spectral efficiency of 0.8 bit/s/Hz is revealed.

In Chapter 6, the possibility of more than 16-fold capacity upgrade of JIH is presented. JIH submarine cable system has the per-fiber capacity of around 50 Gbit/s using 2.5 Gbit/s-based WDM technologies with 100 GHz-spaced NRZ signals. The possibility of terabit-capacity upgrade is investigated by using a higher-channel bit rate of 40 Gbit/s signal with RZ or CS-RZ modulation format and FEC technologies in the transmission lines designed for a 2.5 Gbit/s-based WDM system. Through the numerical and experimental studies, the feasibility of a 100 GHz-spaced 25 x 42.7 Gbit/s transmission with the total capacity of 1 Tbit/s is presented by using proper FEC technologies and signal formats.

In Chapter 7, the substantial knowledge and results from Chapters 2 to 6 are summarized.

Three appendixes A, B, and C are attached to supplementarily explain the equations and schemes used in the thesis. In Appendix A, the fundamental equations describing

the optical pulse propagation in a dispersive nonlinear media are derived from Maxwell's equations, and key parameters for the optical transmissions are reviewed. In Appendix B, after introducing typical modulation formats, the benefit of RZ format against nonlinear impairments is presented by numerical simulations. The basic concept and benefit of FEC technology is explained in Appendix C.

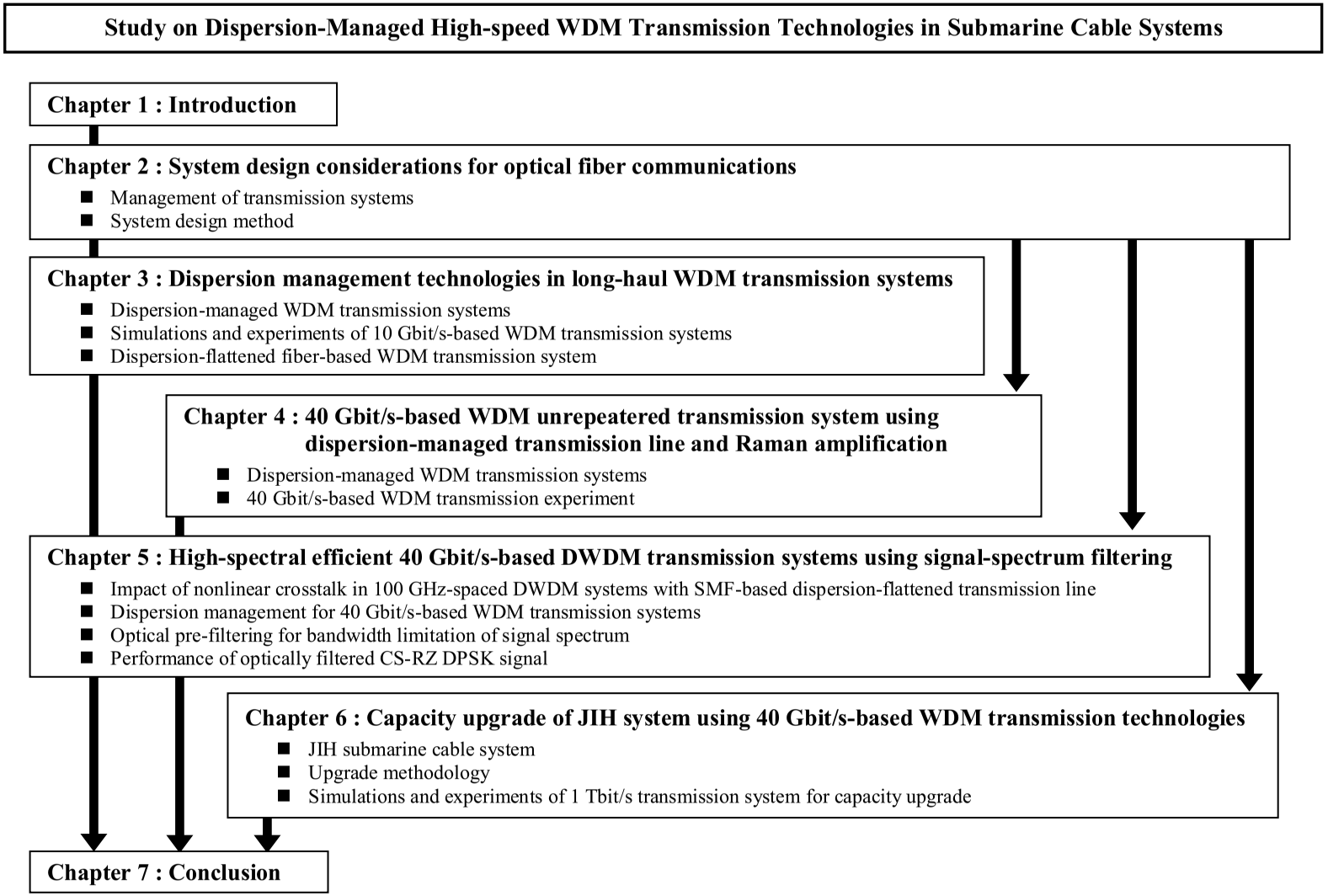

Fig. 1-2 Organization of the thesis.

References

[1] H. Wakabayashi, Y. Namihira, S. Akiba, S. Yamamoto, M. Ohkawa, and H. Yamamoto, “OS-A optical amplifier submarine cable system”, Suboptic1993, paper 4.2, 1993.

[2] N. Bergano and C. R. Davidson, “Wavelength division multiplexing in long-haul transmission systems”, IEEE/OSA J. Lightwave Technol., vol. 14, pp. 1229-1308, 1996.

[3] N. Edagawa and I. Morita, “Recent trends and future perspective of ultrahigh-capacity transoceanic transmission systems”, ECOC2002, 9.1.1, 2002.

[4] E. Desurvire, “Erbium doped fiber amplifiers: principles and applications”, John Wiley and Sons, New York, 1994.

[5] D. Marcuse, A. R. Chraplyvy, and R. W. Tkach, “Effect of fiber nonlinearity on long distance transmission”, IEEE/OSA J. Lightwave Technol., vol. 9, pp. 121-128, 1991.

[6] D. Marcuse, “Single-channel operation in very long nonlinear fibers with optical amplifiers at zero dispersion”, IEEE/OSA J. Lightwave Technol., vol. 9, pp. 356-361, 1991.

[7] D. Marcuse, “Bit-error rate of lightwave systems at the zero-dispersion wavelength”, IEEE/OSA J. Lightwave Technol., vol. 9, pp. 1330-1334, 1991.

[8] D. Marcuse, “RMS width of pulses in nonlinear dispersion fibers”, IEEE/OSA J. Lightwave Technol., vol. 10, pp. 17-21, 1992.

[9] G. P. Agrawal, “Nonlinear fiber optics”, California, USA: Academic Press, 1989.

[10] L. D. Garret, M. Eiselt, and R. Tkach, “Experimental comparison of WDM system capacity in conventional and non-zero dispersion shifted fiber”, OAA 1998, TuB2, 1998.

[11] L. F. Mollenaur, J. P. Gordon, and M. M. Islam, “Soliton propagation in long fiber with periodically compensated loss”, IEEE J. Quantum Electron., vol. 22, pp. 157-173, 1986.

[12] D. Cotter, “Fibre nonlinearities in optical communications”, Opt. and Quantum

Electron., vol. 19, pp. 1-17, 1987.

[13] R. H. Stolen, “Nonlinear properties of optical fibers”, in Optical Fiber Telecommunications, Edited by S. E. Miller and A. G. Chynoweth, New York, USA: Academic Press, 1979.

[14] Y. Aoki, “Properties of fiber Raman amplifiers and their applicability to digital optical communication systems”, IEEE/OSA J. Lightwave Technol., vol. 7, pp. 1225-1239, 1990.

[15] R. H. Stolen and E. P. Ippen, “Raman gain in glass optical waveguides”, Appl. Phys. Lett., vol. 22, pp. 276-278, 1973.

[16] E. Brandon, J. –P. Blondel, F. Boubal, L. Buet, V. Havard, A. Hugbart, L. Labrunie, P. Le Roux, D. Toullier, and R. Uhel, “1.28 Tbit/s (32 x 40 Gbit/s) unrepeatered transmission over 250 km”, ECOC2000, vol. 4, pp. 21-23, 2000.

[17] T. Tsuritani, A. Agata, K. Imai, I. Morita, K. Tanaka, T. Miyazawa, N. Edagawa, and M. Suzuki, “35 GHz-spaced-20 Gbps × 100 WDM RZ transmission over 2700 km using SMF-based dispersion flattened fiber span”, ECOC2000, PD1.5, 2000.

[18] G. Charlet, W. Idler, R. Dischler, J. -C. Antona, P. Tran, and S. Bigo, “3.2Tbit/s (80 x 42.7 Gb/s) C-band transmission over 9 x 100 km of TeraLight fiber with 50 GHz channel spacing”, OAA2002, PDP1, 2002.

[19] T. Tsuritani, I. Morita, A. Agata, and N. Edagawa, “Study on optimum optical pre-filtering condition for highly spectral-efficient ultralong-haul transmission using 40Gbit/s CS-RZ signal and all-Raman repeaters”, OFC2003, FE4, 2003.

[20] A. Agata, I. Morita, T. Tsuritani, and N. Edagawa, “Characteristics of asymmetrically filtered 40Gbit/s CS-RZ signals”, OFC2003, MF78, 2003.

[21] T. Tsuritani, A. Agata, I. Morita, and N. Edagawa, “21.4 Gbit/s x 56 WDM 9170 km transmission using symmetrically dispersion-managed fibre span”, ECOC2001, PD. M1.6, 2001.

[22] A. H. Gnauck, G. Raybon, S. Chandrasekhar, J. Leuthold, C. Doerr, L. Stulz, and E. Burrows, “25 x 40-Gb/s co-polarized DPSK transmission over 12 x 100-km NZDF with 50-GHz channel spacing”, IEEE Photon. Technol. Lett., vol. 15, pp. 467-469, 2003.

[23] B. Zhu, L. E. Nelson, S. Stulz, S. Gnauck, C. Doerr, J. Leuthold, L.

Gruner-Nielsen, M. O. Pedersen, J. Kim, R. Lingle, Y. Emori, Y. Ohki, N. Tsukiji, A. Oguri, and S. Namiki, “6.4-Tb/s (160 x 42.7 Gb/s) transmission with 0.8 bit/s/Hz spectral efficiency over 32 x 100 km of fiber using CSRZ-DPSK format”, OFC2003, PD19, 2003.

[24] T. Tsuritani, K. Ishida, A. Agata, K. Shimomura, I. Morita, T. Tokura, H. Taga, T. Mizouchi, and N. Edagawa, “70 GHz-spaced 40 x 42.7 Gbit/s transmission over 8700 km using CS-RZ DPSK signal, all-Raman repeaters and symmetrically dispersion fiber span”, OFC2003, PD23, 2003.

[25] S. Yamamoto, H. Takahira, and M. Tanaka, “5 Gbit/s optical transmission terminal equipment using forward error correction code and optical amplifier”, Electron. Lett., vol. 30, pp. 254-255, 1994.

[26] H. Yamamoto, H. Tanaka, and K. Goto, “Japan Information Highway – Wideband WDM Technology –”, OECC’98, 15D1-6, 1998.

Chapter 2

System design considerations for optical fiber communications

2-1 Introduction

The advent of optical amplifiers has changed the methodologies of transmission system design, which is an essential work in developing optical transmission systems. The fiber attenuation is no longer limiting factor, and the optical amplifier noise and the signal waveform distortions become major factors to determine the transmission performance. Most of the transmission properties including those limiting factors accumulate with the distance in optically amplified systems, and therefore a careful system design is required especially in long-haul transmission systems.

Key system design parameters and phenomena which should be managed are optical SNR, fiber dispersion, and nonlinearities. The optical SNR of signals passing through a chain of optical amplifiers is degraded by ASE noise, while the attenuation of optical signals is compensated for by optical amplifiers [1]. As the optical SNR practically defines the baseline of acceptable bit-error rate (BER) performance, a high signal launch power to a transmission line and a low ASE property of optical amplifiers are required. Fiber dispersion and nonlinearities induce waveform distortions, which result in the deterioration of the BER performance. In high-speed WDM transmission systems, the difference of dispersion in the signal wavelength band and nonlinear interactions among WDM channels provide a severe impact on the system performance [2]-[6].

In this chapter, firstly, the requirements for managing the system performance in high-speed WDM transmission systems are analytically derived by using the propagation equation in a dispersive nonlinear optical fiber. Based on those requirements, the fundamental concepts of the system design and management schemes of transmission impairments are presented.

The method to estimate or evaluate the system performance precisely is important

in designing the system. Three approaches are used in this thesis: analytical, numerical, and experimental ones. In addition, key system parameters and the relations are also presented.

2-2 Management of transmission systems

The fundamental concept and key parameters for designing the transmission systems are introduced in this section, and the methods for the system design are also explained.

2-2.1 Fundamental concept of system design

The behavior of the envelope of electric field $q(z,t)$ in a fiber is described by the nonlinear Schrödinger (NLS) equation as

$$i\frac{\partial q}{\partial z}-\frac{1}{2}k''\frac{\partial^2 q}{\partial t^2}-\frac{i}{6}k'''\frac{\partial^3 q}{\partial t^3}+\gamma|q|^2 q+i\alpha q=0. \tag{2.1}$$

The derivation of the NLS equation from Maxwell's equations is presented in Appendix A-1. The second and third terms on the left hand side of Eq. (2.1) indicates the second- and third-order dispersion effects, respectively, and the forth term including $|q|^2$ represents the nonlinear effect. The last term represents the attenuation of the signal, where α is the transmission loss coefficient of the optical fiber.

For simplicity, we firstly consider a linear transmission system in the absence of the nonlinear term in Eq. (2.1). The equation describing the evolution of $q(z,t)$ along z-direction can be written in the form:

$$\frac{\partial q}{\partial z}=-\frac{i}{2}k''\frac{\partial^2 q}{\partial t^2}+\frac{1}{6}k'''\frac{\partial^3 q}{\partial t^3}-\alpha q. \tag{2.2}$$

The Fourier transform of the equation yields

$$\frac{\partial \tilde{q}}{\partial z} = \left\{ i\left(\frac{1}{2}k''\omega^2 - \frac{1}{6}k'''\omega^3 \right) - \alpha \right\} \tilde{q} \,, \tag{2.3}$$

where the Fourier transform of $q(z,t)$ is defined as

$$q(t,z) = \frac{1}{2\pi} \int_{-\infty}^{\infty} \tilde{q}(\omega, z) e^{-i\omega t} d\omega \,. \tag{2.4}$$

The solution of Eq. (2.3) is given by

$$\tilde{q}(\omega, z) = \tilde{q}(\omega, 0) e^{-A(z)} e^{-iD(z)} \,, \tag{2.5}$$

where the real and imaginary parts of exponential coefficient, $A(z)$ and $D(z)$, are

$$A(z) = \int_0^z \alpha(\zeta) d\zeta \,, \tag{2.6}$$

$$D(z) = \frac{1}{2}\omega^2 \int_0^z k''(\zeta) d\zeta - \frac{1}{6}\omega^3 \int_0^z k'''(\zeta) d\zeta \,. \tag{2.7}$$

The transmission impairments should be managed so that the spectrum $\tilde{q}(\omega, z)$ does not change from the initial one $\tilde{q}(\omega, 0)$. From Eqs. (2.5)-(2.7), it is clear that the conditions for a penalty-free transmission are

$$\int_0^z \alpha(\zeta) d\zeta = 0 \,, \tag{2.8}$$

$$\frac{1}{2}\omega^2 \int_0^z k''(\zeta) d\zeta - \frac{1}{6}\omega^3 \int_0^z k'''(\zeta) d\zeta = 0 \,. \tag{2.9}$$

These equations express the fundamental concept of system design, and Eqs. (2.8) and (2.9) indicate the transmission loss compensation and dispersion management, respectively.

Next, we consider the effects of fiber nonlinearities on optical signals. Focusing on the only terms associated with fiber nonlinearities, Eq. (2.2) is led to

$$\frac{\partial q}{\partial z} = i\gamma |q|^2 q \,. \tag{2.10}$$

From the equation, the optical signal $q(t, z)$ can be described as

$$q(t,z) = q(t,0)e^{iN(z)z}, \tag{2.11}$$

where the phase $N(z)$ is represented by

$$N(z) = \gamma |q(0,z)|^2 . \tag{2.12}$$

The nonlinear effects arising from the nonlinear index of refraction give rise to an intensity-dependent phase change of the optical signals. Hence, a phase control scheme is necessary to mitigate or compensate for the nonlinear phase change.

2-2.2 Transmission loss compensation

Although the amplitude of the optical pulses decreases due to the transmission loss of fibers, it can be recovered by optical amplifiers which are located discretely at regular intervals. In optically amplified systems, however, the transmission performance is deteriorated by the ASE noise generated in amplifiers, and it accumulates to power levels similar to the data signal. This accumulated noise degrades the system performance by relatively reducing the optical SNR. The ASE noise power P_N is given by

$$P_N = N_f h\nu(G-1)B, \tag{2.13}$$

where N_f is the noise figure, $h\nu$ is the photon energy, G is the amplifier gain, and B is the bandwidth of optical filter following EDF to cut the ASE noise outside of the signal bandwidth [1].

The output power of amplifiers is set to be a fixed constant value, and therefore a portion of the signal in the output power decreases as the ASE noise accumulates with transmission distance. Figure 2-1 shows the relation among the output power from EDFAs, signal power, and accumulated noise power along with transmission distance. As the ASE noise is superimposed at each amplifier, the total noise power is given by multiplying the number of amplifiers N_{amp}. The optical SNR of the signal with an output power P_s from EDFAs is estimated to

$$SNR = \frac{P_S}{P_N N_{amp}} = \frac{P_S}{N_f h\nu(G-1)BN_{amp}} \approx \frac{P_S}{N_f h\nu GBN_{amp}}. \quad (2.14)$$

The ASE noise accompanied with optical amplification degrades the optical SNR, which is one of the most important features of digital transmission systems. Since the required optical SNR is increased with the bit rate linearly, it is necessary to keep a sufficient optical SNR for a higher-channel bit rate on the condition that fiber nonlinearities induced by increasing P_s do not affect the transmission performance.

Eq. (2.14) indicates that optical SNR can be increased by shortening the amplifier spacing. For example, we consider the situation that the amplifier spacing is assumed to be halved from 100 km to 50 km. As the transmission loss of fibers is typically 0.2 dB/km, the amplifier gain G decreases by 10 dB. In this case, the required number of amplifier N_{amp} increases by only 3 dB, and therefore it is found that the SNR eventually increases by 7 dB from Eq. (2.14).

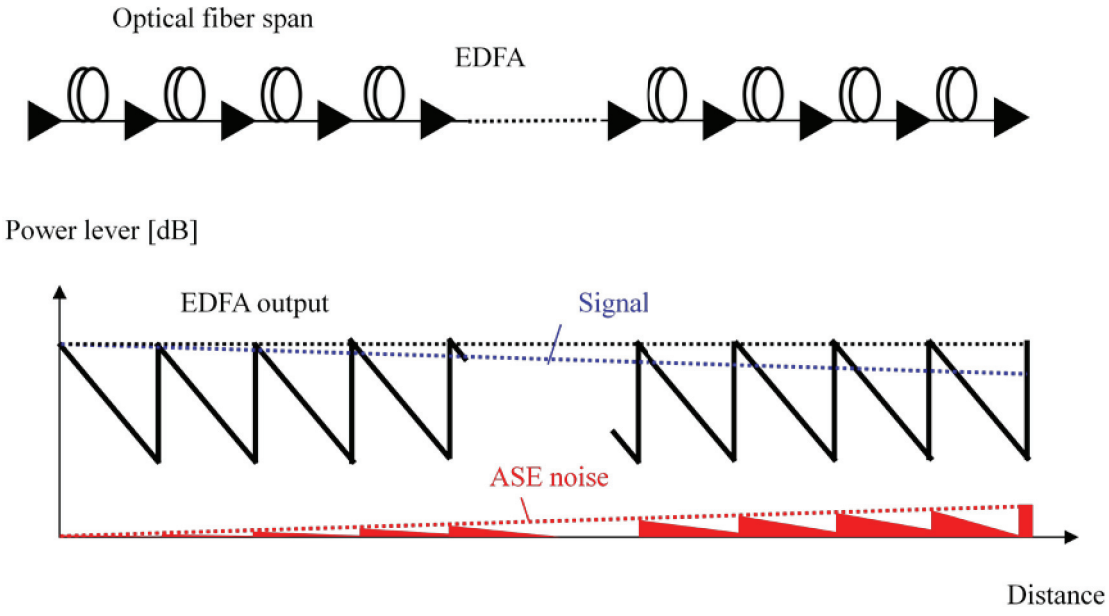

Fig.2-1 Output power from EDFAs, signal power, and accumulated noise power along with transmission distance.

2-2.3 Dispersion management

A solution of Eq. (2.9) describing the concept of dispersion management is given by

$$\int_0^z k''(\zeta)d\zeta = 0\,, \tag{2.15}$$

$$\int_0^z k'''(\zeta)d\zeta = 0\,. \tag{2.16}$$

For single-channel transmissions, the scope of the management is limited in the 2nd-order dispersion as expressed in Eq. (2.15) because the 3rd-order dispersion is negligible within a single-channel spectral window. In contrast, however, for WDM transmission systems in which WDM signal spectral window is wide enough to affect the signal quality, the 3rd-order dispersion compensation as expressed in Eq. (2.16) should be mandatorily considered in addition to the 2nd-order dispersion compensation.

Figure 2-2 shows a transmission line configuration using a 2nd-order dispersion management. The corresponding accumulated dispersion along the distance, which is known as dispersion map, and the dispersion are also illustrated in the figure. The transmission line consists of nine spans of a 50 km-long NZ-DSF and a 50 km-long SMF [7]. The dispersion of the NZ-DSFs and SMF at the center wavelength of the WDM signal (λ_{center}) is -2 and +18 ps/nm/km, respectively. Therefore, the accumulated dispersion of nine NZ-DSF spans is compensated for by using a single span of SMF.

It should be noted that only one channel among many WDM channels can be set to its system dispersion to zero. Although the 2nd-order dispersion compensation is very effective and widely used for single-channel transmission systems, the wavelength dependence of the accumulated dispersion must be considered in long-haul WDM transmission systems. In Fig. 2-2 where the system zero-dispersion is allocated at the center wavelength of the WDM signal, the accumulated dispersion of the edge channels located at far from the zero-dispersion wavelength are not returned to zero due to its wavelength dependency.

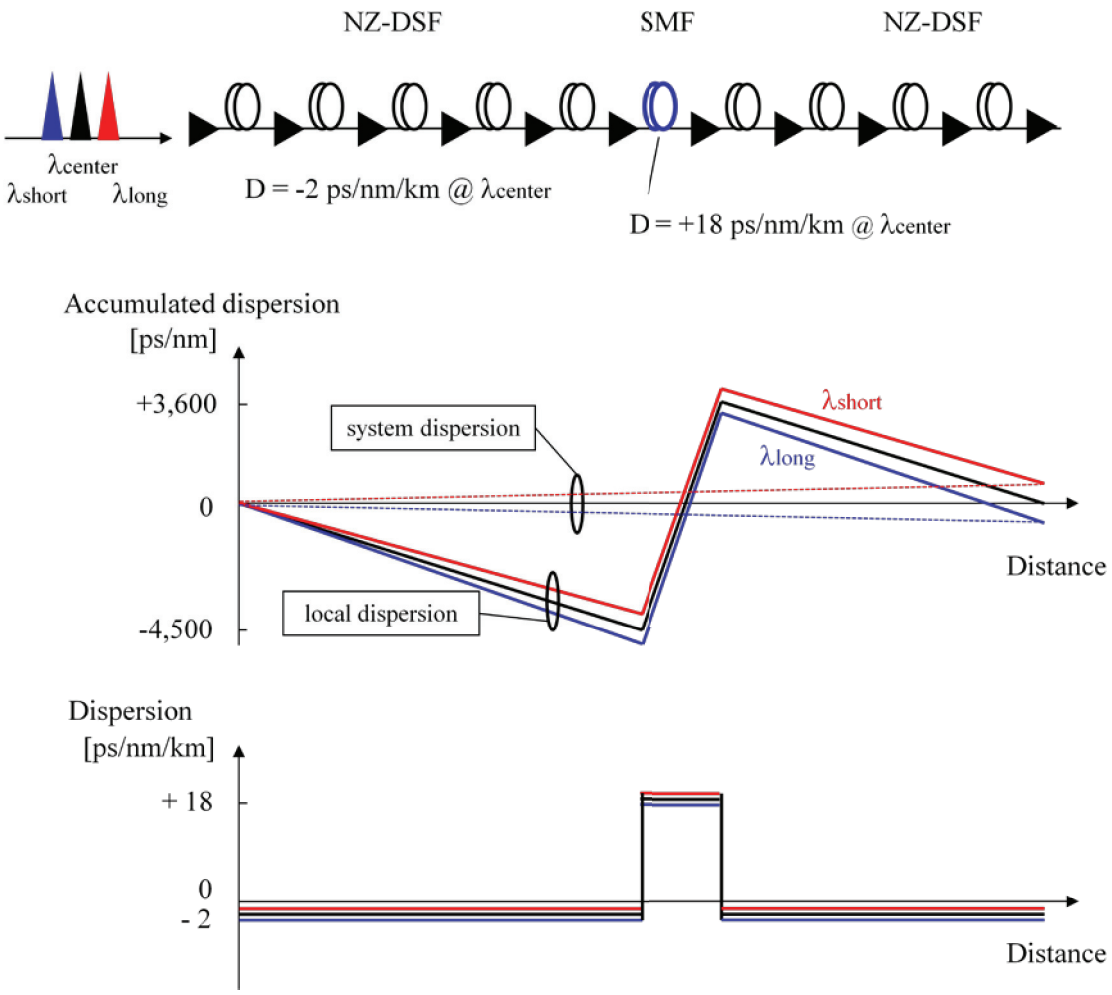

Fig.2-2 Transmission line configuration for dispersion management, the corresponding accumulated dispersion, and the dispersionalong with the transmission distance.

The dispersion with a wavelength dependency $D(\lambda)$ can be described as

$$D(\lambda) = \frac{dD}{d\lambda}(\lambda - \lambda_0)L\,, \tag{2.17}$$

where $\frac{dD}{d\lambda}$ represents dispersion slope, λ_0 is zero-dispersion wavelength, and L is fiber length. Figure 2-3 shows the dispersion property of a WDM signal with a 30-nm wavelength band. The WDM signal has a 2 ps/nm/km dispersion range, since the dispersion slope of conventional fibers is 0.07 ps/nm^2/km. The local dispersion of the

NZ-DSF spans is -3 and -1 ps/nm/km for the shortest and longest wavelengths, respectively, and the corresponding system dispersion becomes -1 and +1 ps/nm/km. The dispersion accumulates with the transmission distance, and the largely accumulated dispersion of the channels located at far from the zero-dispersion wavelength causes signal distortions in WDM transmission systems. It is an important consideration factor in designing long-haul WDM transmission systems to manage the accumulated dispersion over all the signal wavelength range.

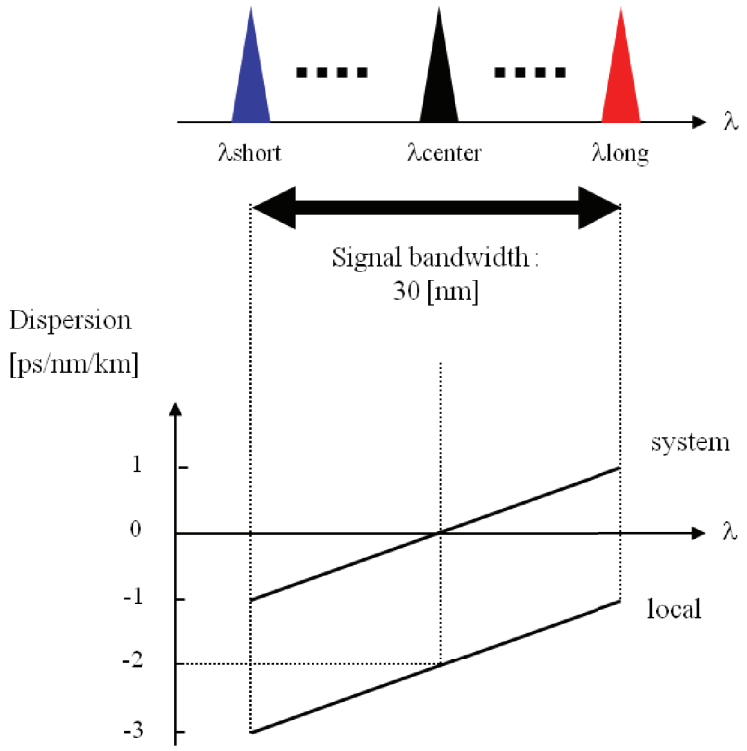

Fig.2-3 Dispersion property of a WDM signal with a 30-nm wavelength band.

2-2.4 Fiber nonlinearity mitigation

The nonlinearities are also inherent characteristics of optical fibers inducing signal distortions, and those can be classified into two categories: stimulated scattering and effects arising from the nonlinear index of refraction. Stimulated scattering such as Brillouin scattering and Raman scattering is manifested as intensity-dependent gain or loss [8]-[12], while effects arising from the nonlinear index such as self-phase modulation (SPM) and cross-phase modulation (XPM) give rise to an intensity-dependent phase change of the optical field as described in Eq. (2.11).

There is a trade-off between optical SNR and fiber nonlinearities in terms of the system performance. A high optical SNR is desired to keep a good system performance, while it induces high nonlinear effects on optical signals and results in the performance degradation. This is an important system design parameter in high-speed transmission systems, and the transmission performance in 10 Gbit/s-based long-haul WDM systems is severely restricted due to the interactions between fiber nonlinearities and largely accumulated chromatic dispersion.

Two approaches are considered to deal with the nonlinear effects. The first approach is to mitigate nonlinearities by applying a proper dispersion management, such as the use of special dispersion maps and span configurations. Dispersion management includes the mitigation of nonlinear behaviors in addition to dispersion compensation. The key fiber parameters are a large A_{eff} and a large local dispersion. It is intuitively understood that a larger A_{eff} should be allocated in a high power portion following an optical amplifier to reduce the nonlinear effects which are inversely proportional to A_{eff}. Chromatic dispersion which makes WDM channels travel at different group velocities contributes to evade the phase matching, and it results in the reduction of nonlinear interactions between WDM channels.

Hybrid-span configuration using a large core fiber (LCF) is a possible solution to reduce nonlinearities in long-haul 10 Gbit/s-based WDM transmission systems [13], [14]. Figure 2-4 shows the configuration of a typical span configuration using a LCF with a non-zero dispersion value. The LCF is located after the EDFA to minimize the

nonlinearities where the signal power level is the highest in a single fiber span. A low dispersion-slope NZ-DSF follows the LCF to alleviate a high dispersion slope property of the LCF, because it has a large dispersion slope as the result of enlarging the A_{eff} .

The second approach is to completely compensate for the induced nonlinear phase change by adding a proper frequency chirp to initial signals or by using soliton as the signal format [15]-[17]. Soliton positively uses the SPM and does not change its shape through the transmission by balancing with a positive dispersion of the fiber.

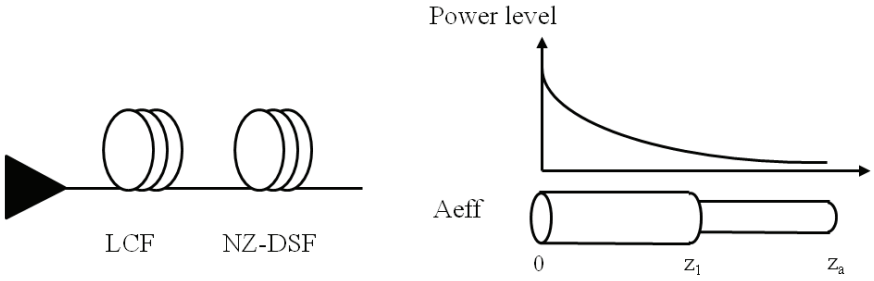

Fig.2-4 Span configuration using a LCF and low dispersion-slope NZ-DSF.

2-3 System design method

As the methods to evaluate the transmission performance, analytical, numerical, and experimental approaches are described in this section.

2-3.1 Analytical method

It is generally difficult to solve the NLS equation analytically except for some specific cases to which the inverse scattering method can be applied [18]. The detailed investigation on the performance should be left to numerical methods by which the

pulse propagation described by the NLS equation can be solved directly. In considering transmission impairments independently, however, analytical approaches are more effective and useful. The dispersive terms of the NLS equation is expressed as linear processes, so that the problem is more easily solved in the frequency domain by using the Fourier transform.

As for fiber nonlinearities, the nonlinear effects can be investigated by focusing the accumulated nonlinearity over a single fiber span $N_{span}(z)$. It is estimated by

$$N_{span}(z) = \int_0^{z_a} \gamma \left| q(t=0,z) \right|^2 dz = \frac{\omega_0 P_0}{c} \int_0^{z_a} \frac{n_2(z)}{A_{eff}(z)} e^{-\alpha(z)z} dz, \tag{2.18}$$

where P_0 is the output power of EDFAs, and z_a is the span length. Kerr coefficient n_2, effective core area A_{eff}, and the fiber loss coefficient α differ according to characteristics of optical fibers.

For example, a two-section span configuration as shown in Fig. 2-4 is considered for the analysis. The accumulated nonlinearity $N_{span}(z_a)$ over the single span with a length of z_a is led to

$$N_{span}(z_a) = \frac{\omega_0 P_0}{c} \left\{ \frac{n_{21}}{\alpha_1 A_{eff_1}} (1 - e^{-\alpha_1 z_1}) + \frac{n_{22}}{\alpha_2 A_{eff_2}} (e^{-\alpha_2 z_1} - e^{-\alpha_2 z_a}) \right\}, \tag{2.19}$$

where the suffixes 1 and 2 indicate the first and second section of the fiber coefficient n_2, α, and A_{eff}, respectively.

The advantages of the two-section span configuration using the LCF followed by the NZ-DSF can be evaluated by Eq. (2.19), in comparison with the reversely allocated two-section span configuration where the NZ-DSF followed by the LCF. The accumulated nonlinearity of the former span configuration in Ref. [13] is 3.3×10^{-4} and smaller than that of the latter one by 1.1 dB. Figure 2-5 shows the accumulated nonlinearity N_{span} along with the distance for the two span configurations: the LCF followed by the NZ-DSF and the NZ-DSF followed by the LCF. From this figure, it is found that the difference is developed in the first section of the span, which is the higher signal power portion.

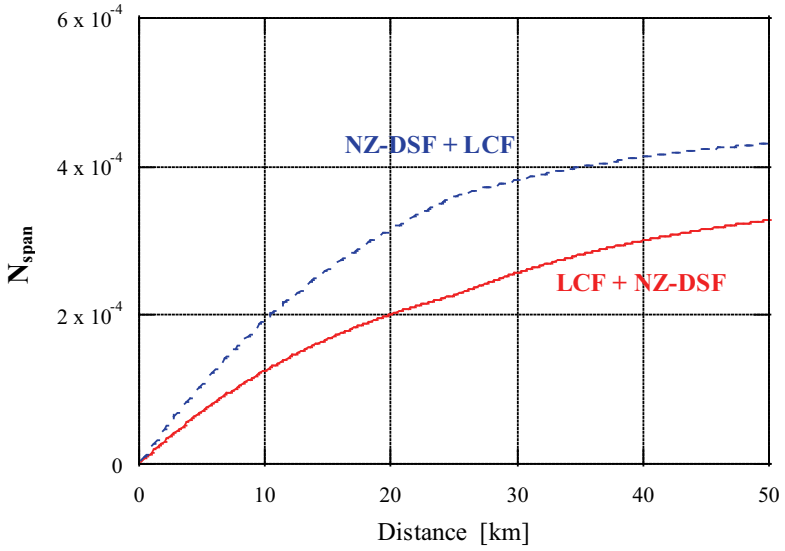

Fig.2-5 Induced nonlinearities for two kinds of span configuration: LCF+NZ-DSF and NZ-DSF+LCF.

2-3.2 Numerical method

Numerical analysis is the only way to solve the NLS equation in practical transmission systems, and it can involve any kinds of fibers and components. The numerical solution of the NLS equation is derived by using the split-step Fourier method. The method separates the effects of the dispersive terms in the frequency domain and those of the nonlinear terms in the time domain, and derives the analytical solution independently for a small incremental distance of Δz in each domain.

In simulations, the NLS equation describing the optical field propagation is solved by the split-step Fourier algorithm on an initial condition. As the initial condition, the data pattern sequence, the pulse shape, and the phase of the field should be defined. Typically, a pseudo-random bit sequence with more than 64 bit-length is used for the data pattern, and the shape of RZ signal is approximated by a super-Gaussian function. A super-Gaussian pulse with an initial chirp is given by

$$q(0,t) = A\exp\left[-\frac{1+iC(0,t)}{2}\left(\frac{t}{t_0}\right)^{2m}\right], \tag{2.20}$$

where A, C, t_0, and m are the amplitude parameter, the chirp parameter, the initial pulse width, and the parameter controlling the degree of edge sharpness. For simulating optical amplified repeaters, the amplitude of optical signals is recovered to the level of the repeater output power at the location of the repeaters, and the optical noise generated by the amplifiers is superimposed to the signal.

2-3.3 Experimental method

The experiment using a straight transmission line configuration is inefficient for the optimization of the system performance at the research stage because it is difficult to change the system parameters of the transmission line frequently and flexibly. For such purposes, recirculating loop technique is used to investigate the performance of long-distance transmission systems [19].

Figure 2-6 shows a schematic diagram of the recirculating loop technique. The recirculating loop consists of a coupler to connect the loop with the transmitter and receiver sides, several spans of the transmission fiber followed by EDFAs, an optical switch for circulating the signal, and an EDFA for compensating for the additional loss of the coupler and the optical switch. At the transmitter side, an optical switch is employed for loading the signal into the loop. The timing states of optical switches and the gate at the receiver side is shown in Fig. 2-7. The timing operation of these two switches is synchronized each other; when the loading switch is closed for feeding the signal into the loop, the state of the circulating switch is closed. In contrast, when the loading switch is opened, the circulating switch is closed for circulating the loaded signals. The time to close the circulating switch corresponds to the target transmission distance, and during the last loop period, the signal forwarded to the receiver side is measured by gating it.

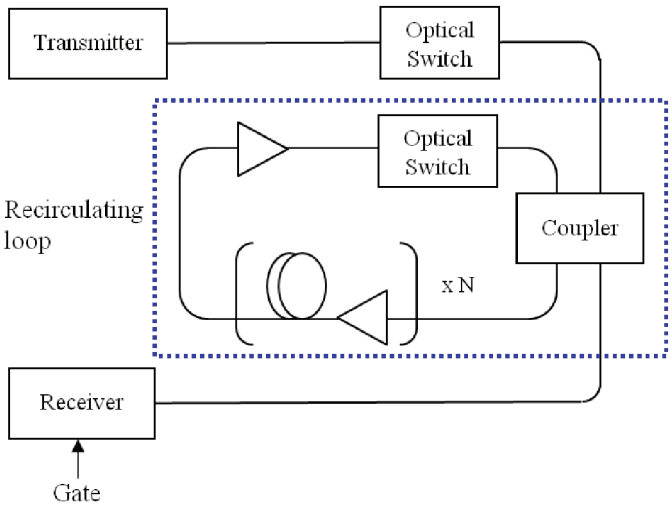

Fig. 2-6 Recirculating loop configuration.

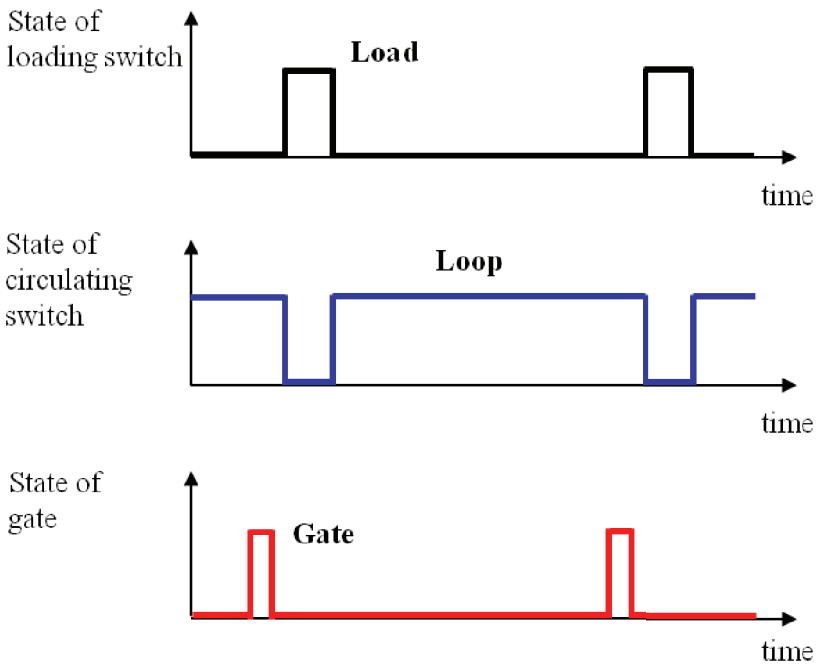

Fig. 2-7 The timing states of optical switches and gate.

2-3.4 Performance evaluation method

The transmission quality in digital transmission systems can be expressed by a BER. As commercial transmission systems operate with very low BERs, these are too small to be measured in experiments and estimated in numerical simulations. The practical method for measuring the transmission performances is to use the Q-factor, which is introduced for the purpose of calculating the BER performance [20].

Figure 2.8 illustrates a Q-factor measurement from obtained BERs by changing decision voltage levels.

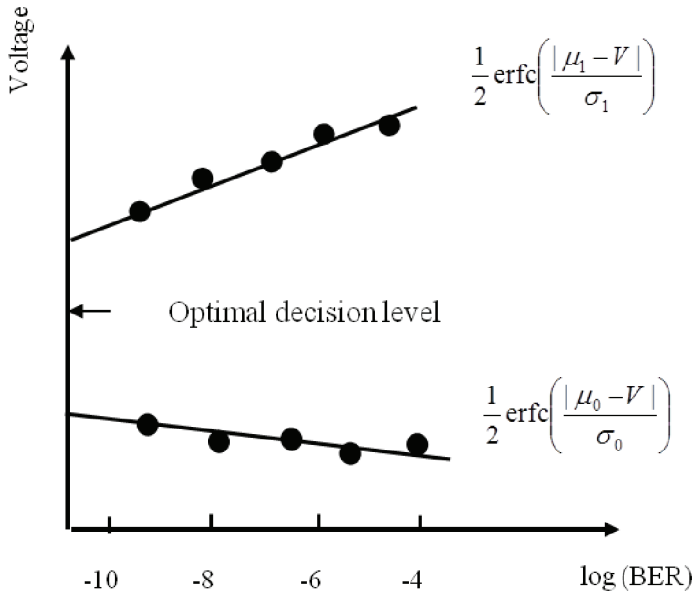

Fig. 2-8 Q-factor measurement in experiments.

In experiments, the Q-factor is estimated by measuring the BER at different threshold settings in the decision circuit. The data are fitted with a curve, assuming Gaussian noise statistics of

$$BER(V) = \frac{1}{2}\left[\text{erfc}\left(\frac{|\mu_1 - V|}{\sigma_1}\right) + \text{erfc}\left(\frac{|V - \mu_0|}{\sigma_0}\right)\right], \tag{2.21}$$

where $\mathrm{erfc}(x)$ is expressed as

$$\mathrm{erfc}(x) = \frac{1}{\sqrt{2\pi}} \int_{x}^{\infty} e^{-\alpha^2/2} d\alpha \,. \tag{2.22}$$

The equivalent values for the means $\mu_{1,0}$ and standard deviations $\sigma_{1,0}$ of the voltages on the marks and spaces are given by the curve fit. The Q-factor is formed as

$$Q \equiv \frac{|\,\mu_1 - \mu_0\,|}{\sigma_1 + \sigma_0}. \tag{2.23}$$

It is usually expressed in decibels as $10\log(Q^2)$ and is translated to *BER* with the following formula,

$$BER = \frac{1}{2}\mathrm{erfc}\left(\frac{Q}{\sqrt{2}}\right) \approx \frac{1}{e\sqrt{2\pi}}\exp\left(-\frac{Q^2}{2}\right). \tag{2.24}$$

A BER of less than 10^{-9}, which is the required quality of error-free transmission, is corresponding to a Q-factor of more than 15.6 dB.

In simulations, Q-factor can be derived from an eye pattern diagram. Figure 2-9 shows the eye pattern generated by overlaying portions of a bit stream that have been delayed by an integer number of bit periods. A histogram is schematically shown to indicate the parameters used in defining the Q-factor. A long bit stream is necessary in the simulations enough to calculate accurate values of the means and standard deviations of the mark and space signals.

It is known that the Q-factor is associated with the SNR of the signals in the definition because $|\,\mu_1 - \mu_0\,|$ and $\sigma_{1,0}$ in Eq. (2.23) indicate the signal and noise levels of mark and space signals, respectively. Considering an ideal situation where only accumulated noise impairs the performance, the Q-factor is described as

$$Q = \frac{2SNR}{1+\sqrt{1+4SNR}}\sqrt{\frac{B_o}{B_e}}\,. \tag{2.25}$$

Here, B_o and B_e are the bandwidth of optical and electrical filters in the receiver, respectively.

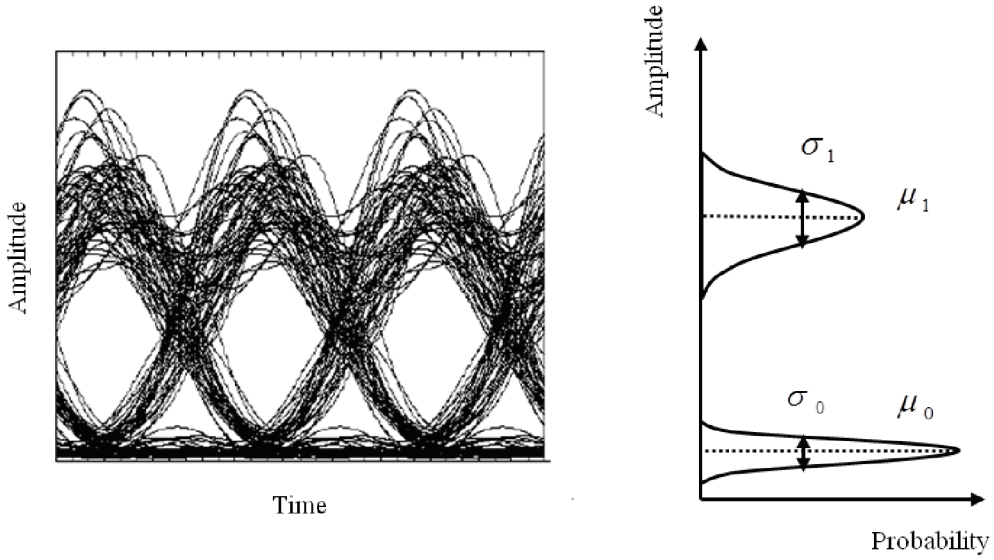

Fig. 2-9 Eye pattern obtained in a simulation and the corresponding histogram of the mark and space signals.

2-4 Conclusion

Fundamental concept of system design has been presented by using pulse propagation equation in optical fibers. Optical SNR, fiber dispersion, and nonlinearities are key technical features determining the transmission performance, and these parameters can be analytically designed with transmission loss compensation, dispersion management, and fiber nonlinearity mitigation, respectively.

As methods for designing systems, three approaches were studied: analytical, numerical, and experimental ones. In the analytical approach, it is effective to investigate transmission impairments independently, and the equation to estimate fiber nonlinearities of a two-section span configuration was analytically derived by focusing on the accumulated nonlinearity over a single fiber span. In addition, a preferable fiber allocation in the span was investigated by using an analytical formula in the case of two-section span configuration. Through these studies, the system design chart was introduced to alleviate fiber nonlinearities, and the results revealed that the nonlinearity

can be mitigated by properly allocated the two kinds of fibers.

Numerical and experimental approaches are necessary to evaluate the transmission performance including all the impairments precisely. Numerical simulations using the split-step Fourier method and transmission experiments using a recirculating loop were described, which are used in the following Chapters. The Q-factor, which is an important key index to express transmission performances, was also explained by associated with BER and SNR.

References

[1] E. Desurvire, “Erbium doped fiber amplifiers: principles and applications”, John Wiley and Sons, New York, 1994.

[2] D. Marcuse, A. R. Chraplyvy, and R. W. Tkach, “Effect of fiber nonlinearity on long distance transmission”, IEEE/OSA J. Lightwave Technol., vol. 9, pp. 121-128, 1991.

[3] D. Marcuse, “Single-channel operation in very long nonlinear fibers with optical amplifiers at zero dispersion”, IEEE/OSA J. Lightwave Technol., vol. 9, pp. 356-361, 1991.

[4] D. Marcuse, “Bit-error rate of lightwave systems at the zero-dispersion wavelength”, IEEE/OSA J. Lightwave Technol., vol. 9, pp. 1330-1334, 1991.

[5] D. Marcuse, “RMS width of pulses in nonlinear dispersion fibers”, IEEE/OSA J. Lightwave Technol., vol. 10, pp. 17-21, 1992.

[6] G. P. Agrawal, “Nonlinear fiber optics”, California, USA: Academic Press, 1989.

[7] L. D. Garret, M. Eiselt, and R. Tkach, “Experimental comparison of WDM system capacity in conventional and non-zero dispersion shifted fiber”, OAA 1998, TuB2, 1998.

[8] Y. R. Shen and N. Bloembergen, “Theory of stimulated Brillouin and Raman scattering”, Phys. Rev. A, vol. 137, pp. 1787-1804, 1965.

[9] D. Cotter, “Fibre nonlinearities in optical communications”, Opt. and Quantum Electron., vol. 19, pp. 1-17, 1987.

[10] R. H. Stolen, “Nonlinear properties of optical fibers”, in Optical Fiber Telecommunications, Edited by S. E. Miller and A. G. Chynoweth, New York, USA: Academic Press, 1979.

[11] E. P. Ippen and R. H. Stolen, “Stimulated Brillouin scattering”, Appl. Phys. Lett., Vol. 21, pp. 539-541, 1972.

[12] D. Cotter, “Stimulated Brillouim scattering in monomode optical fibre”, J. Opt. Commun., Vol. 4, pp. 10-19, 1983.

[13] M. Suzuki, H. Kidorf, N. Edagawa, H. Taga, N. Takeda, K. Imai, I. Morita, S.

Yamamoto, E. Shibano, T. Miyakawa, E. Nazuka, M. Ma, F. Kerfoot, R. Maybach, H. Adelmann, V. Arya, C. Chen, S. Evangelides, D. Gray, B. Pedersen, and A. Puc, “170 Gb/s transmission over 10,850 km using large core transmission fiber”, OFC1998, PD17, 1998.

[14] N. S. Bergano, C. R. Davidson, M. Ma, A. Pilipetskii, S. G. Evangelides, H. D. Kidorf, J. M. Darcie, E. Golvochenko, K. Rottwitt, P. C. Corbett, R. Menges, M. A. Mills, B. Pedersen, D. Peckham, A. A. Abramov, and A. M. Vengsarkar, “320 Gb/s WDM transmission (64 x 5 Gb/s) over 7,200 km using large mode fiber spans and chirped return-to-zero signals”, OFC1998, PD12, 1998.

[15] N. Henmi, T. Saito, and T. Ishida, “Prechirp technique as a linear dispersion compensation for ultrahigh-speed long-span intensity modulation directed detection optical communication systems”, IEEE/OSA J. Lightwave Technol., vol. 12, pp. 1706-1719, 1994.

[16] N. S. Bergano, C. R. Davidson, M. A. Mills, P. C. Corbett, S. G. Evangelides, B. Pedersen, R. Menges, J. L. Zyskind, J. W. Sulhoff, A. K. Srivastava, C. Wolf, and J. Judkins, “Long-haul WDM transmission using optimum channel modulation: a 120 Gb/s (32 x 5 Gb/s) 9,300 km demonstration”, OFC1997, PD16, 1997.

[17] H. Hasegawa and Y. Kodama, “Solitons in optical communications”, Oxford University Press, Oxford, 1995.

[18] V. E. Zakharov and A. B. Shabat, “Exact theory of two-dimensional self-focusing and one-dimensional self-modulation of waves in nonlinear media”, Sov, Phys. JETP, vol.34, pp. 62-69.

[19] N. S. Bergano and C. R. Davidson, “Circulating loop transmission experiments for the study of long-haul transmission systems using erbium-doped fiber amplifiers”, IEEE/OSA J. Lightwave Technol., vol. 13, pp. 879-888, 1995.

[20] N. S. Bergano, F. W. Kerfoot, and C. R. Davidson, “Margin measurements in optical amplifier systems”, IEEE Photonics Technol. Lett., vol.5, pp. 304-306, 1993.

Chapter 3

Dispersion management technologies in long-haul WDM transmission systems

3-1 Introduction

WDM technology is an efficient way to increase the aggregate system capacity of optically amplified transmission systems. In the first generation of WDM undersea cable systems such as SEA-ME-WE 3 (South East Asia Middle West Europe 3) and China-US, a channel bit rate of 2.5 Gbit/s has been adopted for a total system capacity of 20 Gbit/s. For further capacity expansion, both higher-channel bit rate and more WDM channel counts are required.

In such large capacity systems with a channel bit rate of more than 10 Gbit/s, however, nonlinear effects in the transmission fiber severely affect the transmission performance [1]. Considerable efforts have been made to overcome these problems from the viewpoints of both system design and component development.

The use of RZ modulation format is one approach to resolve the problems. NRZ format is employed in the early stages of long-haul WDM transmission systems, because the process of signal generation is simple. Although the NRZ format has advantages in terms of terminal technologies, it is vulnerable against fiber nonlinearities. The NRZ characteristics of the transmitting consecutive mark signals causes pattern-dependent waveform distortions due to nonlinear effects, because the consecutive mark signals of WDM channels occupying the whole bit slot overlap each other in the time domain and induce large nonlinear interactions. RZ format is more tolerable against the pattern-dependent distortion than NRZ format, owing to its nature of the uniform waveform. Most of long-haul submarine cable systems today use the RZ signal format. Appendix B in the thesis reviews typical modulation formats in intensity-modulation direct-direction (IM-DD) systems and shows the benefit of RZ

format in detail.

Another key technology is the use of a hybrid span configuration using a low nonlinear fiber with a large A_{eff} of around 80 μm^2 and a low dispersion-slope fiber [1], [2]. The hybrid span composed of these two NZ-DSFs with a dispersion of around –2 ps/nm/km enables low nonlinearity and moderate dispersion slope over a single fiber span. The low dispersion-slope fiber attributes to alleviate the dispersion accumulation of edge channels located at far from system zero-dispersion wavelength (λ_0), which causes performance degradation through the interactions with fiber nonlinear effects.

A hybrid span configuration of a standard SMF and DCF is another effective approach to achieve a low nonlinearity and small dispersion-slope fiber span. As SC-DCF can compensate for the dispersion and dispersion slope of the SMF simultaneously, the dispersion-flattened fiber span can be constructed by combining the SMF and SC-DCF in each span [3]-[5]. This span configuration satisfies the both requirements of low nonlinearity and small dispersion slope simultaneously, because a large A_{eff} of around 80 μm^2 and a high dispersion property of the SMF contribute to the suppression of fiber nonlinear effects.

There are many differences between NZ-DSF-based and SMF-based systems such as the span loss, local dispersion, and accumulated dispersion over a single fiber span and the transmission line. Although the SMF-based system has an advantage of lower dispersion slope, the accumulated dispersion over the single fiber span is more than one order of magnitude larger than that of the NZ-DSF-based system. In addition, the SC-DCF has a large transmission loss of 0.25 to 0.6 dB/km, which results in a larger span loss and lower optical SNR.

In this chapter, the transmission performance of these two fiber span configurations is investigated by nonlinear impairment analysis, numerical simulations, and transmission experiments, for targeting a 320 Gbit/s WDM transmission over transoceanic distances. This is a challenging work because the transmission capacity has to be doubled from that of PC-1 and Japan-US cable systems installed in 2001. In addition, the potential of dispersion-flattened fiber-based systems is discussed through a 400 Gbit/s (20 x 20 Gbit/s) soliton-based WDM transmission.

3-2 Dispersion-managed WDM transmission systems

3-2.1 NZ-DSF-based system

A hybrid span configuration of the NZ-DSF-based system is illustrated in Fig. 2-4. The LCF with a large A_{eff} and relatively large dispersion slope is placed at the higher signal power portion following EDFAs to reduce fiber nonlinear effects. The low dispersion-slope NZ-DSF with a moderate A_{eff} follows the LCF to reduce overall span-averaged dispersion slope. Table 3-1 lists typical optical parameters of the LCF and the low dispersion-slope NZ-DSF. It should be noted that there is a trade-off between A_{eff} and dispersion slope characteristics. The drawbacks of two types of the fiber, a large dispersion slope for the LCF and a moderate A_{eff} for the low dispersion-slope NZ-DSF, are compensated for each other.

Table 3-1 Typical parameters of the LCF and low dispersion-slope NZ-DSF.

		LCF	NZ-DSF
Dispersion@1550nm	[ps/nm/km]	-2.0	
Dispersion slope	[ps/nm^2/km]	0.11	0.065
A_{eff}	[μm^2]	80	55
n_2	[m^2/W]	2.5 x 10^{-20}	
Loss	[dB/km]	0.22	0.2
Length ratio (LCF : NZ-DSF)		1 : 1	

With this hybrid span configuration, nonlinear effects can be effectively reduced without increasing the dispersion slope, and a 10 Gbit/s-based 160 Gbit/s WDM transmission over 10,850 km was demonstrated with an average Q-factor of 15.5 dB [1].

In this paper, however, the performance of the both edge channels was degraded as shown in Fig. 3-1.

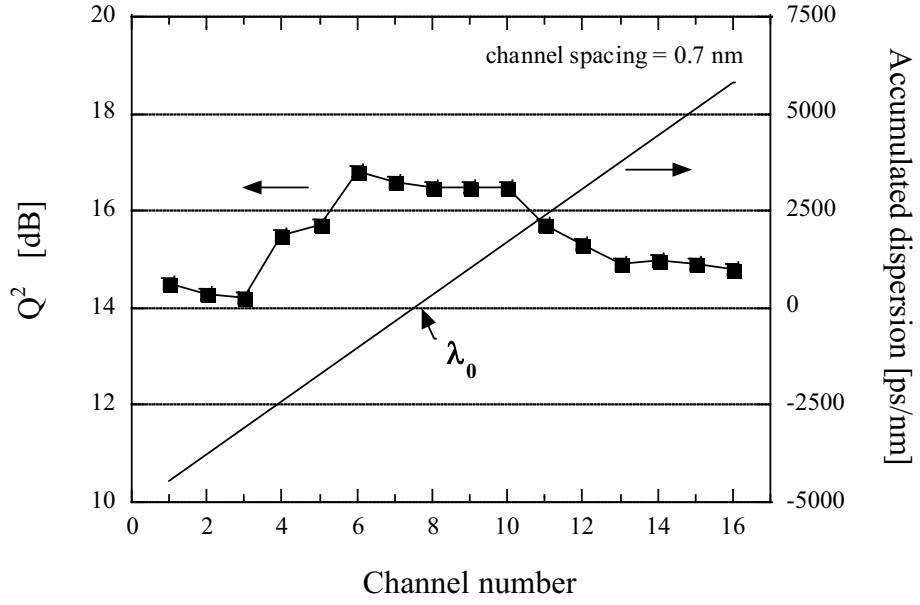

Fig.3-1 Transmission performance and accumulated dispersion of 16 x 10.7 Gbit/s WDM channels over 10,850 km.

Figure 3-1 also shows the accumulated dispersion of each channel after 10,850 km. The performance of the edge channels which are located at far from system zero-dispersion wavelength (λ_0) was degraded, while the average Q-factor (Q^2) was 15.5 dB. It was due to the interactions between their largely accumulated chromatic dispersion and nonlinear effects, and the performance degradation was proportional to the degree of the accumulated dispersion.

A further reduction of nonlinear effects is necessary for the capacity expansion of more than 160 Gbit/s. The span length, repeater output power, and the channel spacing are the candidate parameters for the performance optimization in NZ-DSF-based systems. For doubling the transmission capacity to 320 Gbit/s, the channel spacing should be halved since the amplifier bandwidth is finite and limited.

In this situation, the amplifier output power per channel should be decreased to alleviate fiber nonlinear effects. Even in reducing the amplifier output power per channel, the required optical SNR can be kept by shortening the amplifier spacing.

For example, the amplifier spacing is assumed to be reduced from 50 km to 40 km. The transmission span loss, namely the amplifier gain G, decreases by about 2.0 dB, while the number of amplifiers N_{amp} increases by 0.8 dB. From Eq. (2.14), it is found that the same optical SNR can be kept even with a 1.2-dB smaller amplifier output power in this case. It means that the reduction of the amplifier spacing from 50 to 40km contributes to the reduction of nonlinear effects by 1.2 dB.

3-2.2 SMF-based system

Figure 3-2 shows an example of the hybrid fiber span configuration of SMF-based systems. In SMF-based systems, a large portion of the span is occupied by a SMF with a large A_{eff}, and then a SC-DCF with a negative dispersion and dispersion slope follows to compensate for the both dispersion and dispersion slope of the SMF.

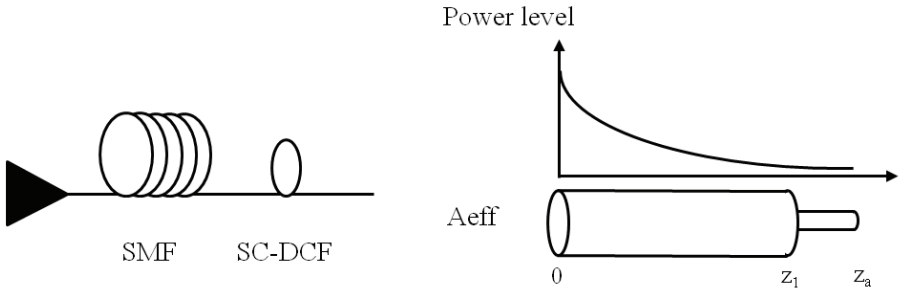

Fig.3-2 Span configuration using a SMF and SC-DCF.

This fiber span configuration contributes to the reduction of fiber nonlinearities

because the SMF with a large A_{eff} is allocated where the optical power level is high. It has another advantage of a high local dispersion, which is effective to suppress the nonlinear effects such as FWM and XPM in long-haul WDM transmission systems [6]. This is a notable feature of SMF-based configurations.

The dispersion parameters of optical fibers can be flexibly designed by changing the refractive index profiles. The dispersion of optical fibers is determined by two factors: material and waveguide geometry. The material dispersion is approximately the same in all silica fibers, and it has an anomalous dispersion and a positive dispersion slope by nature in the transmission window. It is essential to add a considerable waveguide dispersion in order to achieve desirable dispersion and dispersion slope characteristics. W-shaped refractive index profiles, which have two layers in the cladding and the refractive index of the inner cladding is set to be a lower value than that of the outer one, are widely employed for fabricating the fibers with desired characteristics [7]. The fiber parameters can be manipulated by changing the diameters and refractive index difference of core and the first and second claddings in the W-shaped profiles.

The trade-offs among the fiber parameters should be considered in designing span configurations because these are closely related to each other. A refractive index profile achieving a higher negative dispersion and dispersion slope leads to a small A_{eff} and a large micro-bending loss, which results in inducing a higher nonlinearities.

Figures 3-3 (a) and (b) illustrate two typical span configurations of SMF-based systems for the length ratio of SMF and SC-DCF of 5:1 and 1:1, respectively. The SC-DCF in Fig. 3-3 (a) has five-time larger negative dispersion and dispersion slope than those of the SMF, while the SC-DCF in Fig. 3-3 (b) has the opposite values of those of the SMF. Those are examples of SMF-based span configurations, and any combinations regarding the length ratio of the SMF and SC-DCF can be fabricated in principle, by designing the SC-DCF with the desired compensation ratio of both the dispersion and dispersion slope.

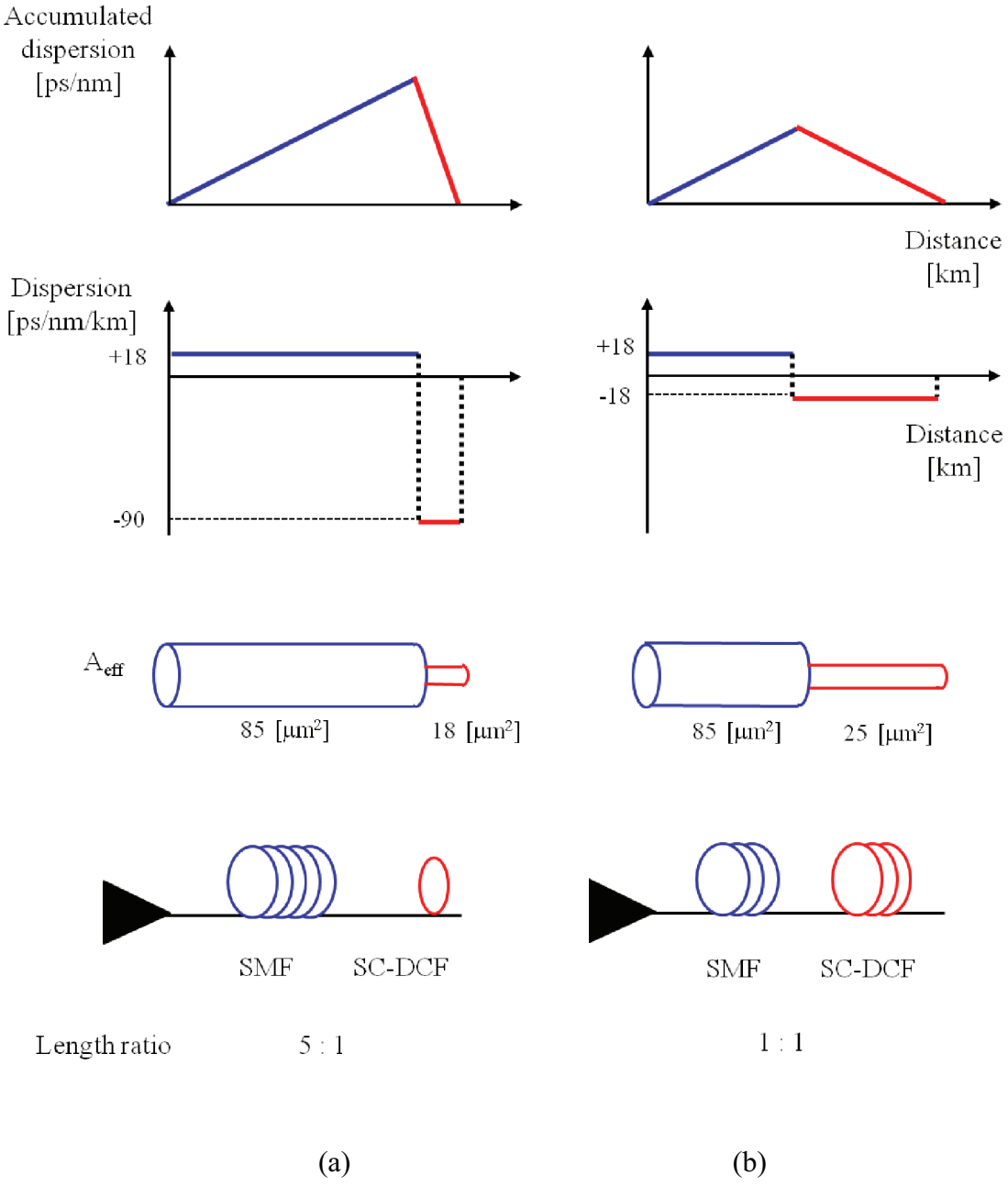

Fig.3-3 SMF-based span configurations with different compensation ratio of SC-DCFs.

Four types of the length ratio are considered as SMF-based span configurations for the evaluation in the following sections. The length ratio of the SMF and SC-DCF are 1:1, 3:1, 5:1, and 7:1, and the corresponding key fiber parameters of SMF and SC-DCFs are listed in Table 3-2 and 3-3, respectively.

Table 3-2 Typical parameters of the SMF used for the evaluation.

		SMF
Dispersion@1550nm	[ps/nm/km]	+18
Dispersion slope	[ps/nm^2/km]	+0.06
A_{eff}	[μm^2]	85
n_2	[m^2/W]	2.3 x 10^{-20}
Loss	[dB/km]	0.20

Table 3-3 Typical parameters of the SC-DCFs used for the evaluation.

		SC-DCF			
Length ratio (SMF : SC-DCF)		1 : 1	3 : 1	5 : 1	7 : 1
Dispersion@1550nm	[ps/nm/km]	-18	-54	-90	-126
Dispersion slope	[ps/nm^2/km]	-0.06	-0.18	-0.3	-0.42
A_{eff}	[μm^2]	25	20	18	15
n_2	[m^2/W]	2.8 x 10^{-20}			
Loss	[dB/km]	0.25	0.35	0.45	0.6

3-2.3 Comparison of NZ-DSF and SMF-based systems

In this section, the transmission characteristics of NZ-DSF and SMF-based systems are compared in terms of the accumulated dispersion over the transmission line and induced nonlinearities over a single fiber span.

Figures 3-4 (a) and (b) illustrate the accumulated dispersion along with the distance, referred to as dispersion map, of NZ-DSF- and SMF-based systems, respectively. In the NZ-DSF-based dispersion map, the difference of accumulated dispersion between channels expands with transmission distance, while the SMF-based dispersion map can provide the same system dispersion for all the channels owing to the flat dispersion characteristics.

A high local dispersion of the SMF, which is effective for suppressing nonlinear impairments, causes a large dispersion accumulation even in a single fiber span. The chromatic dispersion of the SMF is about ten times as large as that of a NZ-DSF. In nonlinear-influenced transmission systems, widely spread pulses cannot be recovered completely to the original waveform even though the SMF is effective for suppressing the nonlinear impairments. In addition, the SC-DCF with a small A_{eff} of 15 to 25 μm^2 induces large nonlinear effects, and a large transmission loss of 0.25 to 0.6 dB/km results in a large SNR degradation.

The induced nonlinearity over a single fiber span can be estimated by using Eq. (2.19). The difference of the span loss was included for the estimation since it is proportional to the EDFA output power. Figure 3-5 shows the effective nonlinear penalties (P_{eff}) of four SMF-based span configurations relative to the NZ-DSF-based one. The P_{eff} is expressed as the sum of the nonlinear penalty (P_{NL}) and additional span loss (P_{loss}) relative to the NZ-DSF-based span configuration. These are shown in Fig. 3-5 by dotted and dashed lines, respectively.

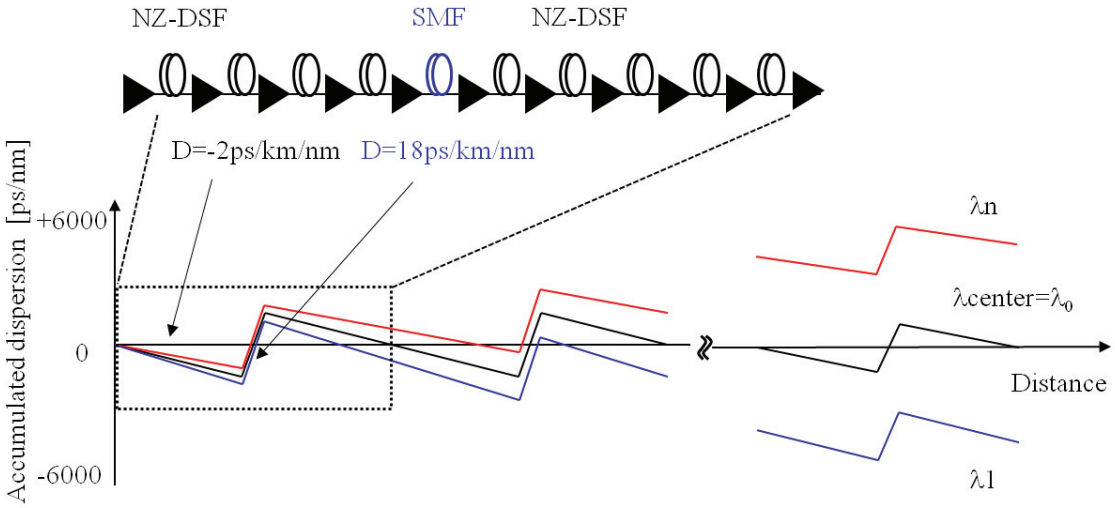

(a) NZ-DSF-based system

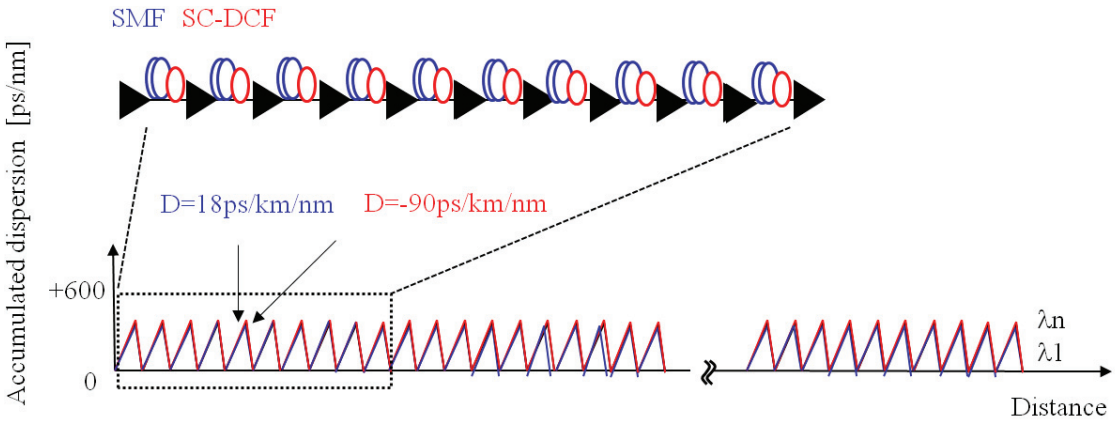

(b) SMF-based system

Fig.3-4 Accumulated dispersion with transmission distance.

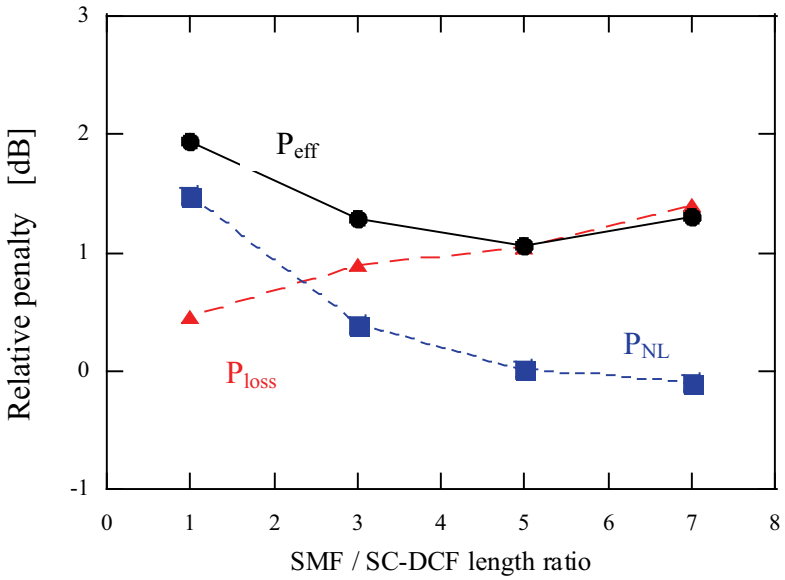

Fig. 3-5 Penalties of SMF-based span configurations relative to NZ-DSF-based one.

Using SC-DCFs with high compensation ratios of more than five, the induced nonlinearities were almost the same level of DSF-based one, while the span loss was deteriorated by about 1 dB. The span loss properties can be improved as the compensation ratio of SC-DCFs reduced. However, it led to a large increase of nonlinear penalties. From Fig. 3-5, it was found that the effective nonlinear penalty was minimized by using the SC-DCF with the compensation ratio of five.

Figure 3-6 show the effective nonlinearities including the span loss along with the distance in the single fiber span for the compensation ratios of one and five. Hereafter, the SC-DCF with the compensation ratio of one and five is referred to as SC-DCF (A) and (B), respectively. A higher nonlinearity was induced at the first segment of the span using SC-DCF (B), because a higher launch power is necessary to keep the same level of optical SNR by compensating for a larger span loss. In contrast, the induced nonlinearity for the span using SC-DCF (B) is relatively small at the second segment, and the induced nonlinearity at the end of the span is smaller than that of SC-DCF (A).

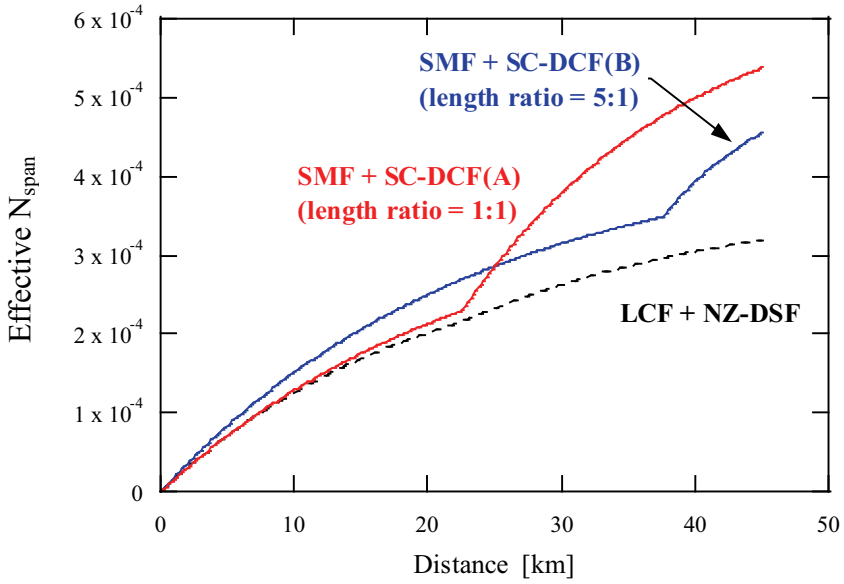

Fig. 3-6 Induced effective nonlinearities along with distance of two kinds of SMF-based span configurations.

3-3 Numerical simulations of 10 Gbit/s-based WDM transmission systems

In this section, the analytical predictions described in the previous sections are validated by numerical simulations. Through the simulations of 320 Gbit/s WDM transmissions over transoceanic distances, the performance of newly proposed dispersion management schemes using SMF-based spans are studied by comparing with NZ-DSF-based one.

3-3.1 NZ-DSF-based system

The transmission performance in the NZ-DSF-based system shown in Ref. [1] was limited by the interactions between the largely accumulated dispersion and nonlinear

effects. In the system where the channel spacing of 16-WDM signals and average dispersion slope were 0.7 nm and 0.08 ps/nm^2/km, respectively, the accumulated dispersion at the edge channels amounts to about 5,000 ps/nm. This value is considered to be the threshold of the acceptable accumulated dispersion in the NZ-DSF-based WDM systems using a channel bit rate of 10 Gbit/s. According to the considerations, the channel spacing was determined so as the accumulated dispersion of the edge channels to be less than 5,000 ps/nm in the simulations. Hence, the channel spacing was set to 0.5 nm for the transoceanic transmissions over 7,000 km. The repeater spacing was set to 40 km, which is considered to be the minimum repeater spacing in practical systems. In order to obtain a Q-factor of higher than 15.6 dB in 32 x 10 Gbit/s transmission systems, it is obvious that the repeater spacing of 50 km, which is used in the 16 x 10 Gbit/s transmission, should be shortened to alleviate fiber nonlinearities furthermore. The reduction of the repeater spacing from 50 km to 40 km is practically equivalent to a 1.2-dB improvement of the nonlinear tolerance as explained in Section 3-3.1; the amplifier gain G and the number of amplifiers N_{amp} in Eq. (2.14) decrease by 2.0 dB and -0.8 dB, respectively. This makes the repeater output power decrease by 2.0 dB, while the number of the repeater increases by 0.8 dB. The system parameters used in the simulations are listed in Table 3-4. Chirped RZ pulse was used as the initial pulse because it is tolerable against fiber nonlinearities [8], [9]. The full width at half maximum (FWHM) of the RZ signal was set to 40 ps, which corresponds to the duty ratio of 40 %. The noise figure of EDFAs was assumed to 4.0 dB

Table 3-4 System parameters in numerical simulations.

	NZ-DSF-based map		SMF-based map
Bit rate / channel [Gbit/s]	10.7		
Channel number	32		
Transmission distance [km]	6,250	7,350	7,000
Input pulse	Chirped RZ (FWHM = 40 [ps])		
Channel spacing [nm]	0.6	0.5	0.5
Noise figure of EDFAs [dB]	4.0		
Repeater spacing [km]	40		45

In the numerical studies, the transmission performance with a channel spacing of 0.6 nm was also investigated. Figure 3-7 shows the simulation result of the 32 x 10.7 Gbit/s over 6,250 km transmission in the NZ-DSF based system with a channel spacing of 0.6 nm. A fluctuation of Q-factor between adjacent channels was due to the inherent uncertainty of numerical simulations using a practical limit of the word length, and the dotted line was indicated supplementally to clarify the transmission characteristics. The figure shows that the performance of the channels near the system zero-dispersion wavelength (λ_0) which was located between channel 16 and 17 were sufficiently good, while ones located at far from λ_0 were on the border of error-free transmission (bit error ratio < 10^{-9}, Q > 15.6 dB). The interactions between nonlinear effects and largely accumulated dispersion severely affected the transmission performance in the edge channel region.

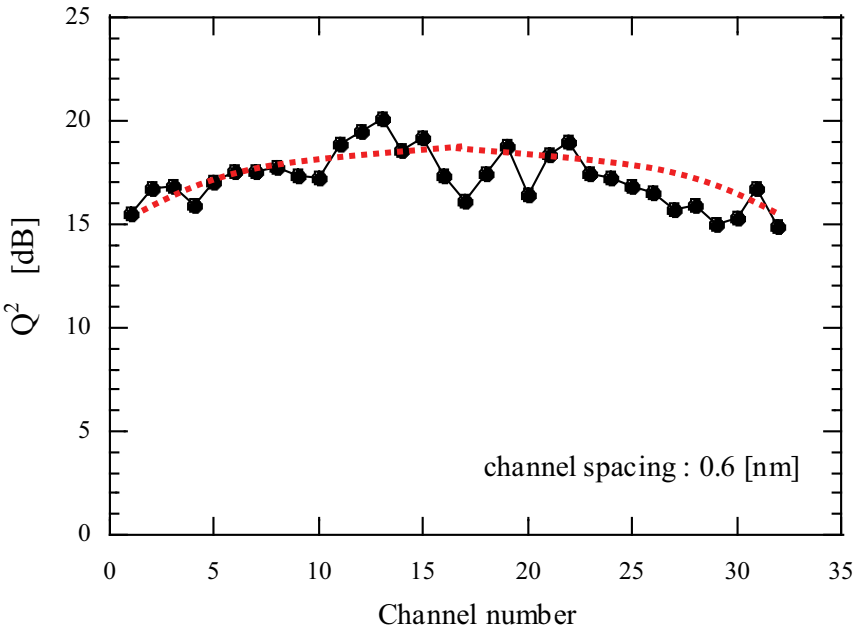

Fig. 3-7 Transmission performance of 10.7 Gbit/s x 32 WDM simulation after 6,250 km in NZ-DSF-based system: Q-factor against channel number.

This tendency increases with distance due to the accumulation of nonlinear effects and dispersion, and further extension of transmission distance cannot be expected in the system with a channel spacing of 0.6 nm. Hence, a channel spacing of 0.5 nm was used for the performance evaluation over 7,350 km. Figure 3-8 shows the Q-factor of all the channels after 7,350 km transmission. The transmission performance of the edge channels was severely degraded to a Q-factor of less than 15.6 dB. From these results, it was found that the performance of the NZ-DSF-based systems was limited by the largely accumulated dispersion. The acceptable accumulated dispersion was approximately estimated to less than 5, 000 ps/nm for the transoceanic distances in 10 Gbit/s-based WDM systems.

For further transmissible distance extension and capacity expansion, other advanced span configurations are necessary to reduce the dispersion slope and to suppress the interactions between the fiber nonlinearities and largely accumulated dispersion.

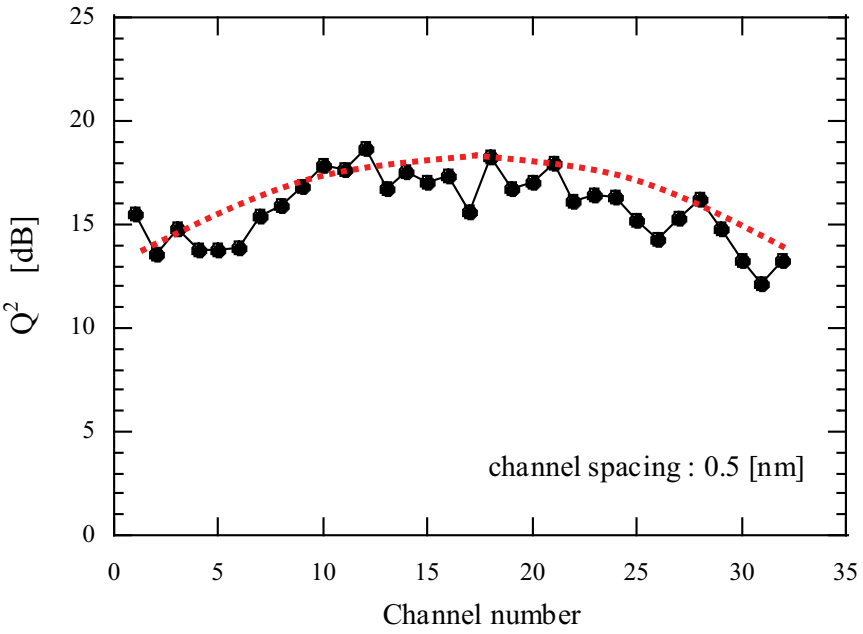

Fig. 3-8 Transmission performance of 10.7 Gbit/s x 32 WDM simulation after 7,350 km in NZ-DSF-based system: Q-factor against channel number.

3-3.2 SMF-based system

In order to confirm the analytical prediction on the optimal configuration of SMF-based transmission span as shown in Fig. 3-5, the transmission performances were numerically evaluated for the SMF/SC-DCF length ratios of one, three, five and seven. The parameters used in the simulations are listed in Tables 3-2 and 3-3.

Figure 3-9 shows the obtained average Q-factor of 32 x 10 Gbit/s channels after 7,000 km transmission. As predicted in Fig. 3-5, the highest Q-factor was obtained by adopting the SMF/SC-DCF length ratio of five. The performance advantage of the SMF/SC-DCF length ratio of five was about 1 dB in comparison with other length ratios.

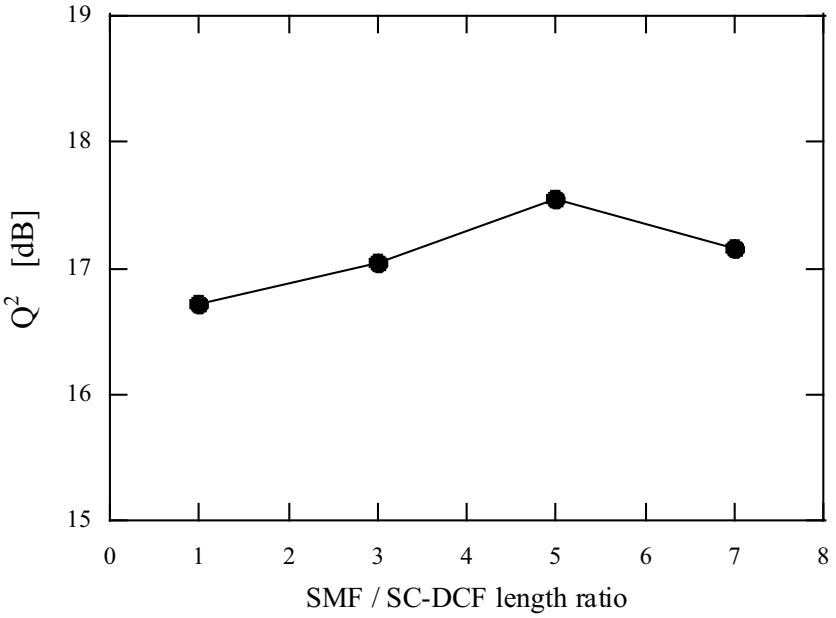

Fig.3-9 Transmission performance of 10.7 Gbit/s x 32 WDM simulation after 7,000 km in SMF-based systems: average Q-factors for the different SC-DCF compensation ratio.

Figure 3-10 shows the Q-factor of all the channels of the 32 x 10 Gbit/s after 7,000 km transmission in the SMF-based system where the SMF/SC-DCF length ratio was five. As shown in Fig.3-10, a flat transmission performance for all the channels was obtained owing to the use of the dispersion-flattened fiber spans, and Q-factors of higher than 15.6 dB were achieved even at the edge channels. A fluctuation of Q-factors observed in the figure was due to the inherent uncertainty of numerical simulations, and the performance indicated by the dotted line is expected in the SMF-based system. Since the performance of SMF-based systems is independent of the signal wavelength, further capacity expansion can be expected by extending the signal wavelength band for extra WDM channels. From these results, the dispersion-flattened SMF-based system is considered suitable for long-haul large-capacity WDM transmission systems.

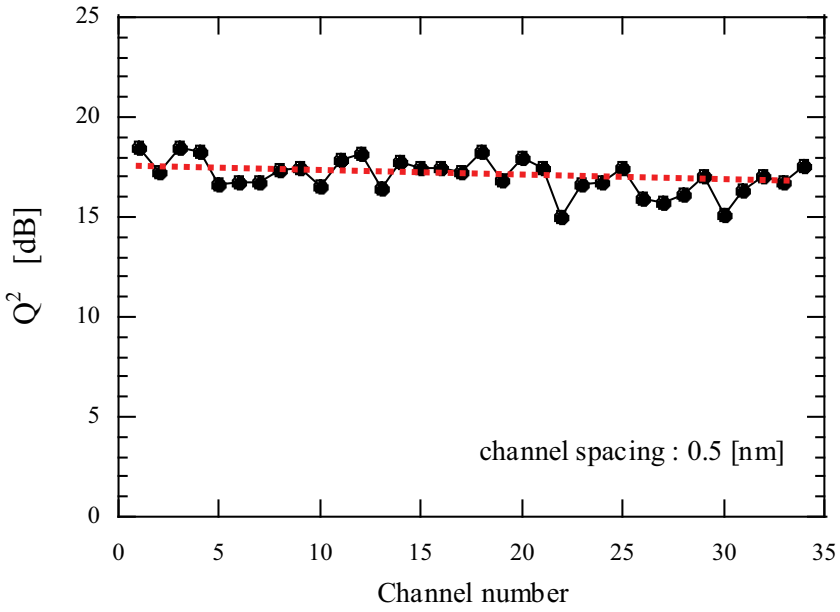

Fig.3-10 Transmission performance of 10.7 Gbit/s x 32 WDM simulation after 7,000 km in SMF-based system: Q-factor against channel number.

3-4 Experiments on 10 Gbit/s-based WDM transmission systems

In order to examine the numerical predictions in the previous section, 320 Gbit/s (32 x 10.7 Gbit/s) WDM transmission experiments are conducted by using two hybrid span configurations.

3-4.1 Experimental setup

Figure 3-11 shows a schematic diagram of the experimental setup. Thirty-two DFB-LDs were used as signal light sources, which were equally spaced by 0.6 nm in the wavelength range from 1542.5 nm to 1561.1 nm for the NZ-DSF-based system and

were equally spaced by 0.5 nm in the wavelength range from 1543.2 nm to 1558.7 nm for the SMF-based system. Each odd and even channels were combined separately with an arrayed waveguide grating (AWG) and then through two $LiNbO_3$ Mach-Zehnder external modulators for data coding and amplitude modulation. In addition, phase modulation was applied for each channel to generate chirped RZ signals. The pulse width was about 40 ps. After producing two sets of pre-chirped 10.7 Gbit/s, 2^{23}-1 RZ signals, they were combined using a polarizing beam splitter and were launched into a transmission line in orthogonal states of polarization with each other [10], [11].

In the transmission experiment of the NZ-DSF-based system as shown in Fig. 3-11 (a), a 402 km-long recirculating loop consisted of ten 40 km-long spans of the transmission fiber and eleven 980 nm-pumped EDFAs. The transmission fiber in the spans consisted of LCF/low dispersion-slope NZ-DSF hybrid fiber with a dispersion of –2 ps/nm/km and standard SMF with a dispersion of +18 ps/nm/km. The ratio of the hybrid fiber span and the SMF span is 9:1 so that the accumulated dispersion around the center wavelength of the WDM signal band periodically returns to zero. In this experiment, the system zero-dispersion wavelength λ_0 was set to 1552 nm. The SMF span was placed in the middle of the recirculating loop. The 980 nm-pumped single-stage EDFAs had an average output power of +11 dBm and a noise figure of 4.3 dB. To obtain 18.6 nm-wide transmission bandwidth, two different long-period fiber grating gain equalizers in each EDFA and a Mach-Zehnder filter with an FSR of 40 nm were employed in the loop. The final EDFA was used to compensate for the excess losses of the Mach-Zehnder filter gain equalizer and other optical components in Fig. 3-11.

In the transmission experiment of the SMF-based system as shown in Fig. 3-11 (b), a 280 km-long recirculating loop consisted of six 47 km-long spans of the transmission fiber and seven 980 nm-pumped EDFAs. Two kinds of fibers were employed to configure all the fiber spans. The first segment following after EDFAs is a standard SMF, and the second segment is a SC-DCF which has a negative dispersion and negative dispersion slope to form dispersion-flattened transmission spans. To compensate for the residual dispersion and dispersion slope of the loop, a SC-DCF with –400 ps/nm/km was inserted at the beginning of the loop. The average dispersion

slope of the recirculating loop was only 0.005 ps/nm^2/km and the average dispersion at 1550 nm was 0.27 ps/nm/km. The loss of the transmission spans including splicing loss was 11.3 dB on average. The EDFAs had an average output power of 11 dBm.

In the receiver, the desired channel was selected by double-pass style optical filters, and the transmission performance was evaluated. Dispersion compensation in the terminals was used to compensate for the residual accumulated dispersion.

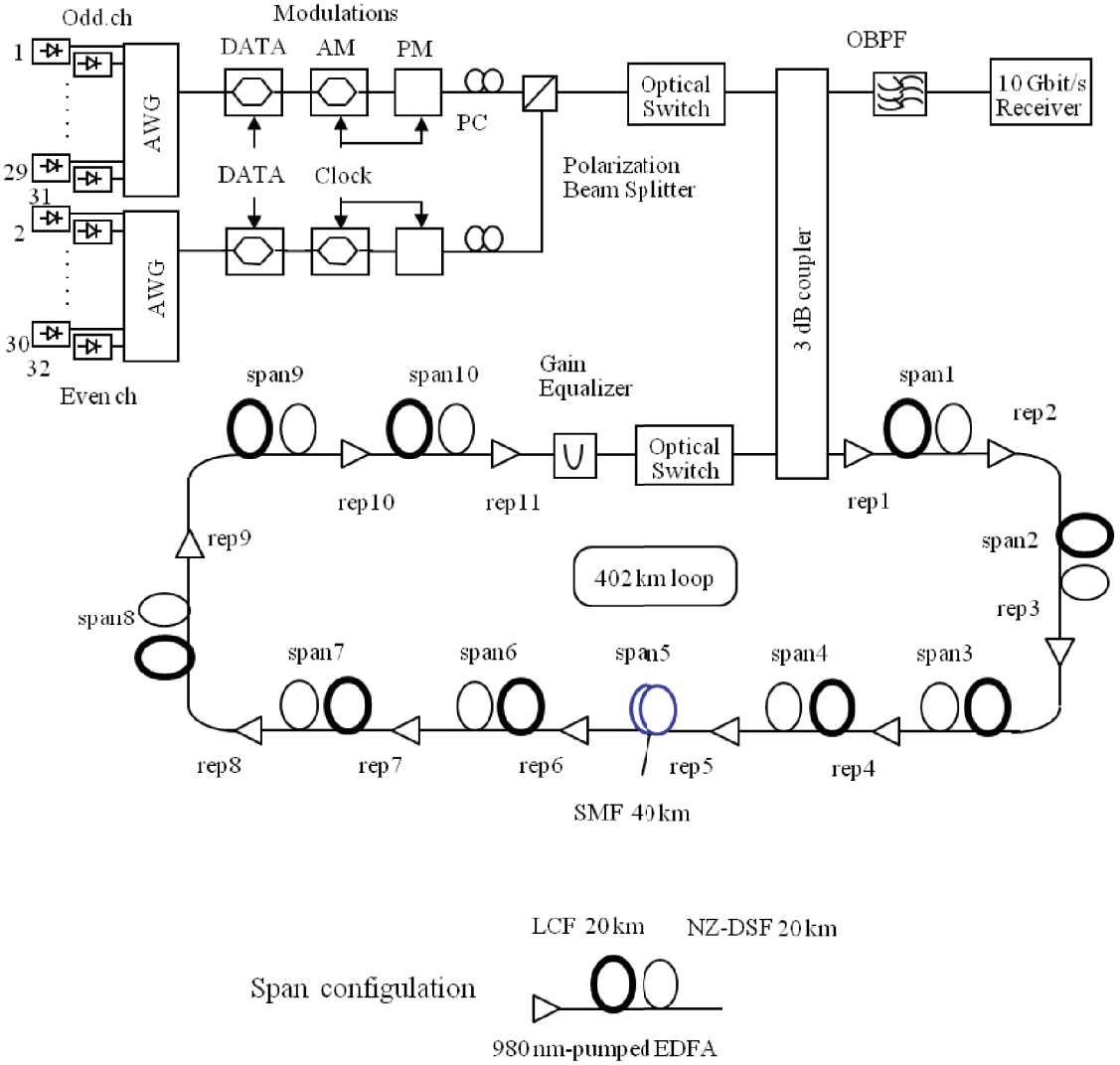

(a) NZ-DSF-based system

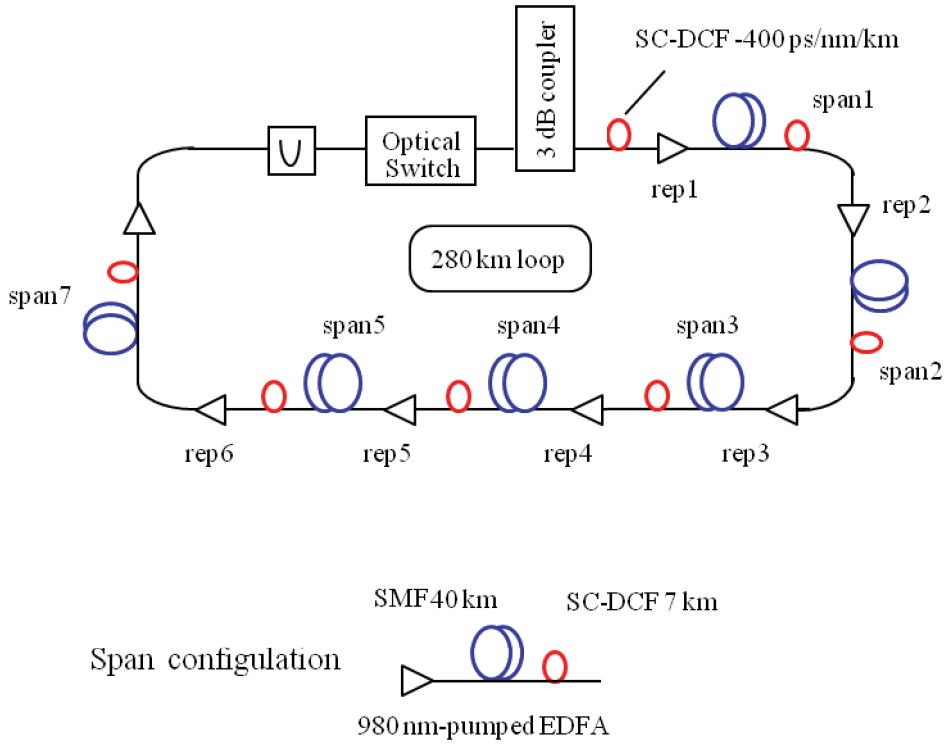

(b) SMF-based system

Fig. 3-11 Experimental setup of 320 Gbit/s (32 x 10.7 Gbit/s) WDM transmissions.

3-4.2 Results and discussion

Figure 3-12 shows the result of the loop experiment in the NZ-DSF-based system after 6,054 km transmission for the repeater output power of +11 dBm. The average Q-factor was 16.2 dB, and the worst Q-factor was 15.5 dB for channels 2 and 28. As was predicted in the simulations, error-free performances were achieved for all the WDM channels at the transmission distance of up to 6,000 km. However, the performance degradation of the edge channels located at far from the zero-dispersion wavelength was observed because of the largely accumulated dispersion.

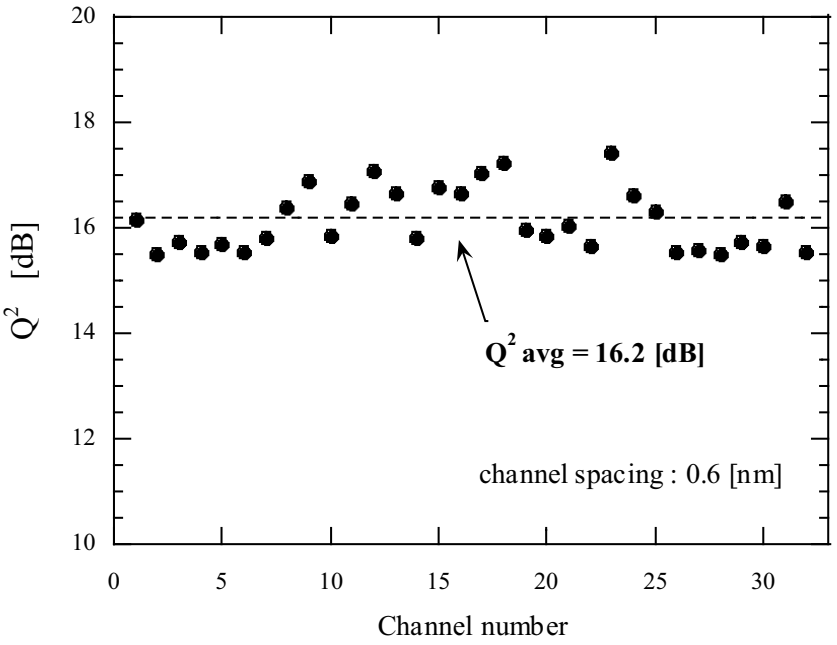

Fig. 3-12 Transmission performance of 10.7 Gbit/s x 32 WDM experiment after 6,054 km in NZ-DSF-based system: Q-factor against channel number.

As for the SMF-based transmission system, the Q-factors of 32-WDM signals are shown in Fig. 3-13. A Q-factor of higher than 15.6 dB was obtained for all the channels after 7,280 km transmission. The average Q-factor was 15.9 dB, and the worst Q-factor was 15.6 dB for channels 1, 10, and 29. A flat transmission performance over the 16-nm wavelength range was achieved using the dispersion-flattened fiber spans, as the numerical simulations were predicted.

In this experiment, the successful large-capacity transmission over transoceanic distances was attributed to the use of the dispersion-flattened transmission spans with high local dispersion.

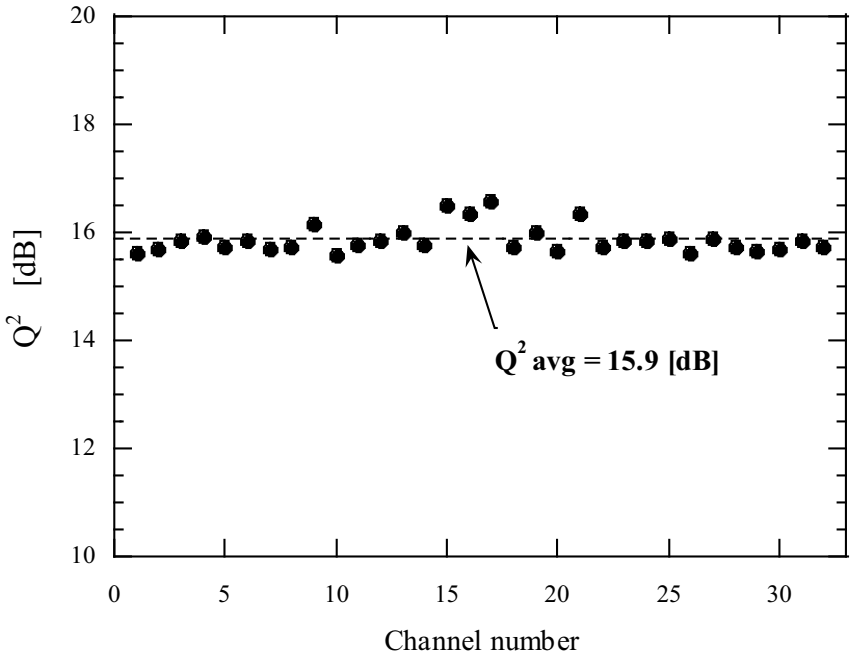

Fig. 3-13 Transmission performance of 10.7 Gbit/s x 32 WDM experiment after 7,280 km in SMF-based system: Q-factor against channel number.

The optical spectrum after 7,280 km transmission is shown in Fig. 3-14. No severe degradation and no significant difference among channels even after long distance transmissions were observed owing to the use of the gain equalization scheme. A pre-emphasis at the transmitter was also applied to both edge channels to precisely equalize the received optical SNR after transmission.

Figures 3-15 and 3-16 show optical eye diagrams before transmission and after 7,280 km transmission for channels 2, 17, and 31, respectively. Significant waveform distortion was not observed after transmission, except random dots which were trigger-related noises in the oscilloscope and were specific to the loop experiment.

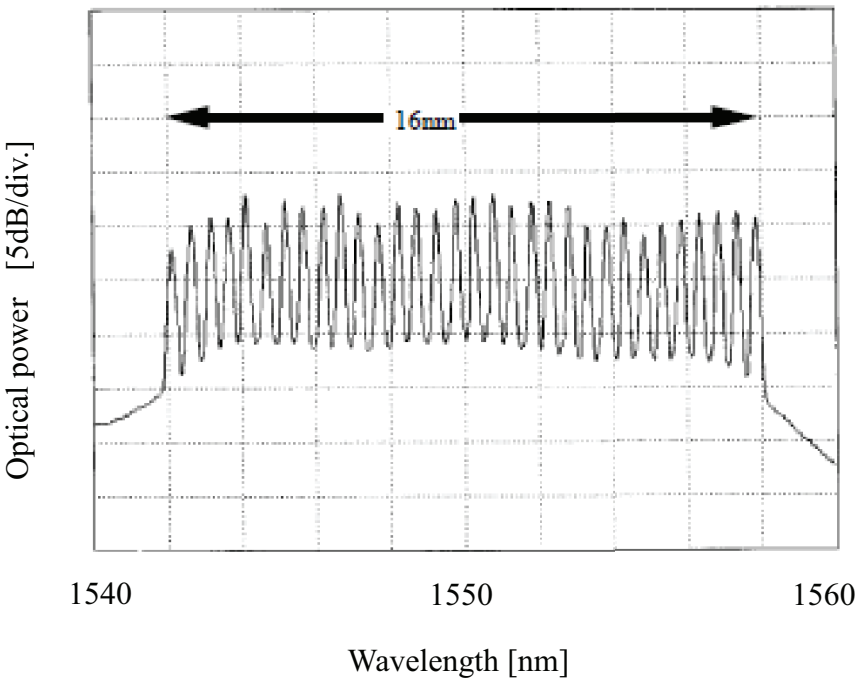

Fig. 3-14 Optical spectrum after 7,280 km transmission.

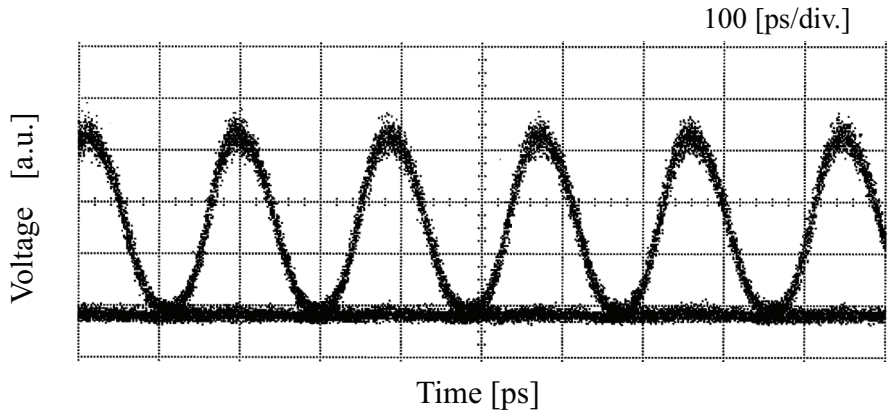

Fig. 3-15 Optical eye diagram before transmission.

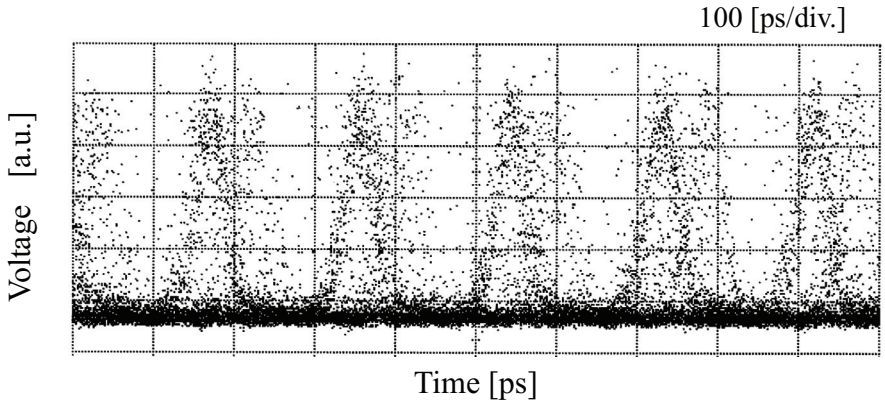

(a) channel 2

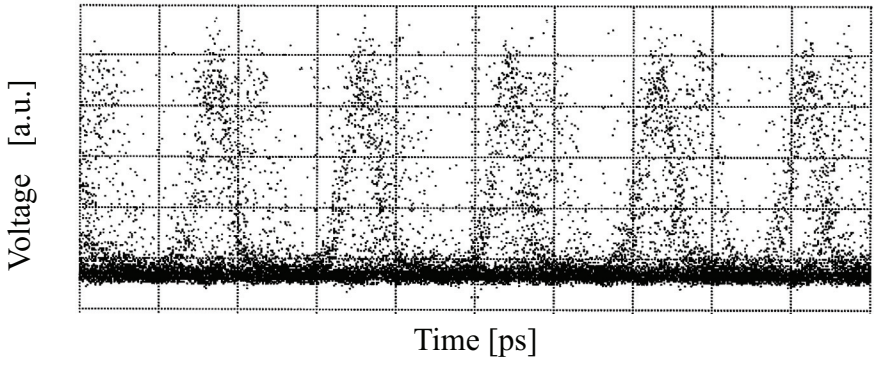

(b) channel 17

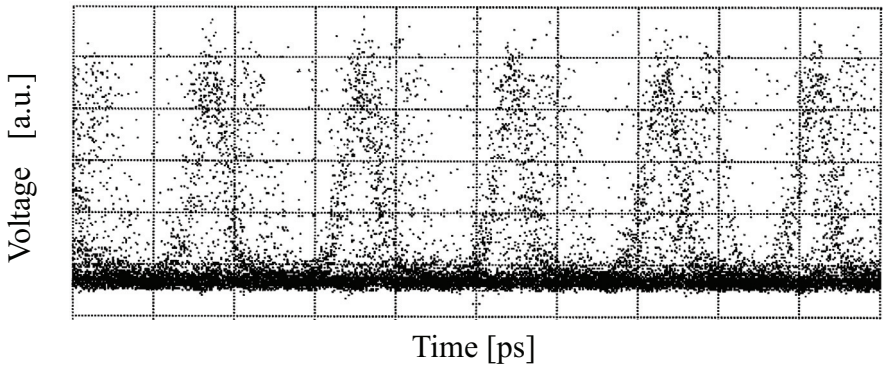

(c) channel 31

Fig. 3-16 Optical eye diagrams after 7,280 km transmission.

As predicted in the previous sections, the dispersion slope has a great impact on long-haul transmission performances, and therefore the dispersion-flattened transmission span is required for further distance extension and capacity expansion. The NZ-DSF-based system has low nonlinear properties, and the transmission capacity can be expanded in the region where the chromatic dispersion does not accumulate too much. For instance, a 500 Gbit/s (50 x 10.7Gbit/s) over 4,036 km transmission was reported with a channel spacing of 0.4 nm, in which the WDM signal wavelength band was 20 nm [11]. For long-haul WDM transmission systems targeting one-terabit capacity, however, the NZ-DSF-based span configuration is not applicable because there is a restriction in accumulated dispersion which is proportional to the system distance and the WDM signal wavelength band. The SMF-based one is a promising solution since the dispersion-flattened fiber span resolves the wavelength dependency of the transmission performance. The system accumulated dispersion is no longer a constraint factor in SMF-based transmission systems, and the capacity can be expanded by increasing the WDM channel count as far as the amplifier bandwidth of cascaded EDFAs covers the signal bandwidth.

3-5 Dispersion-flattened fiber-based WDM transmission system

The straightforward way to flatten the dispersion characteristics of the transmission line is to use a dispersion-flattened fiber [12]. In this section, the potential of the dispersion-flattened fiber is studied through soliton-based WDM transmission.

Soliton-based WDM transmission systems are considered to be a candidate for future high-capacity transoceanic systems since soliton utilizes a principal nonlinear effect of the self-phase modulation positively to form its pulse shape, which contributes to the channel bit rate increase even in nonlinear dispersive media. 20 Gbit/-based 160 Gbit/s soliton-WDM long distance transmissions have been reported [13], [14]. In Ref. [13], the different accumulated dispersion for each channel, which is due to the dispersion slope of the fibers, was compensated for individually by the dispersion compensators inserted in every six spans of the transmission line. The dispersion

compensators consisted of a WDM filter for demultiplexing each WDM channels, DCFs individually optimized for the channels, and a WDM filter for multiplexing the channels again. The results indicate that the dispersion-flattened transmission line is indispensable for soliton WDM transmissions. From this perspective, the transmission line using dispersion-flattened fibers (DFFs) is considered as a more practical approach.

Figure 3-17 show a span configuration using a DFF. The transmission span simply consisted of a single transmission fiber.

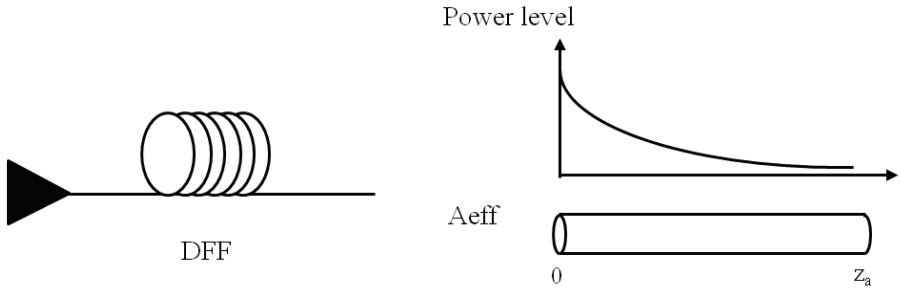

Fig. 3-17 Span configuration using DFF.

The transmission performance in a DFF-based WDM system is experimentally investigated. The channel spacing reported in 20 Gbit/s-based WDM long-distance transmissions was wider than 1.5 nm [13], [14]. In order to increase the aggregate capacity with a finite transmission bandwidth, however, a narrower channel spacing is required. The possibility to reduce the channel spacing to narrower than 1 nm in 20 Gbit/s-based soliton-WDM systems is also investigated, and a 400 Gbit/s (20 x 20 Gbit/s) transmission over 2,000 km with a channel spacing of 0.8 nm is demonstrated using DFFs with pre- and periodic dispersion compensation.

3-5.1 Single-channel transmission experiment

A periodic dispersion compensation scheme in dispersion-managed soliton systems is an effective way to resolve a soliton-inherent constraint of Gordon-Haus timing jitter [15]. It can prevent the generation of the jitter by compensating for the accumulated dispersion periodically to lower the system dispersion in single-channel transmissions.

The transmission performance of WDM systems is also affected by the inter-channel crosstalk caused by FWM and XPM, such as the collision-induced timing jitter [16]. To mitigate such nonlinear effects even in periodically dispersion compensated systems, a higher system dispersion is preferable. In addition, it contributes to increase the packing density of WDM channels by using a small channel spacing, because it makes the signal spectrum to be narrow and avoids the crosstalk among adjacent channels. Figure 3-18 illustrates the relationship between transmissible distance and signal spectral bandwidth against system average dispersion.

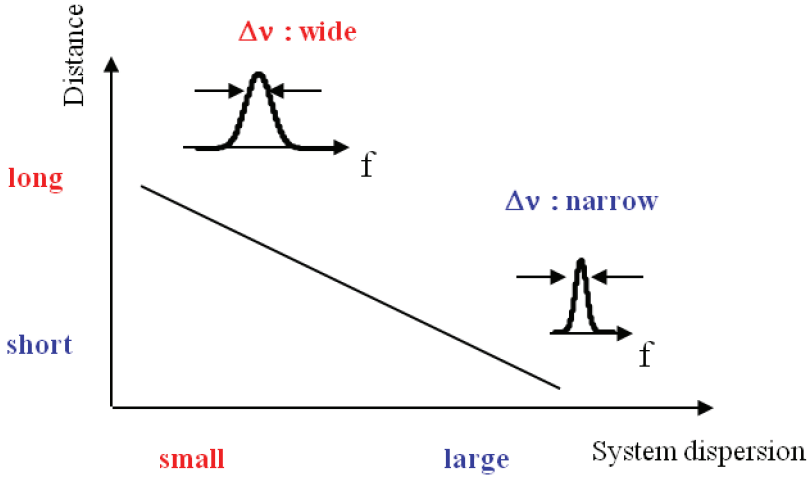

Fig. 3-18 Relationship between transmissible distance and spectral bandwidth against system dispersion.

In the systems using a small system dispersion, the signal spectrum would not be narrow enough to be applicable to a dense WDM transmission, whereas the transmissible distance can be extended. In contrast, a large system dispersion contributes to narrow the signal spectral bandwidth, while the transmissible distance would be restricted.

Firstly, the impact of system dispersion on signal spectral bandwidth and transmissible distance was investigated in a periodically dispersion-compensated soliton-based RZ transmission system by conducting a single-channel transmission experiment. A 215 km-long recirculating loop consisting of six spans of conventional DSF and two spools of DCF was used for the evaluation.

Figure 3-19 shows the transmission distance for a BER of 10^{-9} (depicted as closed circles) and the signal spectral bandwidth at the corresponding distances (depicted as open circles) as a function of system dispersion.

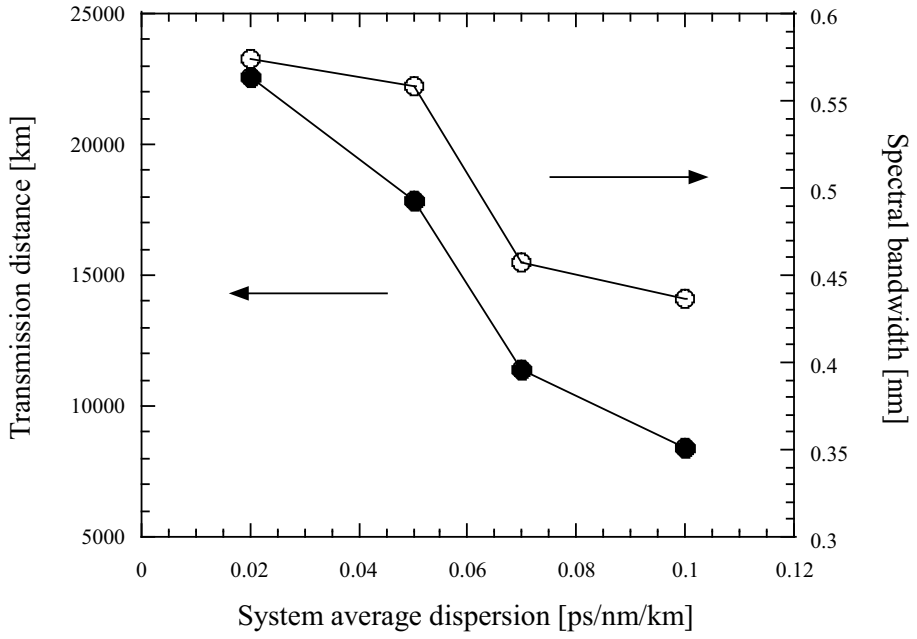

Fig. 3-19 Transmission distance and signal spectral bandwidth against system dispersion in a single-channel soliton transmission experiment.

In the case of a system dispersion of 0.02 ps/nm/km, the transmissible distance was 23,000 km while a large signal spectral spreading was observed. As is shown in Fig. 3-19, there is a trade-off between the transmissible distance and the signal spectral bandwidth. It is also found that the signal spectrum was being narrowed drastically with the system dispersion increased from 0.05 to 0.07 ps/nm/km. It means that the nonlinear effects causing the broadening of the signal spectrum can be suppressed by using a high system dispersion of more than 0.05 ps/nm/km. In considering the spectral bandwidth efficiency and the target transmission distance of longer than 10,000 km with a system margin for WDM transmission impairments, the optimal system dispersion is considered to be around 0.06 ps/nm/km.

The largely accumulated dispersion associated with increasing the system dispersion could cause not only Gordon-Haus timing jitter but also the collision-induced timing jitter for WDM transmissions [15], [16]. To reduce these effects, a pre-dispersion compensation scheme was employed, which does not induce waveform distortions.

From these perspectives, a twenty-channel 20 Gbit/s WDM transmission experiment was constructed in a periodically dispersion-compensated transmission line using the DFFs with a system dispersion of 0.06 ps/nm/km.

3-5.2 WDM transmission experiment

Figure 3-20 shows a schematic diagram of the experimental setup. Four transmitters were used as a 400 Gbit/s transmitter. The wavelengths of twenty channels ranging from 1542 nm to 1557 nm were equally spaced by 0.8 nm. Each transmitter consists of two or three EA-modulator as soliton pulse generators with different wavelengths. Optical soliton data stream with a speed of 20 Gbit/s was produced by using two $LiNbO_3$ intensity modulators operated at 10 Gbit/s with a 2^{11}-1 pseudo-random binary sequence and was optically time-division-multiplexed. In addition, each 20 Gbit/s signal was phase-modulated at 20 GHz by a $LiNbO_3$ phase modulator to improve the transmission performance [17], [18]. After combining twenty-channel 20 Gbit/s signals so as the adjacent channels to be orthogonally polarized, a polarization

scrambler was used to suppress the polarization-hole burning (PHB) of the 980 nm-pumped EDFA repeaters [19], [20].

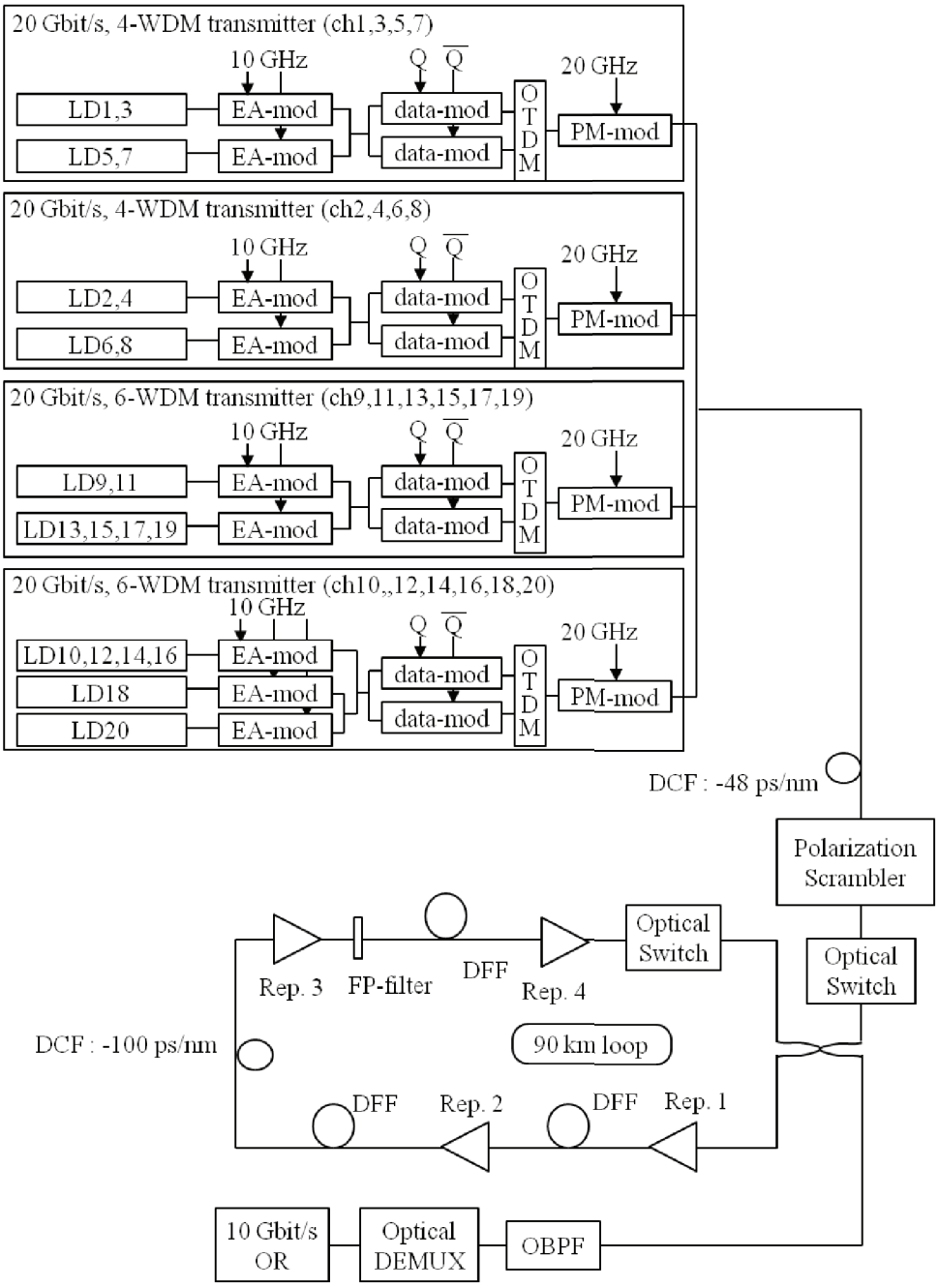

Fig. 3-20 Experimental setup for a twenty-channel 20 Gbit/s WDM transmission.

The transmission line comprised three spans of a 30 km-long DFF and a spool of DCF. The loss of the DFF spans including the splicing loss was about 9 dB on average. The average dispersion slope of the DFF was -0.0002 ps/nm^2/km, and the average chromatic dispersion of the DFF at 1555 nm was 1.0 ps/nm/km. The accumulated chromatic dispersion of the loop was compensated for by a DCF with -100 ps/nm to set the system dispersion of the loop to 0.06 ps/nm/km [17]. The dispersion map in the loop was illustrated in Fig.3-21. The average repeater output power was about 9 dBm. As a frequency guiding filter, a Fabry-Perot-etalon filter with a free spectral range of 0.8 nm was placed in the loop to stabilize the transmission performance.

In the receiver, the desired channel was selected by optical bandpass filters, and the transmitted 20 Gbit/s signals were optically time-division-demultiplexed to a 10 Gbit/s data stream with an optical gate using a sinusoidally-driven EA modulator. Then, the BER for the demultiplexed 10 Gbit/s signals was measured.

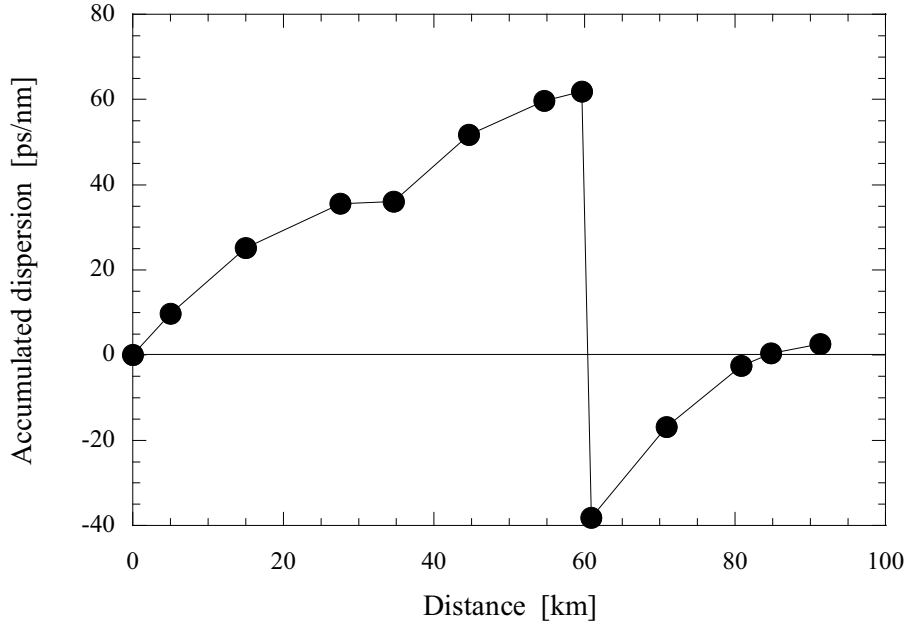

Fig. 3-21 Dispersion map of the recirculating loop.

3-5.3 Results and discussion

Figure 3-22 shows the typical waveforms after 2,000 km transmission for channel 2, 11, and 18. Significant waveform distortion and timing jitter were not observed after transmission.

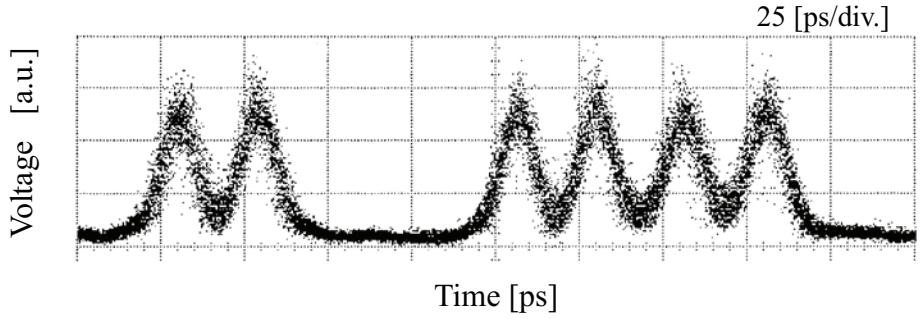

(a) channel 2

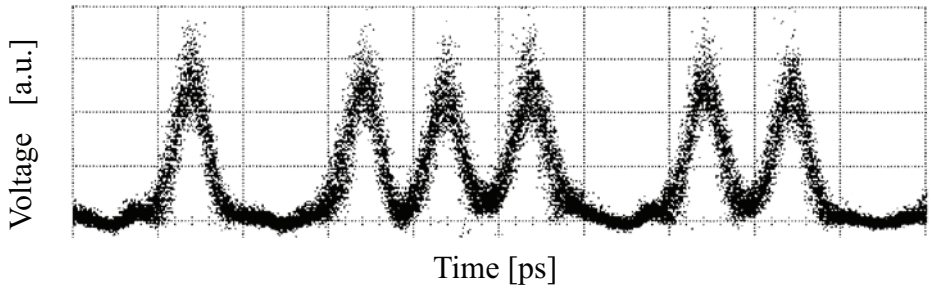

(b) channel 11

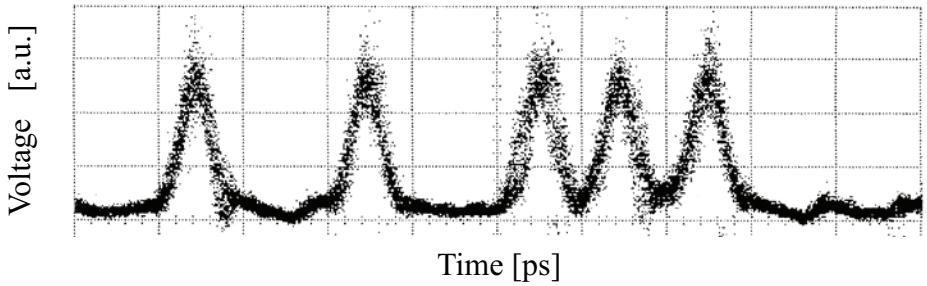

(c) channel 18

Fig. 3-22 Optical waveforms after 2,000 km transmission.

Figure 3-23 shows the optical spectrum before and after 2,000 km transmission. It was found that the spectrum after the transmission was broadening due to the nonlinear effects induced through the transmission.

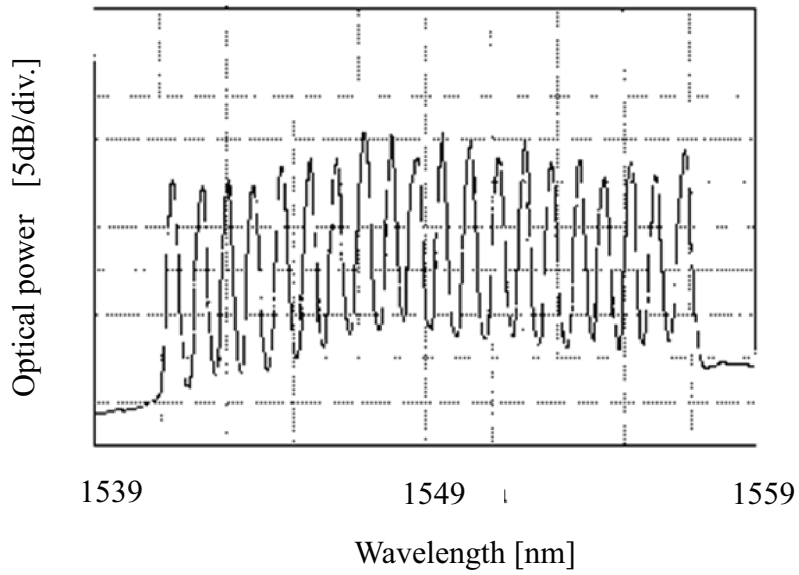

(a) before transmission

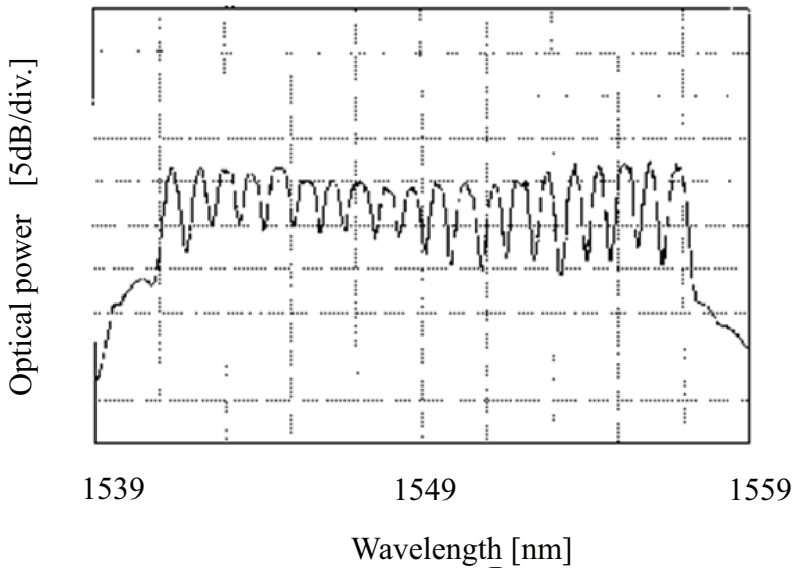

(b) after 2,000 km transmission

Fig. 3-23 Optical spectra of the twenty-channel 20 Gbit/s WDM signal.

Figure 3-24 shows BER performances of twenty channels measured as a function of transmission distance. A BER of less than 10^{-9} was obtained for all the channels after 2,000 km transmission.

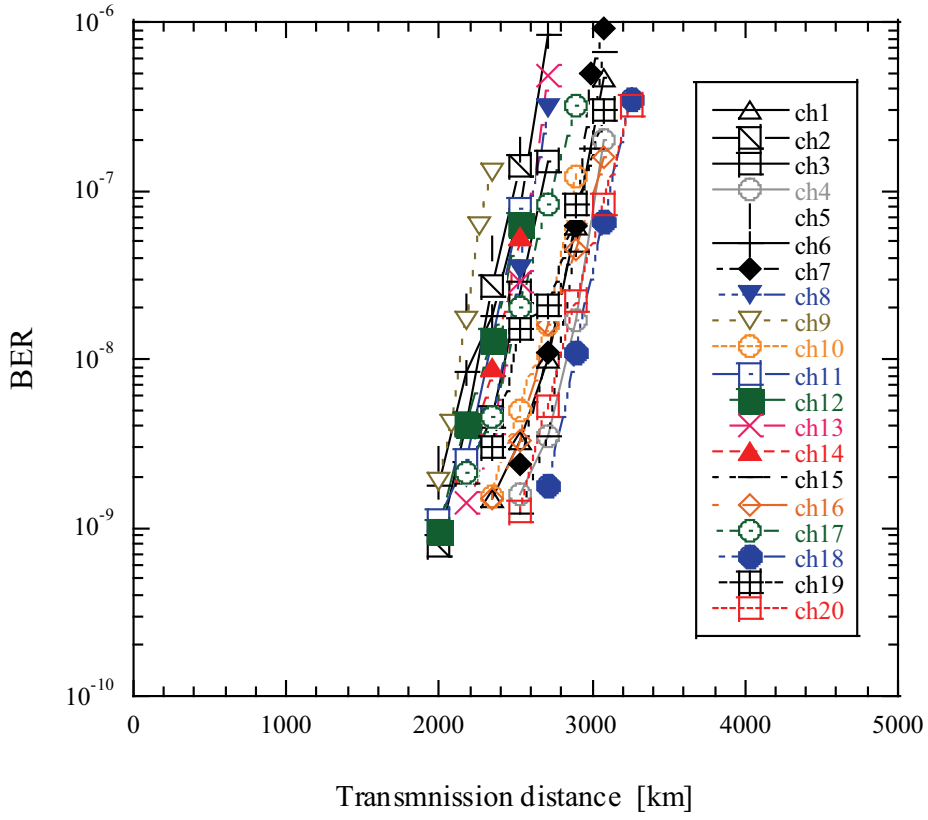

Fig. 3-24 BER performances the twenty 20 Gbit/s WDM channels as a function of transmission distance.

In this experiment, the transmission distance was mainly limited by the optical SNR due to the small signal launch power, the excess loss of the DFFs and the additional EDFA in the small loop. A small effective core area of around 35 μm^2 of the DFFs prevents increasing the signal launch power, and it inherently associates with the dispersion characteristics of the DFFs similarly to SC-DCFs. Further progress in transmission performance can be expected by enhancing the signal launch power with

refining the fiber parameters of the DFFs [22]. The expected improvement in DFF-based systems is estimated in Table 3-5. More than 7-dB SNR improvement is expected by using the DFFs with moderate values of effective core area and transmission loss.

Table 3-5 Expected improvement in DFF-based systems.

	this experiment	expected value	improvement
A_{eff}	30 ~ 35 μm^2	> 70 μm^2	3.7 ~ 3.0 dB
Transmission loss	0.30 dB/km	0.20 dB/km	3.0 dB
# of effective EDFAs	4/3	N/N = 1	1.2 dB

In addition to the improvement listed in Table 3-4, a higher dispersion of the DFFs is necessary to suppress nonlinear interactions. The WDM transmission performance in this experiment was considered to be restricted by inter-channel interactions between adjacent WDM channels. A large performance difference was observed between the single-channel transmission shown in Fig. 3-19 and the WDM transmission. The performance of the WDM transmission was severely degraded as the number of the WDM channel increases due to a high-nonlinear property of the DFFs. The inter-channel interactions can be suppressed by using higher-dispersion fibers, because the high dispersion contributes to the reduction of interacting time when different WDM channels overlap. The trade-offs of fiber parameters such as dispersion, dispersion slope, and effective core area, which are associated with the waveguide design of the fiber, is the key issue for the further improvement of transmission performances in the DFF-based systems.

3-6 Conclusion

Through the analytical, numerical, and experimental studies on the transmission performance of two kinds of fiber span configurations, it has been shown that WDM transmission systems over transoceanic distances require not only low fiber nonlinearity but also flat dispersion characteristics. The wavelength dependency of the transmission performance observed in the LCF/NZ-DSF-based system was resolved in the SMF-based system because of the flat dispersion characteristics of the SMF/SC-DCF span configuration. For a 320 Gbit/s (32 x 10.7 Gbit/s) system, error-free transmission distance has been extended up to 7,280 km with the use of the SMF/SC-DCF span configuration. Through these studies, it was confirmed that the dispersion-flattened SMF/SC-DCF-based system is a promising solution for long-haul high-speed WDM transmission systems targeting terabit capacity.

As for the DFF-based system, a 400 Gbit/s (20 x 20 Gbit/s) soliton-based WDM transmission over 2,000 km was demonstrated with a channel spacing of 0.8 nm using the DFFs. Meanwhile, the result revealed the drawbacks of the DFF-based system. The nonlinearities induced by the small effective core area degraded the transmission performance. The performance is expected to be improved by resolving the trade-offs between the dispersion and effective core area characteristics inherently associated with the DFFs.

References

[1] M. Suzuki, H. Kidorf, N. Edagawa, H. Taga, N. Takeda, K. Imai, I. Morita, S. Yamamoto, E. Shibano, T. Miyakawa, E. Nazuka, M. Ma, F. Kerfoot, R. Maybach, H. Adelmann, V. Arya, C. Chen, S. Evangelides, D. Gray, B. Pedersen, and A. Puc, "170 Gb/s transmission over 10,850 km using large core transmission fiber", OFC1998, PD17, 1998.

[2] N. S. Bergano, C. R. Davidson, M. Ma, A. Pilipetskii, S. G. Evangelides, H. D. Kidorf, J. M. Darcie, E. Golvochenko, K. Rottwitt, P. C. Corbett, R. Menges, M. A. Mills, B. Pedersen, D. Peckham, A. A. Abramov, and A. M. Vengsarkar, "320 Gb/s WDM transmission (64 x 5 Gb/s) over 7,200 km using large mode fiber spans and chirped return-to-zero signals", OFC1998, PD12, 1998.

[3] D. LeGuen, S. DelBurgo, M. L. Moulinard, D. Grot, M. Henry, F. Favre, and T. Georges, "Narrow band 1.02 Tbit/s (51 x 20 Gbit/s) soliton DWDM transmission over 1000km of standard fiber with 100 km amplifier spans", OFC1999, PD4, 1999.

[4] M. X. Ma, M. Nissov, H. Li, A. Mills, G. Yang, H. D. Kidorf, A. Srivastava, J. Sulhoff , C. Wolf, Y. Sun, and D. W. Peckham, "765 Gb/s over 2,000 km transmission using C- and L-band erbium doped fiber amplifiers", OFC1999, PD16, 1999.

[5] T. Matsuda, M. Murakami, and T. Imai, "340 Gbit/s (34 x 10 Gbit/s) WDM transmission over 8,514 km using broadband gain equalization technique for transoceanic systems", Electron. Lett., vol. 35, pp. 1090-1091, 1999.

[6] D. Marcuse, A. R. Chraplyvy, and R. W. Tkach, "Effect of fiber nonlinearity on long distance transmission", IEEE/OSA J. Lightwave Technol., vol. 9, pp. 121-128, 1991.

[7] Y. Akasaka, R. Sugizaki, S. Arai, Y. Suzuki, and T. Kamiya, "Dispersion flat compensation fiber for dispersion shifted fiber", ECOC1996, TuP.01, 1996.

[8] N. Henmi, T. Saito, and T. Ishida, "Prechirp technique as a linear dispersion compensation for ultrahigh-speed long-span intensity modulation directed detection optical communication systems", IEEE/OSA J. Lightwave Technol., vol.

12, pp. 1706-1719, 1994.

[9] N. S. Bergano, C. R. Davidson, M. A. Mills, P. C. Corbett, S. G. Evangelides, B. Pedersen, R. Menges, J. L. Zyskind, J. W. Sulhoff, A. K. Srivastava, C. Wolf, and J. Judkins, "Long-haul WDM transmission using optimum channel modulation: a 120 Gb/s (32 x 5 Gb/s) 9,300 km demonstration", OFC1997, PD16, 1997.

[10] K. Inoue, "Arrangement of orthogonal polarized signals for suppressing fiber four-wave mixing in optical multichannel transmission systems", IEEE Photon. Technol. Lett., vol. 6, pp. 560-563, 1991.

[11] K. Imai, T. Tsuritani, N. Takeda, K. Tanaka, N. Edagawa, and M. Suzuki, "500 Gbit/s (50 x 10 Gbit/s) WDM transmission over 4,000 km using broadband EDFAs and low dispersion slope fiber", OFC1999, PD5, 1999.

[12] N. Edagawa, I. Morita, M. Suzuki, S. Yamamoto, K. Tanaka, and S. Akiba, "Long distance soliton WDM transmission using a dispersion-flattened fiber", OFC1997, PD19, 1997.

[13] M. Suzuki, I. Morita, K. Tanaka, N. Edagawa, S. Yamamoto, H. Taga, and S. Akiba, "160 Gbit/s (8 x 20 Gbit/s) soliton WDM transmission experiments using dispersion f1attened fibre and periodic dispersion compensation", Electron. Lett., vol. 34, pp. 475-476, 1998.

[14] M. Nakazawa, K. Suzuki, H. Kubota, A. Sahara, and E. Yamada, "160 Gbit/s WDM (20 Gbit/s x 8 channels) soliton transmission over 10,000 km using inline synchronous modulation and optical filtering", OAA1998, PD10, 1998.

[15] J. P. Gordon and H. A. Haus, "Random walk of coherently amplified solitons in optical fiber communication", Opt. Lett., vol. 11, pp. 665-667, 1986.

[16] L. F. Mollenaur, J. P. Gordon, and M. N. Islam, "Soliton propagation in long fiber with periodically compensated loss", IEEE J. Quantum Electron., vol. 22, pp. 157-173, 1986.

[17] I. Morita, M. Suzuki, N. Edagawa, K. Tanaka, S. Yamamoto, and S. Akiba, "Performance improvement by the initial phase modulation in 20 Gbit/s soliton-based RZ transmission with periodic dispersion compensation", Electron. Lett., vol. 33, pp. 1021-1022, 1997.

[18] T. Georges and B. Charbonnier, "Reduction of the dispersive wave in periodically amplified links with initially chirped solitons", IEEE Photon. Technol. Lett., vol.

9, pp.127-129, 1997.

[19] P. Wysocki and V. Mazurczyk, “Polarization dependent gain in erbium-doped fiber amplifiers: computer model and approximate formulas”, IEEE/OSA J. Lightwave Technol., vol. 14, pp. 572-584, 1996.

[20] A. N. Pilipetskii, B. Bakhshi, M. Vaa, M. Nissov, and N. S. Bergano, “The interaction between fiber PMD and polarization hole burning in long-haul transmission systems”, OFC2005, OTuA2, 2005.

[21] M. Suzuki, I. Morita, N. Edagawa, S. Yamamoto, H. Taga, and S. Akiba, “Reduction of Gordon-Haus timing jitter by periodic dispersion compensation in soliton transmission ”, Electron. Lett., vol. 31, pp. 2027-2029, 1995.

[22] N. J. Smith, W. Forysiak, and N. J. Doran, “Reduced Gordon-Haus jitter due to enhanced power solitons in strongly dispersion managed systems ”, Electron. Lett., vol. 32, pp. 2085-2086, 1996.

Chapter 4

40 Gbit/s-based WDM unrepeatered transmission system using dispersion-managed transmission line and Raman amplification

4-1 Introduction

The transmission systems using a higher-channel bit rate of 40 Gbit/s have commercial advantages over 10 Gbit/s-based systems such as the increase in spectral efficiency and the significant reduction of WDM channel count in keeping the same capacity. From these practical viewpoints, telecom engineers have been making relentless efforts on the development of higher-channel bit rate transmission systems, and as the result, successful 40 Gbit/s-based transmission experiments for ultra long-distance unrepeatered system application have been reported [1]-[4].

In order to achieve such 40 Gbit/s-based long-distance unrepeatered transmissions, the problems associated with fiber nonlinearities must be overcome. It induces the degradation of transmission performances through SPM, XPM, and FWM effects [5]-[10]. In addition, the fiber nonlinearities prevent the pump light for Raman amplification from being launched into the transmission line with high power levels, which is indispensable for long-distance unrepeatered transmissions [11]. Another problem is the fact that 40 Gbit/s signals have much lower tolerance for the accumulated dispersion than 10 Gbit/s signals due to the small time-slot of 25 ps.

The longest unrepeatered transmission distance in 40 Gbit/s-based WDM signals was 250 km. It was achieved by using an 115 μm^2-A_{eff} fiber, Raman amplification, and a remote-EDFA with a separate transmission line dedicated for a high-power pump-light transmission to excite the remote-EDF [1]. In the demonstration, the input signal power was 158 mW, the pump power for Raman amplification was 1.4 W, and

the pump power for the remote-EDFA was 1.9 W. To extend the transmission distance, the signal launch power and pump power for the remote EDF must be increased, which requires significantly further suppression of the fiber nonlinearities in the transmission line. In addition, for enhancing the system practicality by reducing the complexities, the fiber for the pump-light transmission should be eliminated.

In this chapter, firstly, key issues of system design and remedies for the extension of transmission distance are presented. After describing a dispersion-managed transmission line configuration for Raman amplification, a 40 Gbit/s-based terabit -capacity unrepeatered transmission over 306 km has been demonstrated, for the first time, by using 175 μm^2-A_{eff} fibers placed at each end of the transmission line without using a dedicated fiber for the pump-light transmission.

4-2 Dispersion-managed WDM transmission systems

4-2.1 Key issues of system design

In unrepeatered transmission systems which include no active repeaters in the transmission line, the remedies to keep a sufficient optical SNR at the receiver are quite important to extend the transmissible distance. The straightforward way to increase optical SNR is to launch a higher power signal to the transmission line. The distributed amplification using stimulated Raman scattering (SRS) and remotely pumping EDF schemes are also effective to increase the optical SNR during the transmission [9]-[14]. SRS is a nonlinear process induced in optical fibers, and a small fraction of the optical wave launched from an end of the transmission line is converted to another wave called as Stokes wave with a wavelength upshifted by about 70 nm [15]. In this manner, the Raman scattering effect acts as distributed amplification of 1.55-μm signals by pumping optical beams with a wavelength of around 1.48 μm. The growth of the Stokes wave is described by

$$\frac{dI_S}{dz} = g_R I_P I_S , \tag{4.1}$$

where I_S is the Stokes intensity, I_p is the pump intensity, and g_R is the Raman-gain coefficient [13]. Since the intensity is defined as a power per unit effective core area P/A_{eff}, the amplification gain is proportional and inversely proportional to the pump power and effective core area of the fiber, respectively.

All the remedies associated with the increase of optical SNR require a high input power to the optical fiber to attain a high optical SNR. The fiber nonlinearities, however, limit the signal launch power to the fiber. In particular, stimulated Brillouin scattering (SBS) generates a backward-propagating Stokes wave causing instabilities of the pump wave once the pump power reaches the Brillouin threshold [15]-[17]. The key for designing unrepeatered systems is to mitigate the nonlinear effects such as SPM, XPM, FWM, and SBS for a higher input power of the signal and pump waves, while utilizing the useful nonlinear effect of SRS for the amplification. One of the most promising solutions to overcome the problem is to use an ultra-large A_{eff} fiber. Newly developed fibers with an A_{eff} of more than 160 μm^2 (hereafter, this type of fibers is referred to as "effective-area enlarged single mode fiber: EE-SMF") are suitable for 40 Gbit/s-based transmissions owing to their inherent low-loss and low-PMD properties [18], [19].

Regarding another problem of a low dispersion tolerance of 40 Gbit/s signals, a possible solution is to use a transmission line which has a small accumulated dispersion and low nonlinear properties. It can be constructed by employing a hybrid line configuration of EE-SMFs and NZ-DSFs with a negative dispersion value. The suppression of the total amount of the accumulated dispersion is important for 40 Gbit/s-based long-distance transmissions to mitigate the intra-channel interactions between adjacent bit-slot pulses.

Unlike in the case of 10 Gbit/s-based repeatered systems, large core fibers of EE-SMFs must be placed at both edges of the transmission line to increase the threshold of SBS generation. The A_{eff}-enlarged property of EE-SMFs allows a higher launch power to the transmission line of both forward-propagating signal and backward-propagating pump light for Raman amplification, and as the results, a high

optical SNR can be obtained. In addition, it effectively contributes to the reduction of fiber nonlinearities by allocating a large-A_{eff} fiber in higher optical power portions. NZ-DSFs with a negative dispersion value work positively to reduce the accumulated dispersion in EE-SMFs.

From these perspectives, the hybrid transmission line configuration where a NZ-DSF is inserted in the middle of EE-SMFs as shown in Fig. 4-1 is considered to be advantageous to satisfy both a low nonlinear property and a small accumulated dispersion. Furthermore, the configuration is beneficial in terms of the SNR property, because it contributes to the reduction of ASE noise in Raman amplification [4]. This low-noise amplification feature is an essential factor for extending the transmissible distance in ultra long-haul unrepeatered transmission systems.

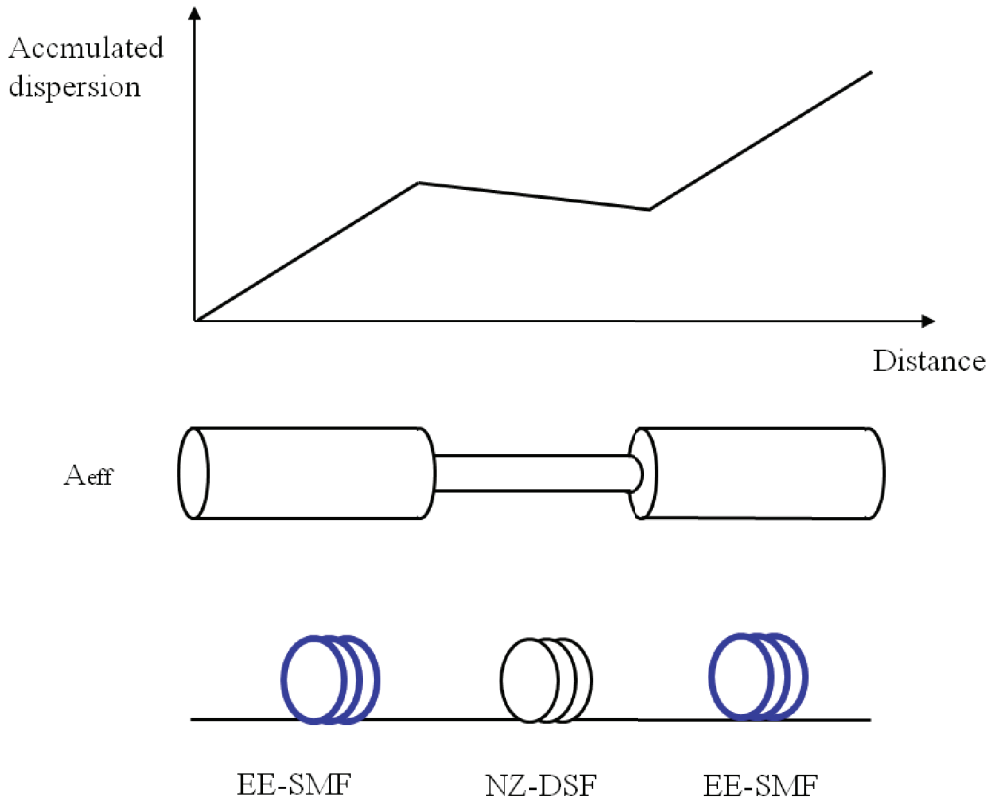

Fig. 4-1 Hybrid line configuration using EE-SMFs and NZ-DSF for ultra long-haul unrepeatered transmission systems.

Figure 4-2 shows a schematic diagram of the transmission line configuration using Raman amplification and remote EDFA. The transmission line consisted of a 98 km-long EE-SMF followed by a 110 km-long NZ-DSF, a remote EDF, and a 98 km-long EE-SMF. Two optical isolators were inserted in the transmission line to reject the propagation of the backward-scattering light. The key parameters of the EE-SMF and NZ-DSF are summarized in Table 4-1.

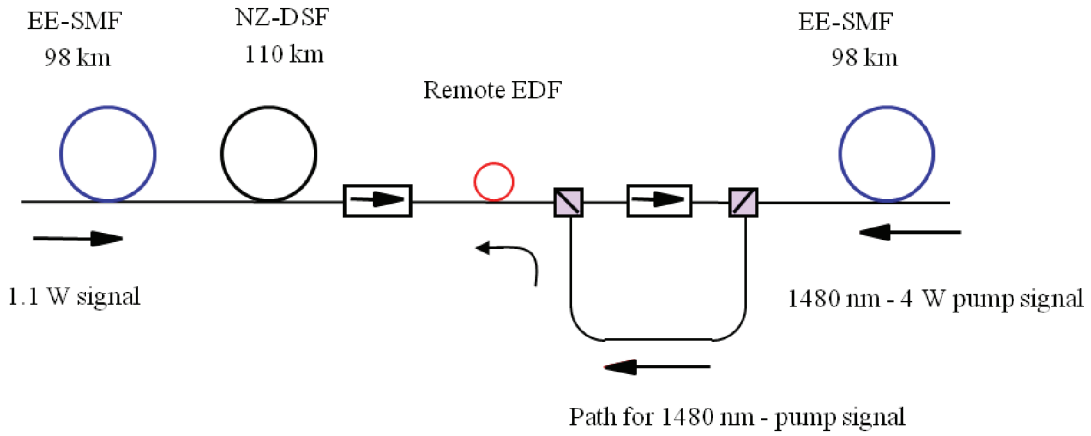

Fig. 4-2 Transmission line configuration for Raman amplification and remote EDFA.

Table 4-1 Key parameters of EE-SMF and NZ-DSF.

	EE-SMF	NZ-DSF
Dispersion@1550nm [ps/nm/km]	+22	-2
A_{eff} [μm^2]	175	55
Loss [dB/km]	0.18	0.20

This transmission line involves two key technological schemes: a hybrid fiber configuration to achieve a low nonlinear property and small accumulated dispersion and a remote EDFA to extend the transmissible distance without a dedicated fiber for pump-light transmission. From practical viewpoints, no separate fiber for pumping a remotely located EDF is strongly desired.

4-2.2 Hybrid transmission line configuration

In the hybrid transmission line configuration, the EE-SMFs and NZ-DSF mainly contribute to the reduction of fiber nonlinearities and accumulated dispersion, respectively. The ultra-large A_{eff} of 175 μm^2 of the EE-SMF used at the transmitter side allows to launch a high power signal to the transmission line without inducing nonlinear effects of SBS, SPM, and XPM. Similarly, the large A_{eff} of the EE-SMF at the receiver side allows to launch a high pump power stably for Raman amplification and remote EDFA and to avoid undesirable noise problems through the Raman amplification process.

The NZ-DSF with a negative dispersion value placed at the middle part of the transmission line enables to suppress the accumulation of dispersion. Figure 4-3 shows the dispersion map corresponding to the transmission line configuration in Fig. 4-2. The solid line indicates the accumulated dispersion of the hybrid configuration, and the dotted line indicates that of the homogeneous fiber configuration of the EE-SMF. By using the hybrid configuration, the accumulated dispersion after 306 km transmission is significantly reduced to less than two-thirds of a homogeneous fiber configuration since the accumulated dispersion of the hybrid and homogeneous configurations are 4,092 ps/nm and 6,732 ps/nm, respectively. The signal power in the NZ-DSF is considered to be too small to induce nonlinear effects, because the signal power decreases by about 18 dB at beginning of the NZ-DSF

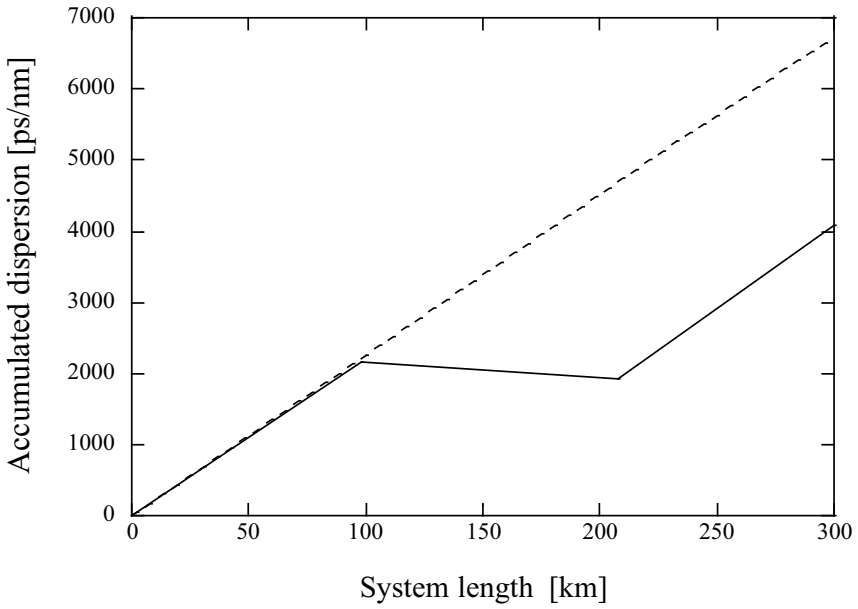

Fig. 4-3 Dispersion map of the hybrid transmission line configuration.

4-2.3 Remote EDF scheme

The location of a remote EDF to extend the transmissible distance effectively is an important system design issue, since it affects the overall optical SNR property at the receiver side. As the allocation of a remote EDF, a far site from the receiver is preferable to attain a high optical SNR, while a large amount of pump power from the receiver side is required to excite the remote EDF. In this situation, an ultra-low nonlinear fiber at the receiver side works effective for remote-EDF amplification as well as Raman amplification, because the maximum launch power of the pump light to the transmission line is restricted by SBS threshold.

The trade-off between the optical SNR and nonlinear impairments was experimentally evaluated to determine the location of the remote EDF. There were two candidates of the remote EDF location: the front and rear sides of the NZ-DSF, and the better SNR performance was obtained by allocating the remote EDF at the rear side of the NZ-DSF. In the configuration where the remote EDF was located at the front of

the NZ-DSF, a sufficient pump power was not fed to the EDF due to a large transmission loss of about 40 dB.

Optical isolators were placed at each side of the remote EDF as shown in Fig. 4-2 for low noise and stable operations. To feed the pump light from the receiver side to the remote EDF, a set of WDM couplers was used to bypass the optical isolator.

4-3 40 Gbit/s-based WDM transmission experiment

By using the hybrid transmission line configuration, a transmission experiment was conducted toward a terabit-capable 40 Gbit/s-based WDM unrepeatered transmission over 300 km.

4-3.1 Experimental setup

Figure 4-4 shows a schematic diagram of the experimental setup using the transmission line as explained in the previous section. The transmitter consisted of twenty-five DFB-LDs, the wavelength of which ranged from 1547.0 nm to 1566.4 nm with a channel spacing of 100 GHz (0.8 nm). The light sources for odd (even) channels were combined with an arrayed-waveguide grating (AWG) followed by two 20 Gbit/s $LiNbO_3$ intensity-modulators for data modulation and RZ pulse formatting. The 20 Gbit/s RZ signals (a 2^{15}-1 pseudo-random binary sequence) produced through the $LiNbO_3$ modulator chain were divided into two identical 20 Gbit/s data streams, and they were optically time-division-multiplexed in the same state of polarization to generate 40 Gbit/s RZ signals with an optical delay to alleviate the correlation between the two 20 Gbit/s data streams. Then, the odd and even channels were combined with a polarization beam splitter (PBS) in the orthogonal state of polarization [20].

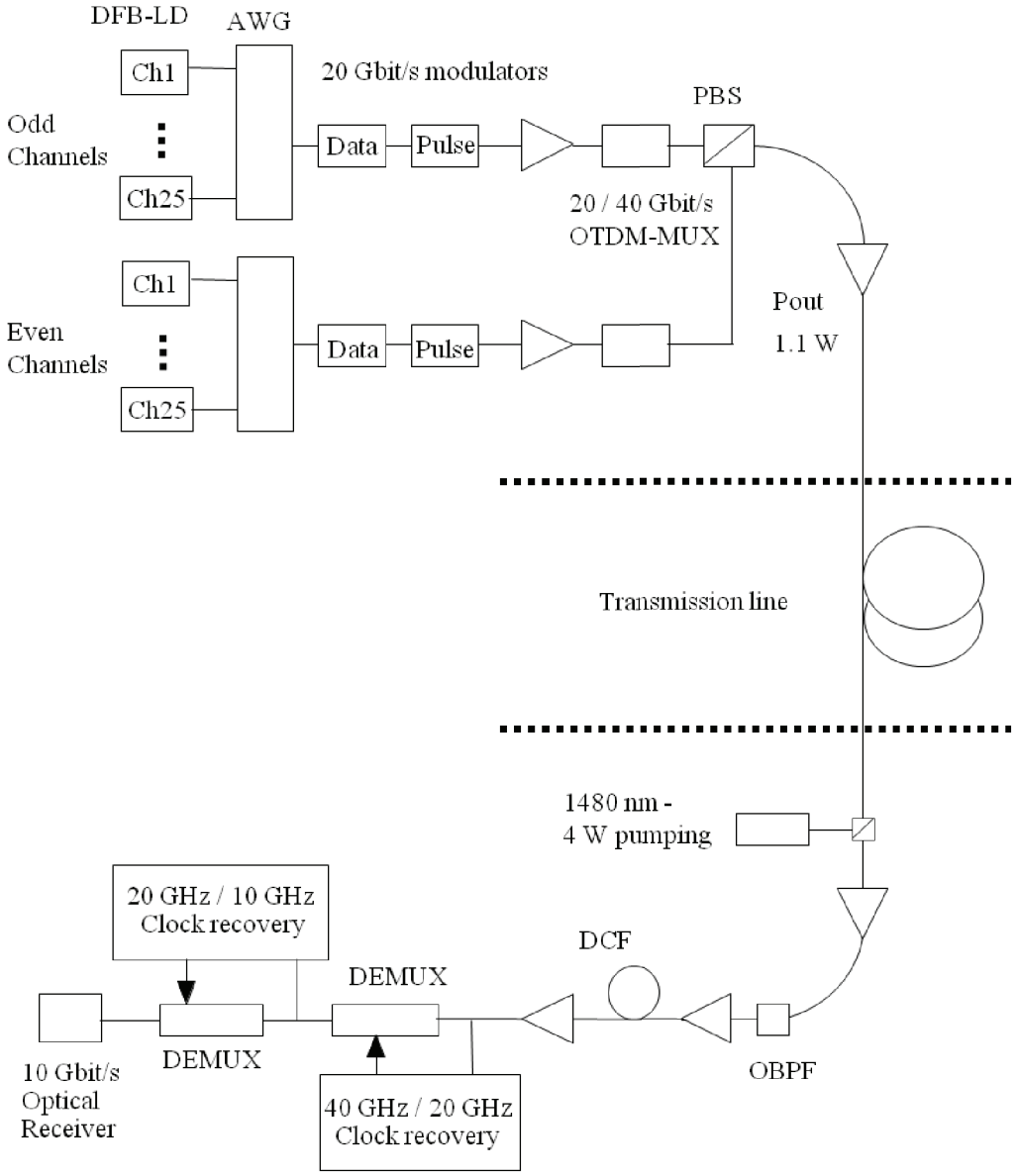

Fig. 4-4 Experimental setup for a 40 Gbit/s-based WDM unrepeatered transmission.

The pulse width was about 10 ps. The total power of the 25 WDM signals fed into the transmission line was boosted to 1.1 W. In this experiment, no channel pre-emphasis was applied. The input signal power was as high as 1.1 W, and the pump light source was a 1.48-μm fiber laser with an output power of 4 W. The optical gain obtained by the remote EDFA and Raman amplification was around 15 dB and 17 dB, respectively

as shown in Fig. 4-5. The accumulated dispersion in the transmission line was compensated for by DCFs after transmission.

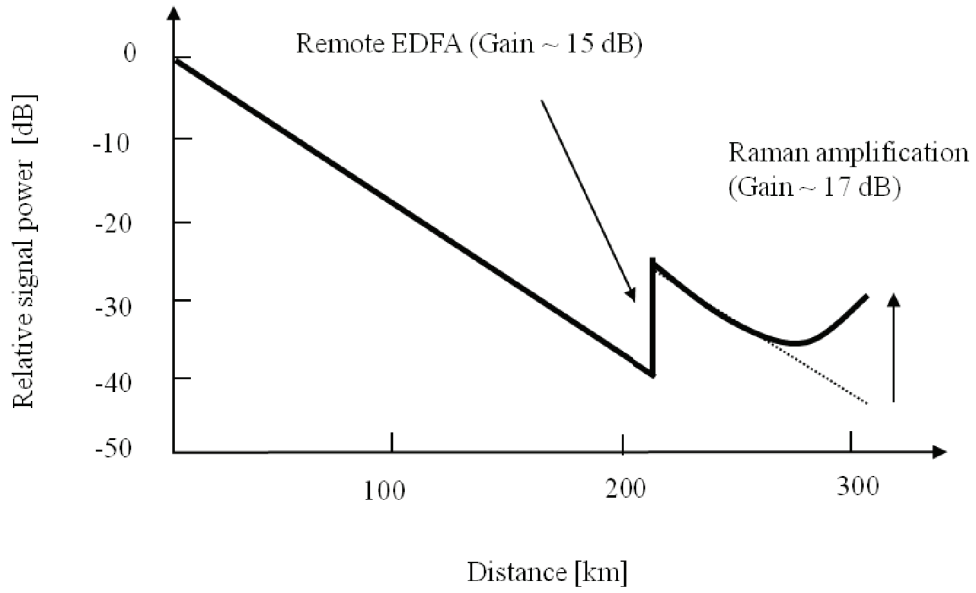

Fig. 4-5 Signal level diagram along the transmission line using a remote EDFA and Raman amplification.

In the receiver, the desired channel was selected by using two cascaded 1 nm optical bandpass filters (OBPF). No polarization demultiplexing was applied. The received 40 Gbit/s signals were optically time-division-demultiplexed (OTDM DEMUX) to 10 Gbit/s signals with a two-stage optical gate using sinusoidally driven polarization insensitive EA modulators [21]. The transmission performance was evaluated by taking the average of the BER of the four 10 Gbit/s data streams, which can be easily attained by periodically re-synchronizing the clock recovery circuit in the OTDM-DEMUX stage at around 500 Hz so that the 10 Gbit/s tributaries fed into the receiver were selected randomly [22].

4-3.2 Results and discussion

Figures 4-6 (a) and (b) show the monitored signal spectra before and after 306 km transmission. As shown in Fig. 4-6 (b), sufficient optical SNRs of more than 18 dB at the resolution of 0.2 nm were obtained for all the channels. The tilt of the signal level observed after transmission was mainly due to the mismatch between the signal bandwidth and the gain peak of Raman amplification in the last portion of the transmission line.

Figure 4-7 shows the eye diagrams after 306 km transmission. Despite of a fairly large accumulated dispersion due to the long-distance unrepeatered transmission, clear eye opening was obtained for the edge and center channels of the WDM signal band. The results indicate that the nonlinear effects in this experiment were well suppressed owing to the ultra-large A_{eff} of the EE-SMF. Figure 4-8 shows the Q-factor corresponding to the measured BER after 306 km transmission for all the channels. The average and the worst Q-factors were 15.9 dB and 15.6 dB, respectively. EE-SMF has low PMD characteristics by nature, and therefore the use of EE-SMF will play an important role in 40 Gbit/s-based ultra long-distance unrepeatered systems.

Finally, to clarify the impact of pumping direction of the remote EDF on the transmission performance, the pumping directions was changed from backward direction in Fig. 4-2 to forward direction as shown in Fig. 4-9. Figure 4-10 (a) shows the signal spectrum before the remote EDF (dotted line), and Fig. 4-10 (b) shows the signal spectra after the remote EDF for backward (solid line) and forward (dashed line) pumping configurations. No distinct difference neither in signal spectra nor in optical SNR was observed between these two pumping configurations. Note that the signal level variation among 25 WDM channels was not so significant, and almost the same optical SNR was attained for all the channels after the remote EDF amplification even without applying any pre-emphasis at the transmitter side. This can be attributed to the ultra-low nonlinearity of the transmission line that avoids the impact of the Raman tilt induced at the beginning of the transmission line [23].

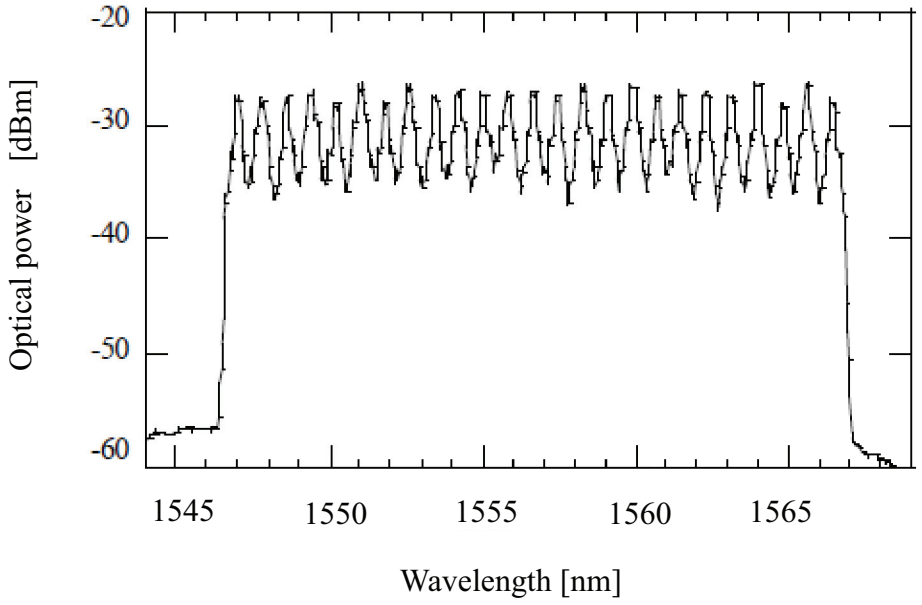

(a) before transmission

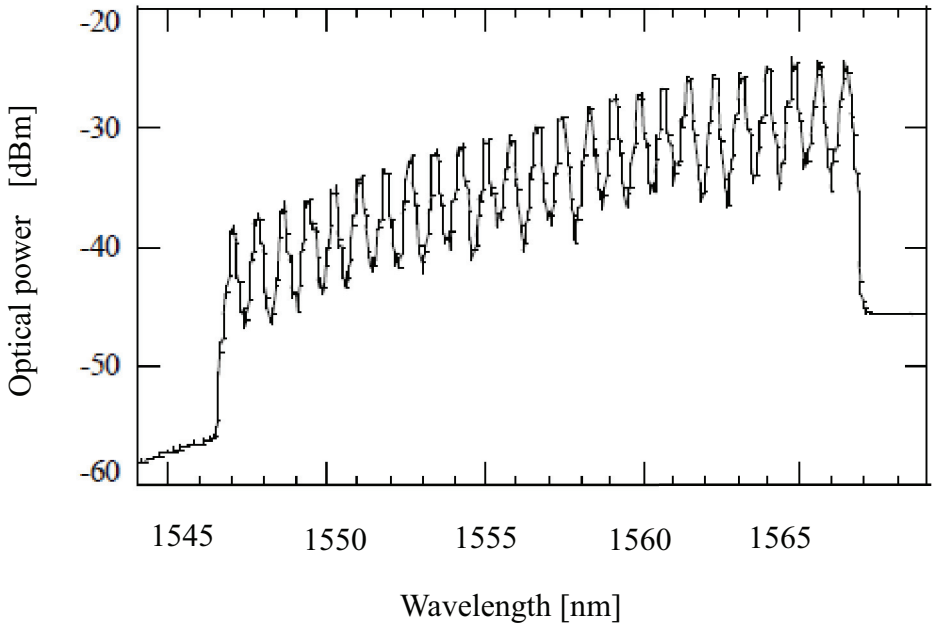

(b) after transmission

Fig. 4-6 Optical spectra of 40 Gbit/s x 25 WDM signals.

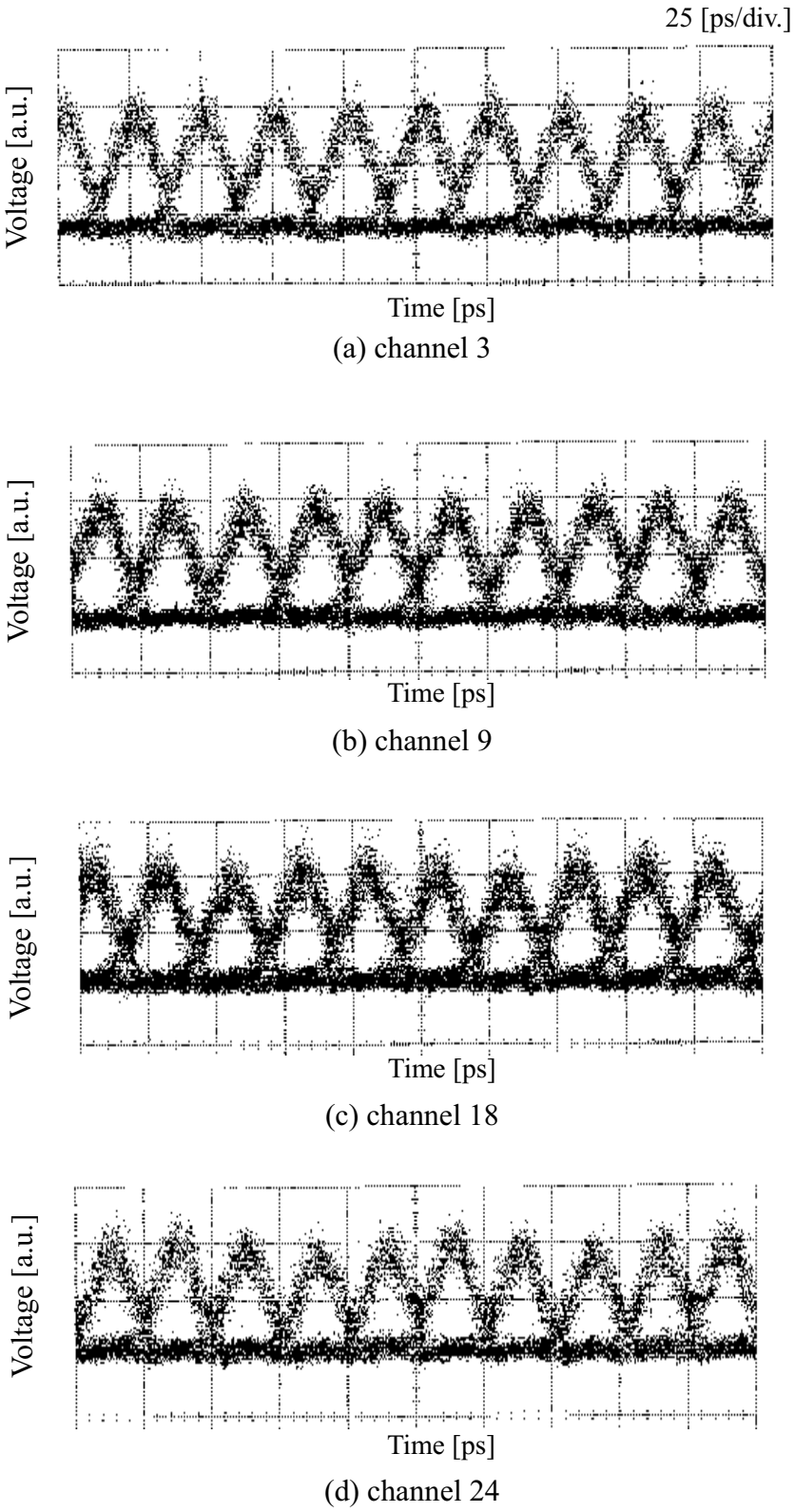

Fig. 4-7 Eye diagrams after 306 km transmission.

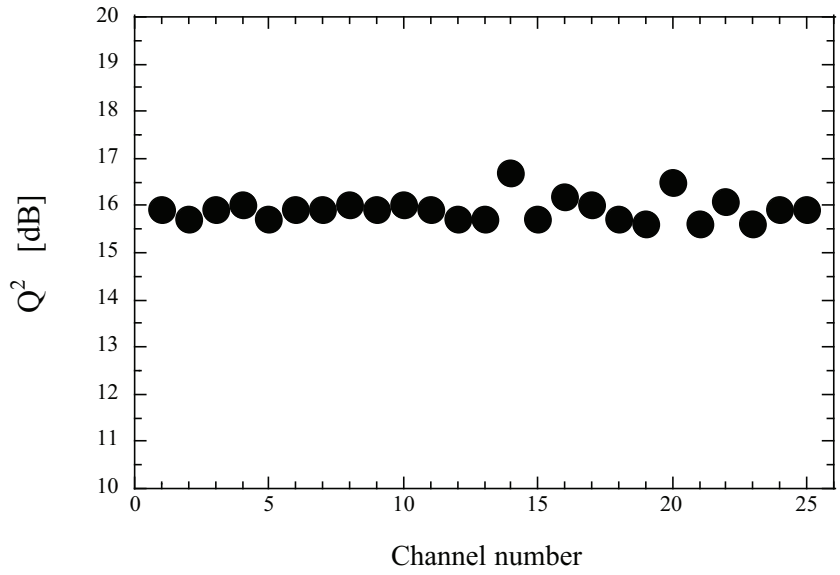

Fig. 4-8 Q-factor after 306 km transmission.

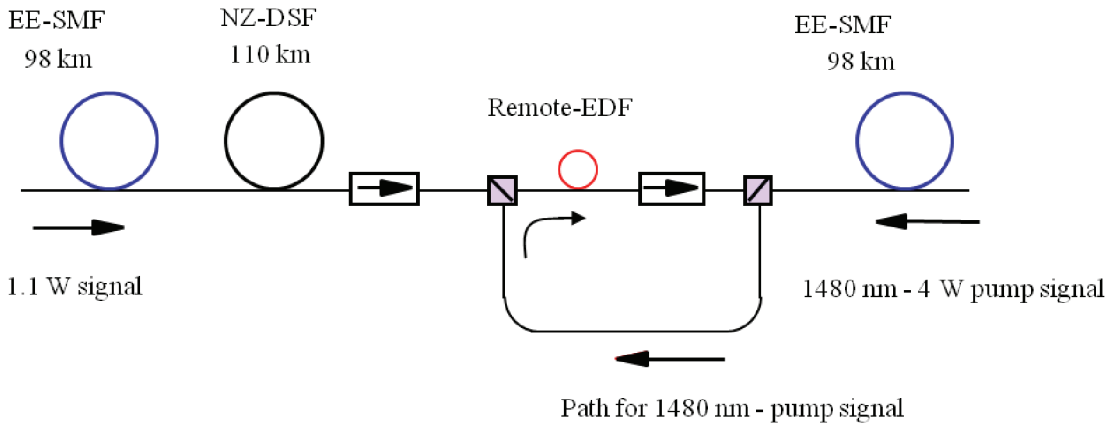

Fig. 4-9 Transmission line configuration for forward-pumping scheme.

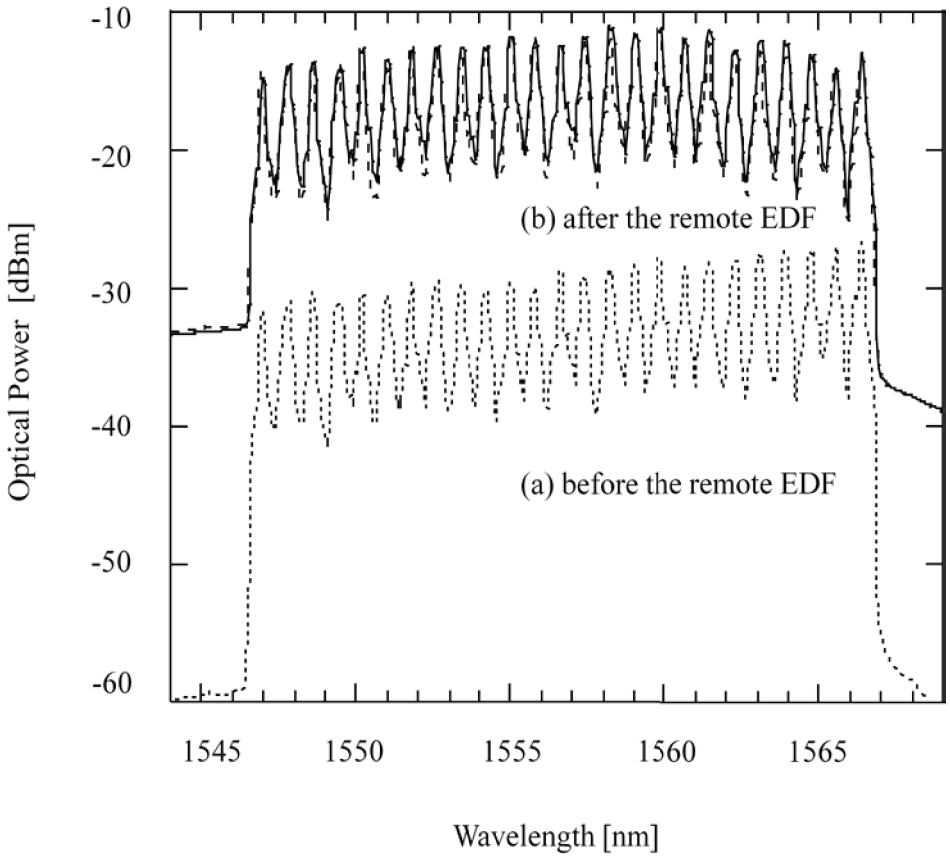

Fig. 4-10 Optical spectra: (a) before the remote EDF(dotted line) and (b) after the remote EDF for backward (solid) and forward (dashed) pumping schemes.

4-4 Conclusion

The 40 Gbit/s-based unrepeatered terabit-capacity WDM transmission over 306 km has been successfully demonstrated for the first time, even without using a separate fiber for pump power transmission. This longest-distance transmission was attributed to the adoptions of 175 μm^2-A_{eff} fiber and proper dispersion map configured with the EE-SMFs and NZ-DSF. The reduction of the accumulated dispersion is an important system design issue for 40 Gbit/-based unrepeatered transmission systems, in addition to the suppression of fiber nonlinearities.

The development of ultra large-A_{eff} SMF cables would be the key to achieve 40

Gbit/s-based ultra long-distance unrepeatered systems. With further improvement of the remote EDF scheme and the adoption of strong FEC technologies, much longer 40 Gbit/s-based unrepeatered transmissions would be expected in the near future.

References

[1] E. Brandon, J. –P., Blondel, F. Boubal, L. Buet, V. Havard, A. Hugbart, L. Labrunie, P. Le Roux, D. Toullier, and R. Uhel, "1.28 Tbit/s (32 x 40 Gbit/s) unrepeatered transmission over 250 km", ECOC2000, vol. 4, pp. 21-23, 2000.

[2] K. Shimizu, K. Kinjo, N. Suzuki, K. Ishida, S. Kajiya, K. Motoshima, and Y. Kobayashi, " Fiber-effective-area managed fiber lines with distributed Raman amplification in 1.28-Tb/s (32 x 40 Gb/s), 202-km unrepeatered transmission", OFC2001, TuU2, 2001.

[3] J. Berger, U. Feiste, R. Ludwig, C. Schubert, C. Schmidt, and H. G. Weber, "40 Gb/s RZ unrepeatered transmission over 252 km SMF using Raman amplification", OFC2001, TuU3, 2001

[4] T. Miyakawa, I. Morita, K. Tanaka, H. Sakata, and N. Edagawa: "2.56 Tbit/s (40 Gbit/s x 64 WDM) unrepeatered 230 km transmission with 0.8 bit/s/Hz spectral efficiency using low-noise fiber Raman amplifier and 170 μm^2-A_{eff} fiber", OFC2001, PD26, 2001.

[5] D. Marcuse, A. R. Chraplyvy, and R. W. Tkach, "Effect of fiber nonlinearity on long distance transmission", IEEE/OSA J. Lightwave Technol., vol. 9, pp. 121-128, 1991.

[6] D. Marcuse, "Single-channel operation in very long nonlinear fibers with optical amplifiers at zero dispersion", IEEE/OSA J. Lightwave Technol., vol. 9, pp. 356-361, 1991.

[7] D. Marcuse, "Bit-error rate of lightwave systems at the zero-dispersion wavelength", IEEE/OSA J. Lightwave Technol., vol. 9, pp. 1330-1334, 1991.

[8] D. Marcuse, "RMS width of pulses in nonlinear dispersion fibers", IEEE/OSA J. Lightwave Technol., vol. 10, pp. 17-21, 1992.

[9] G. P. Agrawal, "Nonlinear fiber optics", California, USA: Academic Press, 1989.

[10] D. Cotter, "Fibre nonlinearities in optical communications", Opt. and Quantum Electron., vol. 19, pp. 1-17, 1987.

[11] P. Le Roux, E. Brandon, J. –P. Blondel, L. Labrunie, D. Toullier, and G. Zarris, "Error-free 2.5 Gbit/s unrepeatered transmission over 570 km", ECOC2000, vol. 4,

pp. 45-47, 2000.

[12] Y. R. Shen and N. Bloembergen, “Theory of stimulated Brillouin and Raman scattering”, Phys. Rev. A, vol. 137, pp. 1787-1804, 1965.

[13] R. H. Stolen, “Nonlinear properties of optical fibers”, in Optical Fiber Telecommunications, Edited by S. E. Miller and A. G. Chynoweth, New York, USA: Academic Press, 1979.

[14] Y. Aoki, “Properties of fiber Raman amplifiers and their applicability to digital optical communication systems”, IEEE/OSA J. Lightwave Technol., vol. 7, pp. 1225-1239, 1990.

[15] R. H. Stolen and E. P. Ippen, “Raman gain in glass optical waveguides”, Appl. Phys. Lett., vol. 22, pp. 276-278, 1973.

[16] E. P. Ippen and R. H. Stolen, “Stimulated Brillouin scattering”, Appl. Phys. Lett., vol. 21, pp. 539-541, 1972.

[17] D. Cotter, “Stimulated Brillouim scattering in monomode optical fibre”, J. Opt. Commun., Vol. 4, pp.10-19, 1983.

[18] K. Aikawa, T. Suzuki, T. Suzuki, and A. Wada, “Single-mode optical fiber with effective core area larger than 160 μm^2”, ECOC1999, vol. 1, pp. 302-303, 1999.

[19] K. Osono, K. Kotani, K. Murakami, Y. Bing, T. Yamazaki, and H. Shimane, “The study of ultra large effective area fiber & mating dispersion slope compensating fiber for dispersion flattened hybrid optical fiber DWDM link”, IWCS2001, pp. 483-487, 2001.

[20] K. Inoue, “Arrangement of orthogonal polarized signals for suppressing fiber four-wave mixing in optical multichannel transmission systems”, IEEE Photon. Technol. Lett., vol. 6, pp. 560-563, 1991.

[21] I. Morita, K. Tanaka, N. Edagawa, and M. Suzuki, “40 Gbit/s single-channel soliton transmission over transoceanic distance by reducing Gordon-Haus timing Jitter and soliton-soliton interaction”, IEEE/OSA J. Lightwave Technol., vol. 7, pp.2506-2511, 1999.

[22] J. –X. Cai, M. Nissov, A. N. Pilipetskii, C. R. Davidson, R. –M. Mu, M. A. Mills, L. Xu, D. Foursa, R. Menges, P. C. Corbett, D. Sutton, and N. S. Bergano, “1.28 Tb/s (32 x 40 Gb/s) transmission over 4,500 km”, ECOC2001, PD.M.1.2, 2001.

[23] S. Bigo, S. Gauchard, A. Bertaina, and J.-P. Hamaide, “Experimental investigation of stimulated Raman scattering limitation of WDM transmission over various types of fiber infrastructures”, IEEE Photon. Technol. Lett., vol. 11, pp. 671-673, 1999.

Chapter 5

High-spectral efficient 40 Gbit/s-based DWDM transmission systems using signal-spectrum filtering

5-1 Introduction

A high-channel bit rate of 40 Gbit/s is commercially beneficial in long-haul repeatered systems in a similar manner to unrepeatered systems as described in Chapter 4. However, a massive 40 Gbit/s-based WDM transmission is very challenging, and many bottlenecks for high-speed transmissions must be overcome.

The first bottleneck is the trade-off on the local dispersion of the transmission line. A smaller local dispersion is preferable for a higher bit-rate transmission because of its small dispersion tolerance. The optimum local dispersion for 40 Gbit/s single-channel soliton transmissions was found to be around 0.3 ps/nm/km, and the transmission over 8,600 km was achieved [1]. Furthermore, by adopting polarization-division-multiplexing to reduce the soliton-soliton interactions, the transmissible distance was extended from 8,600 km to 10,200 km [2], [3]. For WDM transmissions, however, the local dispersion must be set to a larger value to reduce the inter-channel interactions among WDM channels as mentioned in Chapter 3. In addition, flat dispersion characteristics of the transmission line is also necessary for WDM transmissions, and the SMF-based span configuration is considered to be a prospective candidate to meet the above mentioned requirements.

The second bottleneck is to increase the packing density, namely spectral efficiency of 40 Gbit/s-based WDM systems. Spectral efficiency is a key issue to enhance aggregate capacity and cost-effectiveness of optical transmission systems. In order to achieve a high spectral efficiency, the bandwidth limitation of the signal spectrum by using optical filtering before transmission (i.e. *pre-filtering*) is an attractive solution, and many successful demonstrations using the scheme have been reported [4]-[19]. Regarding OOK signals, detailed studies on the benefits of asymmetric pre-filtering

have been already reported for CS-RZ signals [14], [15]. However, regarding DPSK signals, which is a promising format for high-speed bit-rate long-haul system applications, no similar study has been reported, whereas remarkable demonstrations of 40 Gbit/s-based DWDM transmission have been already reported by using symmetrically pre-filtered DPSK signals [16]-[19].

In this chapter, firstly, the impact of nonlinear crosstalk on 50 GHz-spaced 40 Gbit/s DWDM transmissions is experimentally explored to clarify the transmissible distance and the penalties induced by inter-channel interactions in a SMF-based transmission system. Then, the optimum dispersion map is investigated for 40 Gbit/s DWDM systems. Next, the optical pre-filtering scheme is described as a practical method to reduce the linear crosstalk for achieving a high-spectral efficient transmission, and a 50 GHz-spaced 40 Gbit/s x 25 WDM transmission over 480 km is presented by using signal bandwidth-limited RZ signals. Finally, the optimum pre-filtering conditions for CS-RZ DPSK signals are numerically and experimentally investigated for a spectral efficiency of 0.8 bit/s/Hz, and the transmission performance of symmetrically and asymmetrically pre-filtered CS-RZ DPSK signals have been also evaluated by conducting long-haul transmission experiments up to 9,000 km.

5-2 Impact of nonlinear crosstalk in 100 GHz-spaced 40 Gbit/s DWDM systems using SMF-based dispersion-flattened transmission line

As discussed in Chapter 3, a small local dispersion causes significant inter-channel crosstalk due to fiber nonlinearities in high-speed DWDM transmission systems. For 40 Gbit/s-based massive DWDM transmissions, the dispersion of NZ-DSF is too low to suppress inter-channel interactions, and the properties of a high dispersion and low nonlinearity are required to the transmission line. The SMF-based span configuration satisfies these demands and is considered to be a promising approach to achieve high-speed massive DWDM transmissions. In this section, to evaluate nonlinear crosstalk in SMF-based DWDM systems, the impact of nonlinear penalty due to the

increase of channel count is investigated in a 0.8 nm-spaced SMF-based 40 Gbit/s DWDM system.

5-2.1 Experimental setup

Figure 5-1 shows a schematic diagram of the experimental setup. In the transmitter, a 16 x 40 Gbit/s WDM signal were generated. Sixteen LDs were used as signal light sources, which were equally spaced by 0.8 nm in the wavelength range from 1543.6 nm to 1555.6 nm. Odd and even channels were combined separately with an AWG and then put into modulator chains. A 20 Gbit/s RZ data stream was produced with a 20 GHz $LiNbO_3$ pulse generator driven by a 10 GHz sinusoidal signal and a 20 Gbit/s $LiNbO_3$ data modulator driven by electrically time-division-multiplexed (ETDM) 20 Gbit/s data signals with a 2^{15}-1 pseudo-random binary sequence. Then, the 20 Gbit/s signals were optically time-division-multiplexed (OTDM) to generate 40 Gbit/s signals. The pulse width was about 10 ps. Even and odd channels were combined using a polarization beam splitter and were launched into the transmission line in orthogonal state of polarization.

The 143 km-long recirculating loop consisted of four 36 km-long spans of SMF-based transmission fiber and five 980 nm-pumped EDFAs. Two kinds of fibers were used to configure all the fiber spans. The first segment following EDFAs was a standard SMF, and the second segment was a SC-DCF with a negative dispersion and negative dispersion slope to form a dispersion-flattened transmission span. Figure 5-2 shows the dispersion map of the loop. The dispersion of the SMF was +18 ps/nm/km, the maximum accumulated dispersion in the loop was 550 ps/nm. A DCF with –17 ps/nm was inserted at the beginning of the loop to compensate for the residual dispersion and dispersion slope of the loop. The average dispersion slope of the loop was only –0.002 ps/nm/km, and the average dispersion at 1550 nm (channel 9) was 0.03 ps/nm/km. The loss of each spans including splice loss was 9.6 dB on average. To obtain flat transmission bandwidth, a Mach-Zehnder filter with an FSR of 32 nm was employed.

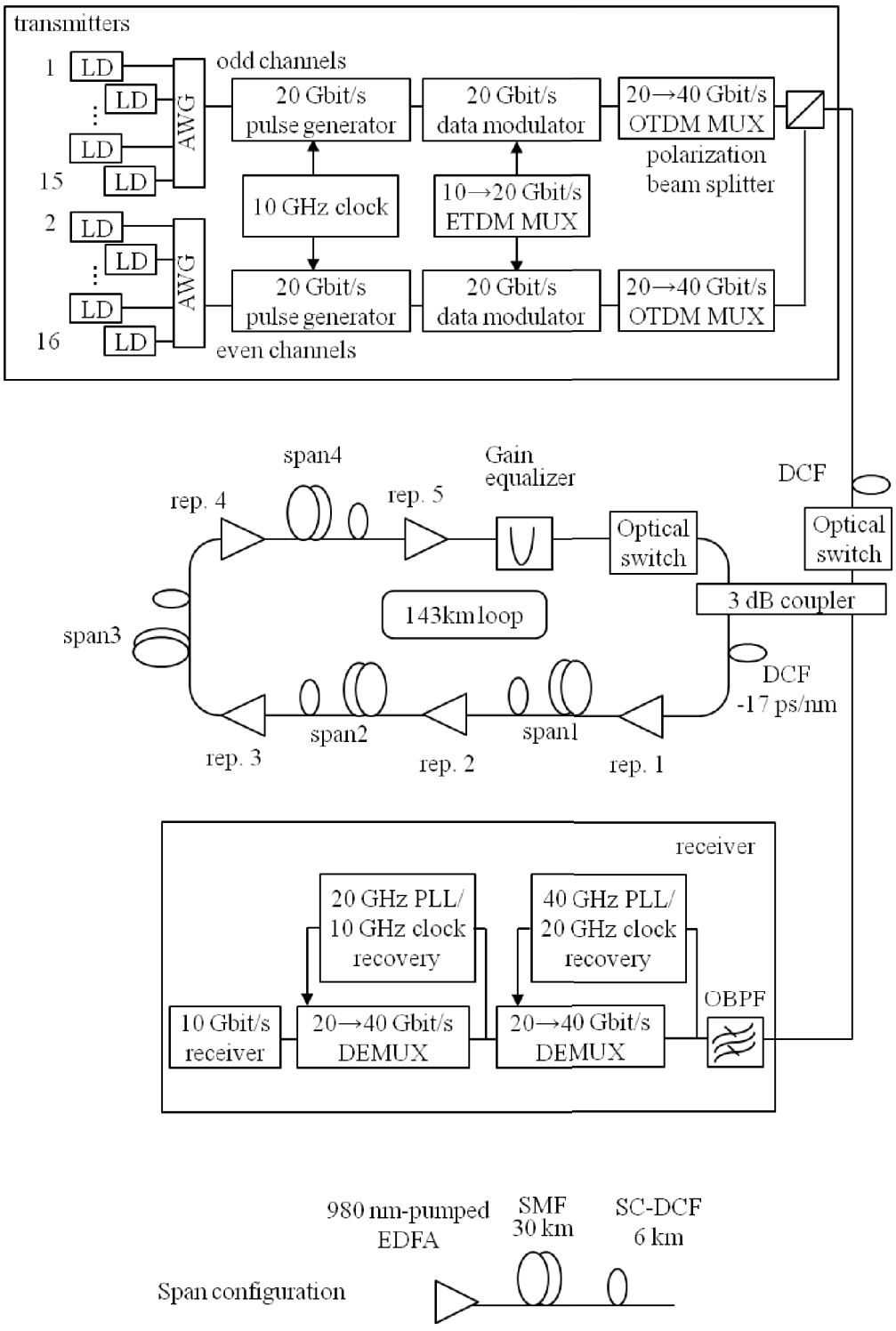

Fig. 5-1 Experimental setup for 100 GHz-spaced 40 Gbit/s DWDM transmission.

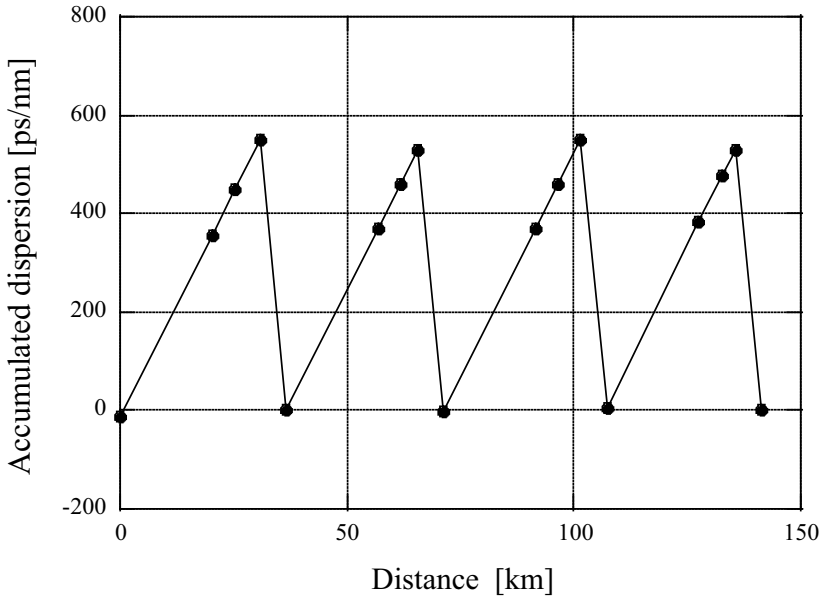

Fig. 5-2 Dispersion map of the loop.

In the receiver, the center channel of the WDM signals, channel 9, was selected by optical bandpass filters, and the transmitted 40 Gbit/s signals were optically time-division-demultiplexed to 10 Gbit/s signals with a two-stage optical gate using sinusoidally-driven polarization insensitive EA modulators. The transmission performance was measured for the demultiplexed 10 Gbit/s signals.

5-2.2 Result and discussion

Figure 5-3 shows the measured Q-factor of channel 9 as a function of the number of WDM channel for transmission distances of 1,000, 1,290, and 1,570 km. The repeater output power was adjusted to obtain the optimum transmission performance, and it was almost proportional to the number of WDM channel. The figure indicates that the induced nonlinear penalty by increasing the number of WDM channel from one to sixteen was as small as 0.4 dB for 1,000 km transmission. Even after 1,560 km transmission, the penalty was less than 1 dB even in the 16 WDM transmission.

Figure 5-4 shows the observed eye diagrams of the 40 Gbit/s signals and time-division-demultiplexed l0 Gbit/s signals of channel 9 after the 40 Gbit/s-based 16 -WDM transmission over 1,000 km. These waveforms were measured with a high-speed photo-detector with a bandwidth of 32 GHz. Significant waveform distortion and timing jitter were not observed.

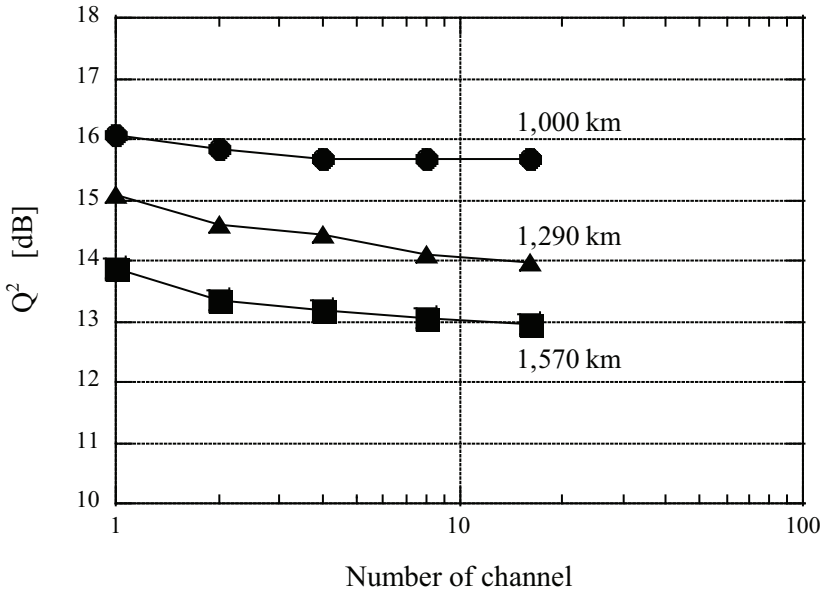

Fig. 5-3 Q-factor of channel 9 against the number of WDM channel.

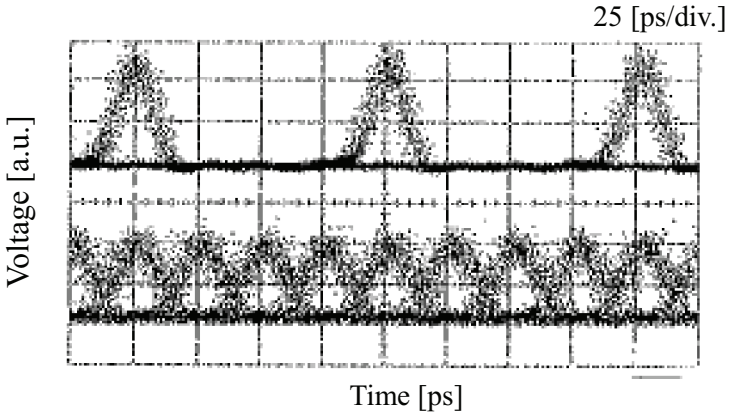

Fig. 5-4 Eye diagrams of channel 9 for 40 Gbit/s-based 16-WDM transmission over 1,000 km.

From these results, it was considered that most of the penalties associated WDM transmissions in the SMF-based system were induced by only a few neighboring channels. The results indicate that further capacity expansion can be expected without increasing the penalty significantly.

Finally, the performances of all the WDM channels were measured, and it was confirmed that a 640 Gbit/s (16 x 40 Gbit/s) error-free transmission (BER < 10^{-9}) over 1,000 km was achieved as shown in Fig. 5-5.

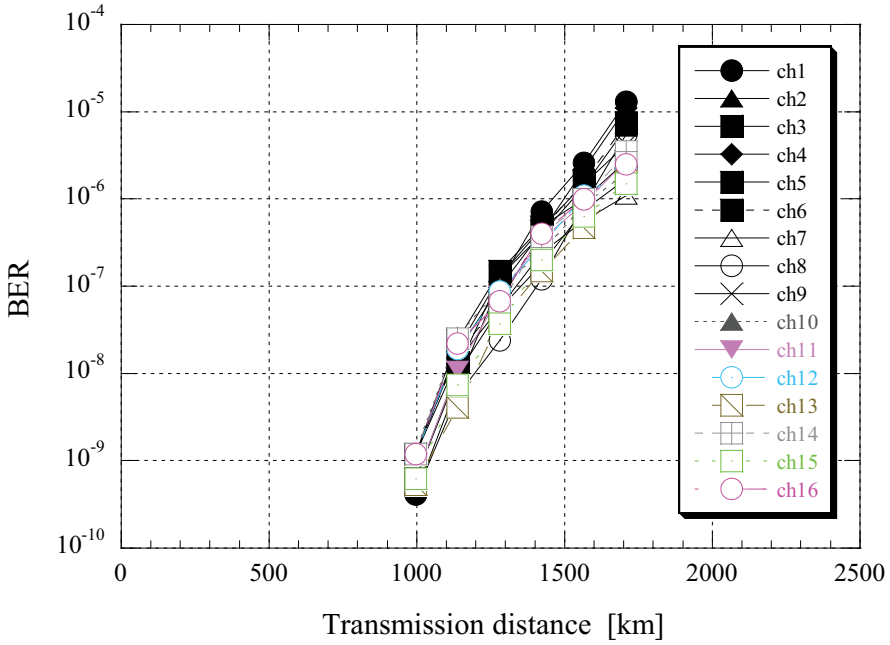

Fig. 5-5 BER performance against transmission distance for 16 WDM channels.

Through these experiments, it was found that in the SMF-based 40 Gbit/s DWDM systems with high local dispersion, the transmission performance is not so sensitive to the increase of the channel count when the number exceeds more than several channels. In comparison with the transmissible distance of 20 Gbit/s-based soliton WDM transmissions using the DFF-based span configuration, which was decreased from 15,000 km to 2,000 km by adopting the WDM scheme, the inter-channel crosstalk in the SMF-based span configuration was dramatically suppressed. In addition, since the

transmission performance is not sensitive to the increase of channel counts, the channel spacing can be expected to be narrowed to less than 0.8 nm with a small nonlinear penalty.

The problem of the SMF/SC-DCF span configurations is that the transmission distance was limited to 1,000 km. A high-dispersion property of the SMF causes a wide spread of the RZ pulses and induces interactions between the neighboring pulses. The intra-channel interactions deteriorate the transmission performance in SMF-based systems. The key issues for a long-haul high-density WDM transmission are the extension of the transmissible distance and the reduction of linear crosstalk for increasing the packing density of the WDM signals.

5-3 Dispersion management for 40 Gbit/s-based WDM transmission systems

A largely accumulated dispersion of SMF-based span configurations causes the intra-channel interactions between adjacent pulses, while a high-local dispersion of the SMF is effective to suppress the inter-channel interactions between WDM channels. In this section, the dispersion map to mitigate the intra-channel interactions is investigated.

5-3.1 Single-channel transmission

The intra-channel interactions are attributed to a largely accumulated dispersion, especially in high-speed transmission systems. In the dispersion map which uses a span configuration for the length ratio of SMF and SC-DCF of 5:1 as shown in Fig. 5-2, the dispersion accumulates up to +550 ps/nm in a single fiber span. The performance of the dispersion maps reducing the accumulated dispersion was explored by 40 Gbit/s single-channel transmission experiments.

Figure 5-6 shows three kinds of dispersion maps used for the evaluation. The

corresponding span configurations, the effective core area, and dispersion of each optical fiber are also illustrated in the figure. Dispersion map 1 shown in Fig.5-6 (a) is the map used for the evaluation of the inter-channel interactions in the previous section. The different dispersion maps 2 and 3 are shown in Fig. 5-6 (b) and (c), respectively. The magnitudes of the dispersion and dispersion slope of the SC-DCF employed in maps 2 and 3 are the same as ones of the SMF, and the signs are opposite. The transmission span is configured by the same length of the SMF and SC-DCF. The accumulated dispersion of the map 2 is +400 ps/nm, and that of the map 3 decreases to +200 ps/nm by placing the SC-DCF in the middle of the span.

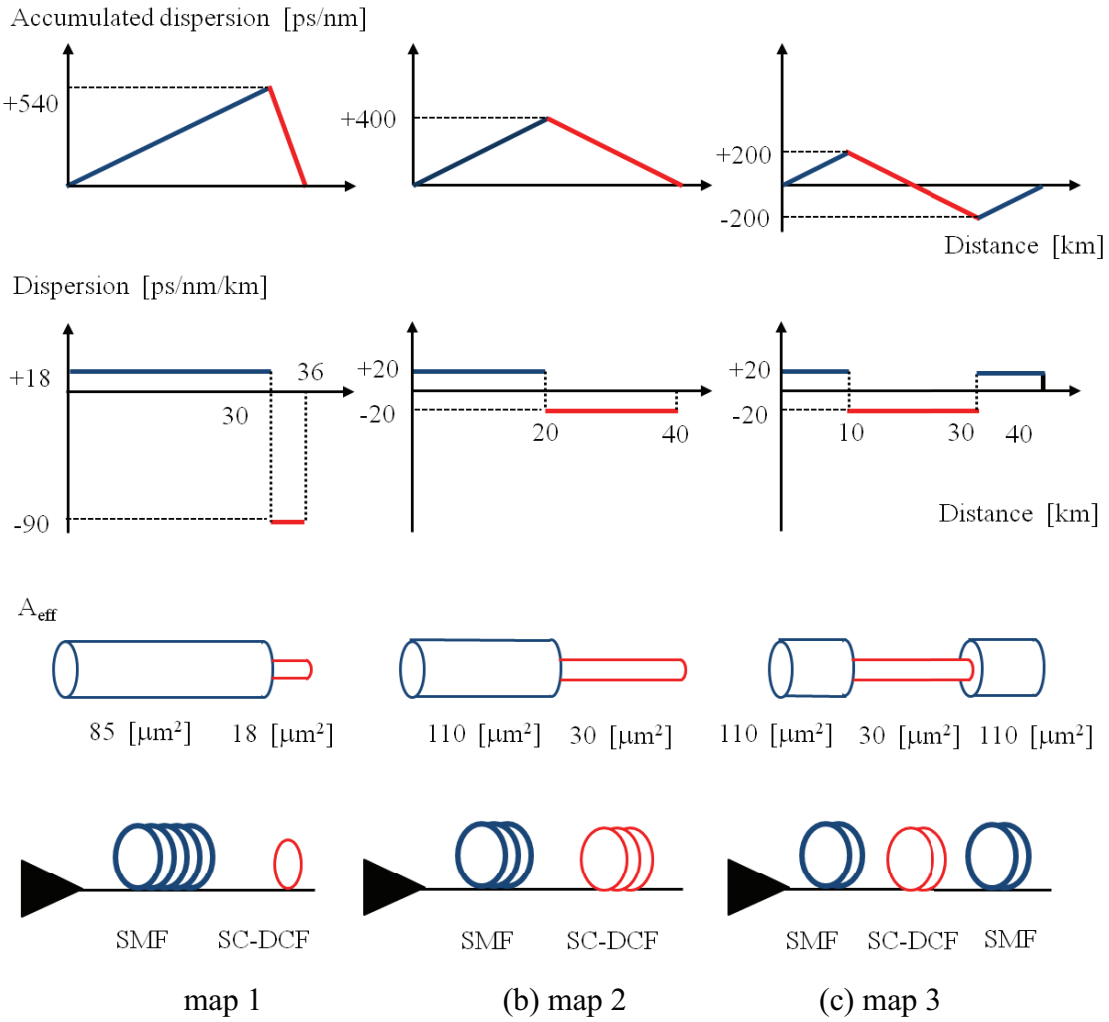

Fig. 5-6 Dispersion maps for evaluating the impact of the accumulated dispersion on single-channel transmission performances.

The BER performances of 40 Gbit/s signal-channel transmissions in three kinds of dispersion maps are shown in Fig. 5-7. The transmission conditions such as repeater output power and phase modulation were optimized for each dispersion map.

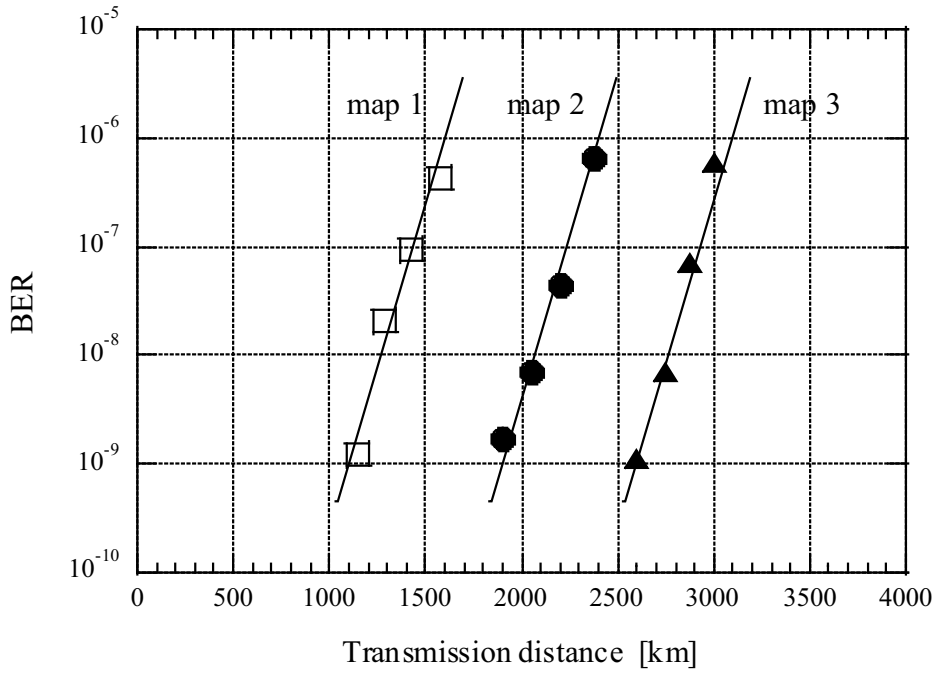

Fig. 5-7 BER performances of 40 Gbit/s single-channel transmissions in three kinds of dispersion maps.

From Fig.5-7, it was found that the transmission performance was improved as the accumulated dispersion in a single span was decreased. A transmission distance over 2,500 km was achieved in map 3 where the accumulated dispersion is the minimum among three kinds of the maps. These results indicate that the dispersion map to inhibit the accumulation of the dispersion is effective to suppress the intra-channel interactions for single-channel transmissions.

5-3.2 WDM transmission

The transmissible distance in 40 Gbit/s single-channel transmissions can be extended by using dispersion map 3 in Fig. 5-6 owing to the reduction of the intra-channel interactions. In a similar manner to adopt map 3, dispersion maps whose accumulated dispersion is smaller than that of map 3 is expected to be effective for extending the transmission distance furthermore. For example, considering the dispersion map as shown in Fig. 5-8 where a fundamental segment consisted of SMF/SC-DCF/SMF is allocated repeatedly within a single fiber span, the accumulated dispersion over the span can be inhibited by increasing the number of repetition. In contrast, however, to compensate for the dispersion of the SMF by the SC-DCF in the front portion of the span may increase fiber nonlinearities, because the effective core area of the SC-DCF is much smaller than that of the SMF.

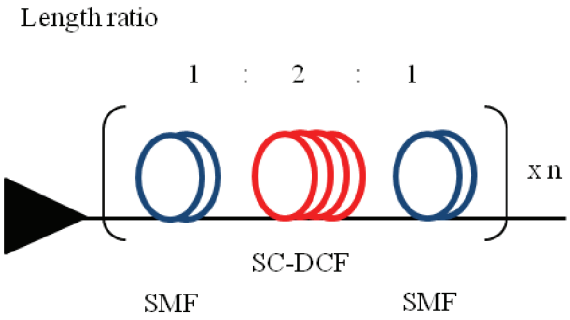

Fig. 5-8 Dispersion map for inhibiting the accumulation of dispersion.

For WDM transmissions, the inter-channel interactions may restrict the transmission performance. In order to evaluate the trade-offs between the intra-channel and inter-channel interactions, numerical simulations were conducted for both single-channel and 16-WDM transmissions over 3,000 km.

Figure 5-9 shows the obtained Q-factors as a function of the SMF/SC-DCF/SMF-fundamental segment number. As the span length was fixed to 40 km for all the cases in the simulations, the length of SMF/SC-DCF/SMF-fundamental

segment was 10 km for the repetition number of four. As is shown in Fig. 5-9, no significant difference was observed between the repetition number of one and two in 16-WDM transmissions, while the best performance was obtained at the repetition number of two in the single-channel transmission. It can be predicted that for further large-capacity WDM transmissions with the channel number of more than 16, the transmission performance of multiple repetition number of fundamental segment would be inferior to that of single one. From these perspectives, the dispersion map 3 in Fig. 5-6 (c) is confirmed to be optimum for 16 WDM transmissions.

Although the dispersion map was optimized for extending the transmission distance, the distance was limited to shorter than 3,000 km even for the single-channel transmission. For 40 Gbit/s-based large-capacity transoceanic transmissions, additional technologies are necessary to extend the transmission distance.

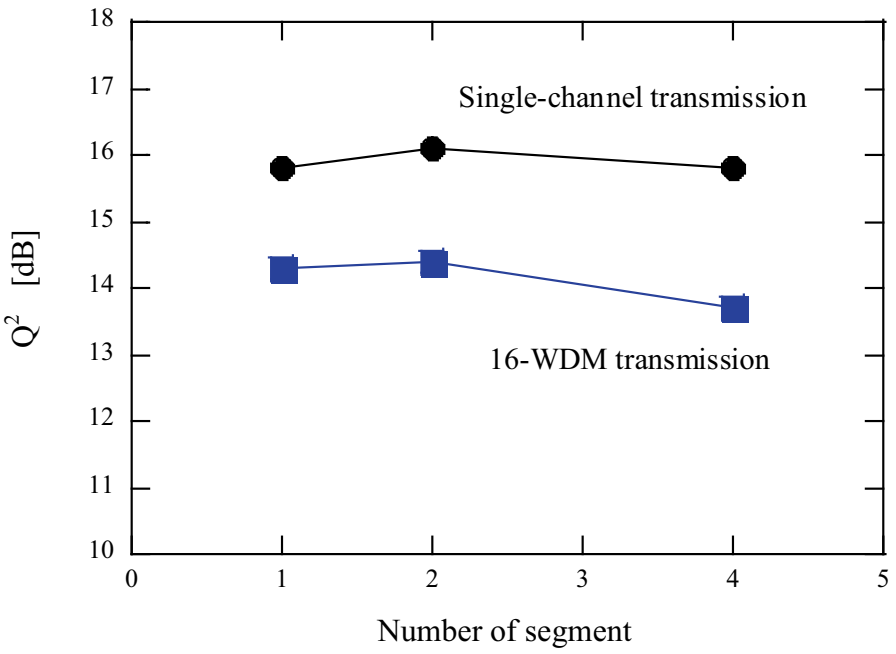

Fig. 5-9 40 Gbit/s x 16 WDM-3,000 km transmission performance as a function of the repetition number of the fundamental segment.

5-4 Optical pre-filtering for bandwidth limitation of signal spectrum

In the previous section, SMF-based dispersion map was optimized for 40 Gbit/s-based WDM transmissions. The advantage of the SMF-based transmission line is a low inter-channel-crosstalk property. This feature is advantageous to increase the packing density of WDM channels for high spectral efficiency.

From these perspectives, many schemes to mitigate linear crosstalks between adjacent channels were proposed and studied for reducing the channel spacing of WDM signals. The highest spectral efficiency reported at 40 Gbit/s channel bit rate was 0.8 bit/s/Hz, which was demonstrated in 186 km NRZ transmission with polarization-demultiplexing of the adjacent WDM channels at the receiver [19]. In practical conditions, however, the use of automated polarization-demultiplexer may introduce too much complexity and cost increase. Without the polarization demultiplexing, the highest spectral efficiency in 40 Gbit/s-based WDM transmissions was 0.64 bit/s/Hz, demonstrating a 300-km NRZ transmission [5]. NRZ format was suitable for short-distance transmissions because of the simplicity of transmitter and the narrow spectral bandwidth. In contrast, NRZ format is vulnerable against fiber nonlinearities as shown in Appendix B, and therefore it is not applicable to long-haul transmission systems.

In this section, the optical pre-filtering of RZ format is introduced as a practical solution to reduce the linear crosstalk to achieve a high spectral efficiency for targeting long-haul transmissions.

5-4.1 Bandwidth limitation of signal spectrum

The system architecture to use a signal bandwidth limitation for mitigating the linear crosstalk between adjacent channels is schematically illustrated in Fig. 5-10. In this system, the signal spectrum is trimmed by an optical filter with a sharp transmission characteristic, and then the bandwidth-limited signal is combined to a WDM signal. A

WDM multiplexing device simultaneously trims the signal spectrum of each channel in DWDM systems, owing to the flat-passband and sharp-edged amplitude characteristics of the device.

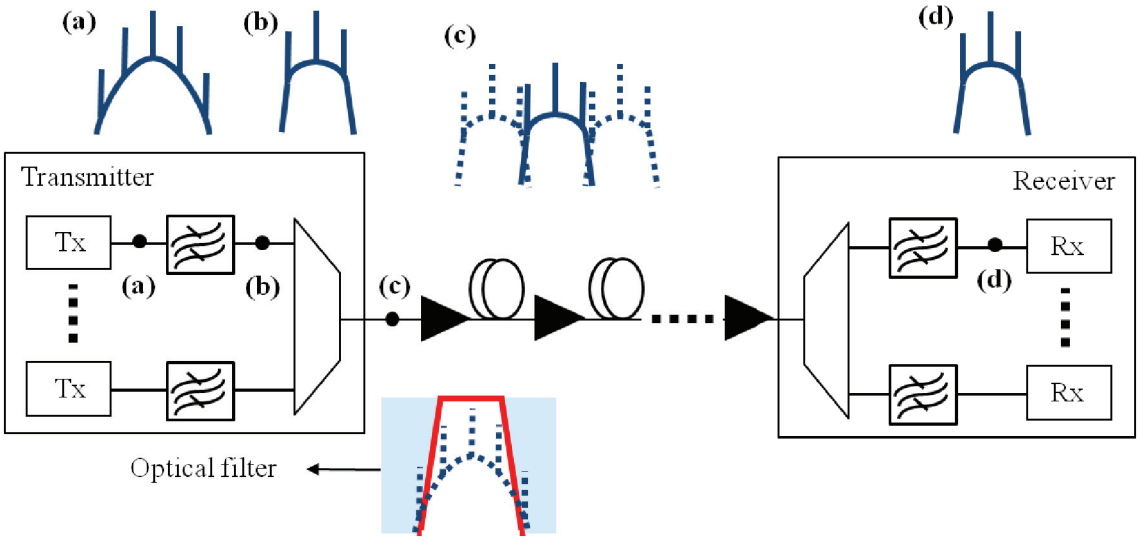

Fig. 5-10 Architecture of optically bandwidth-limited transmission system.

The effectiveness of the optical bandwidth limitation has been reported through many transmission experiments [4]-[19]. One of the key design factors is the filtering condition associated with the position of the center frequency. There are two typical filtering approaches: symmetrical and asymmetrical filtering. Figures 5-11 (a), (b), and (c) show examples of the optical spectra for no filtered, symmetrically filtered, and asymmetrically filtered signals, respectively. The bandwidth of the optical filter was set to 75 GHz. The corresponding waveforms to the optical spectra in Fig. 5-11 are indicated in Fig. 5-12. There was no significant difference between symmetrically and asymmetrically filtered signals in Fig. 5-12. In addition, no severe waveform distortion was observed, while the spectra were trimmed and the side-bands at the data-rate frequency were also slightly filtered as shown in Fig. 5-11.

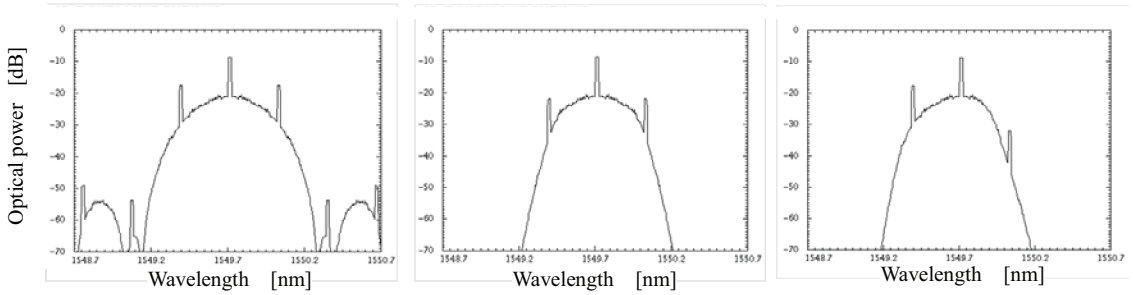

(a) no filtering (b) symmetric filtering (c) asymmetric filtering

Fig. 5-11 Spectra of optically filtered 40 Gbit/s signals.

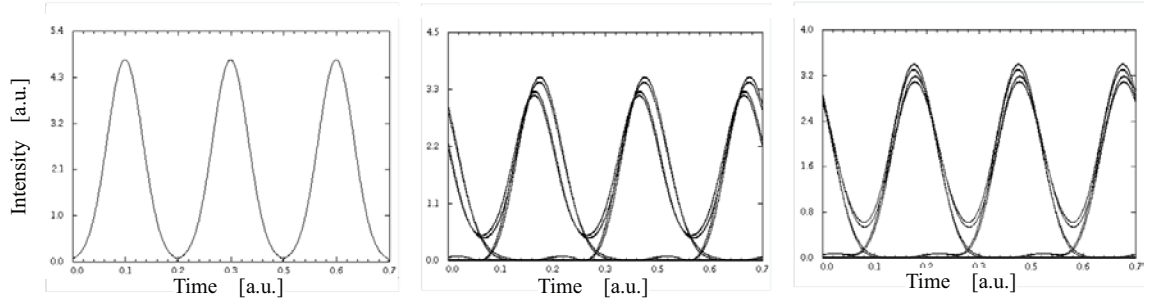

(a) no filtering (b) symmetric filtering (c) asymmetric filtering

Fig. 5-12 Waveforms of optically filtered 40 Gbit/s signals.

Next, in order to investigate the impact of the bandwidth limitation on the performance of 40 Gbit/s-based transmissions, numerical simulations of 40 Gbit/s single-channel transmissions were conducted for both symmetrically and asymmetrically filtered signals. For the simulations, dispersion map 3 illustrated in Fig. 5-6 was used. Figure 5-13 shows the obtained Q-factors after 3,000 km transmission as a function of the bandwidth of the optical filter for trimming the signal bandwidth. The closed circles and squares show the results of symmetrically and asymmetrically signals, respectively. In addition, the transmission performance of no filtered RZ signal is also indicated as closed triangle in the figure.

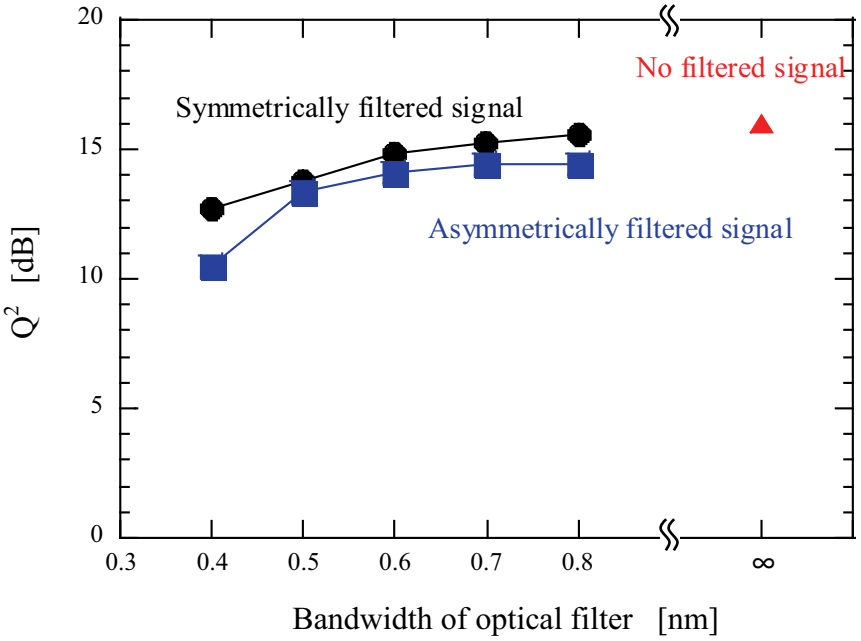

Fig. 5-13 40 Gbit/s single-channel performances after 3,000 km transmission as a function of the optical filter bandwidth for the bandwidth limitation.

The performances of symmetrically filtered signals were superior to those of asymmetrically filtered one for all the optical bandwidth, and the degradation by narrowing the filter bandwidth was relatively small in comparison with the asymmetrically filtered one. These results revealed that the symmetric filtering was desirable for the bandwidth limitation for 40 Gbit/s-based RZ signals.

5-4.2 WDM transmission experiments

The impact of the bandwidth limitation on WDM transmission performance was investigated through 40 Gbit/s x 25 WDM transmission experiments targeting a high spectral efficiency of 0.8 bit/s/Hz. Figure 5-14 shows the characteristics of the optical filter used for the spectral limitation. It has a flat 3 dB-passband of the 45 GHz bandwidth and sharp edges for mitigating the linear crosstalk from the adjacent channels in 50 GHz-spaced WDM systems.

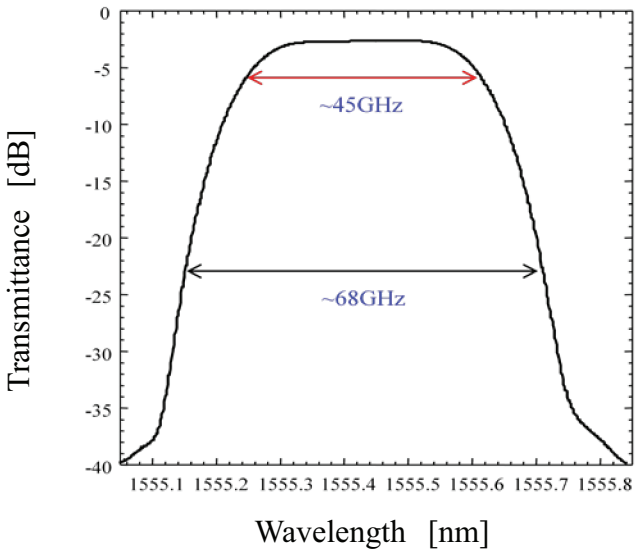

Fig. 5-14 Characteristics of the optical filter for the limitation of spectral bandwidth.

Figures 5-15 (a) and (b) show the optical spectra and waveforms of 40 Gbit/s RZ signal without and with the limitation of spectral bandwidth, respectively. In this experiment, the center wavelength of the filter is set to the signal wavelength for symmetric filtering. As shown in the figure, no significant waveform distortion was observed, while the spectral bandwidth was intentionally reduced.

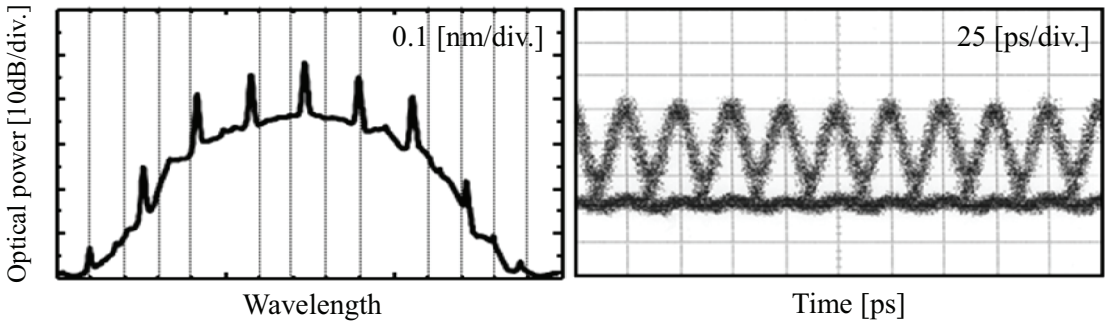

(a) no filtered signal spectrum and waveform

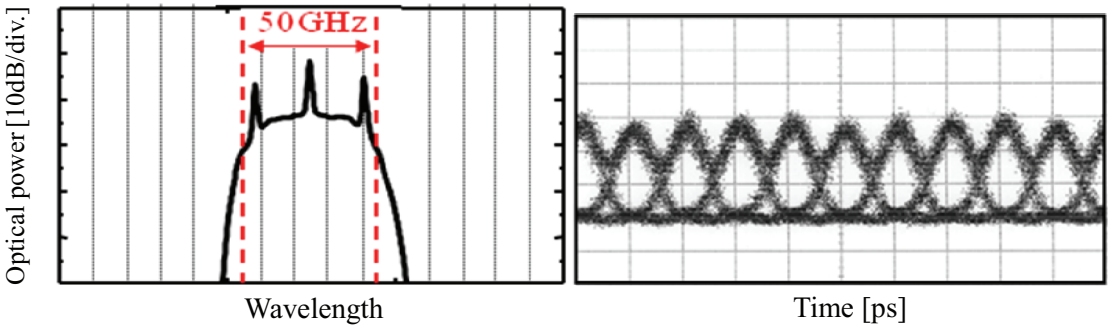

(b) symmetrically filtered signal spectrum and waveform

Fig. 5-15 Optical spectra and waveforms of 40 Gbit/s RZ signals.

Figure 5-16 shows a schematic diagram of the experimental setup. In the transmitter, twenty-five DFB-LDs were used and the wavelengths were equally spaced by 50 GHz from 1545.5 nm to 1555.2 nm. Even and odd channels were combined separately and fed into two modulators in cascade for data coding with a 2^{15}-1 pseudo-random binary sequence and RZ formatting to produce 10 ps signal pulses. Then, a 40 Gbit/s signal was generated by optical time-division-multiplexing (OTDM) in the same state of polarization. To mitigate the spectral overlapping between tightly-packed DWDM signals, optical filters with very sharp transmission characteristics as shown in Fig. 5-14 were used at the next stage. At the last stage of transmitter, the even and odd channels were combined using a polarization beam splitter and were launched into the transmission line in the orthogonal state of the polarization.

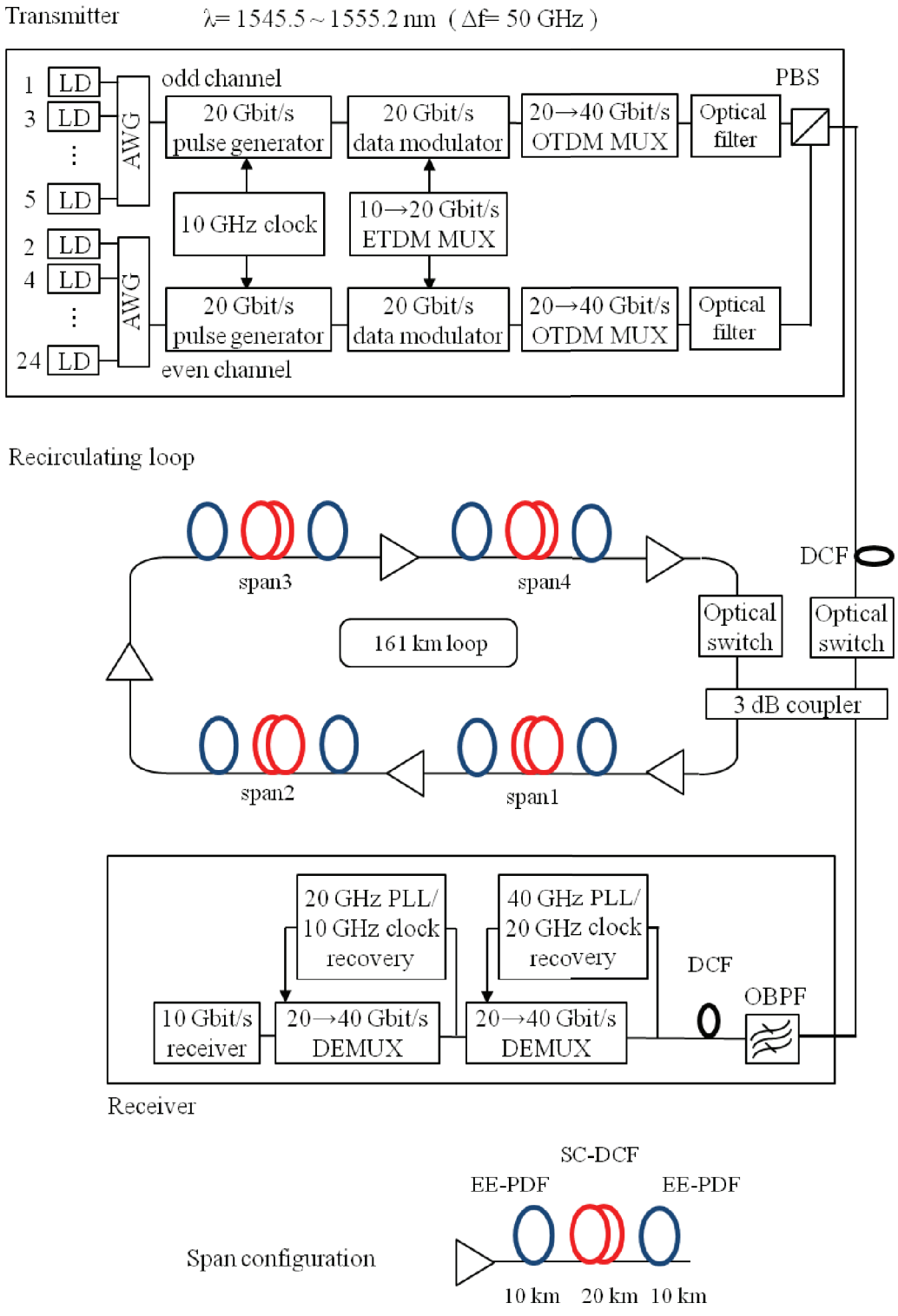

Fig. 5-16 Experimental setup.

The 161 km-long recirculating loop consisted of four spans of transmission fiber and five EDFA repeaters pumped at 980 nm. The average repeater output power was 12 dBm. The transmission line consisted of SMF-based EE-PDFs (effective-area-enlarged positive-dispersion fibers) and a SC-DCF to configure a dispersion-flattened fiber span reducing intra-span dispersion excursion.

The dispersion, dispersion slope, and effective area of EE-PDF were +20 ps/nm/km, +0.06 ps/nm^2/km, and 110 μm^2, respectively. The magnitudes of dispersion and dispersion slope of the SC-DCF was the same as ones of the EE-PDF, and the signs were opposite. The system dispersion at 1550 nm and dispersion slope of the transmission line were 0.03 ps/nm/km and -0.005 ps/nm^2/km, respectively. The loss of transmission spans including splice loss was 9.4 dB on average.

In the receiver, the measured channel was selected with a cascade of optical filters. Then, the transmitted 40 Gbit/s signals were optically time-division-demultiplexed to 10 Gbit/s signals with a two-stage optical gate using sinusoidally-driven polarization insensitive EA modulators. The transmission performance was evaluated with a BER averaged over four 10 Gbit/s demultiplexed channels. To obtain the best transmission performance, the accumulated dispersion for WDM channels was optimized with the DCFs inserted before and after the transmission line.

Firstly, in order to grasp the transmission characteristics of the optically bandwidth-limited signals, the impact of the bandwidth limitation on single channel and WDM transmissions were investigated. Figure 5-17 shows the BER characteristics of demultiplexed 10 Gbit/s signals for the single channel transmissions with and without bandwidth limitation and the four-WDM transmission with bandwidth limitation. Although the transmissible distance was reduced from 2,000 km to 800 km by using the bandwidth limitation, the inter-channel nonlinear crosstalk associated with the increase of channel number was considered to be moderate despite of the narrow channel spacing.

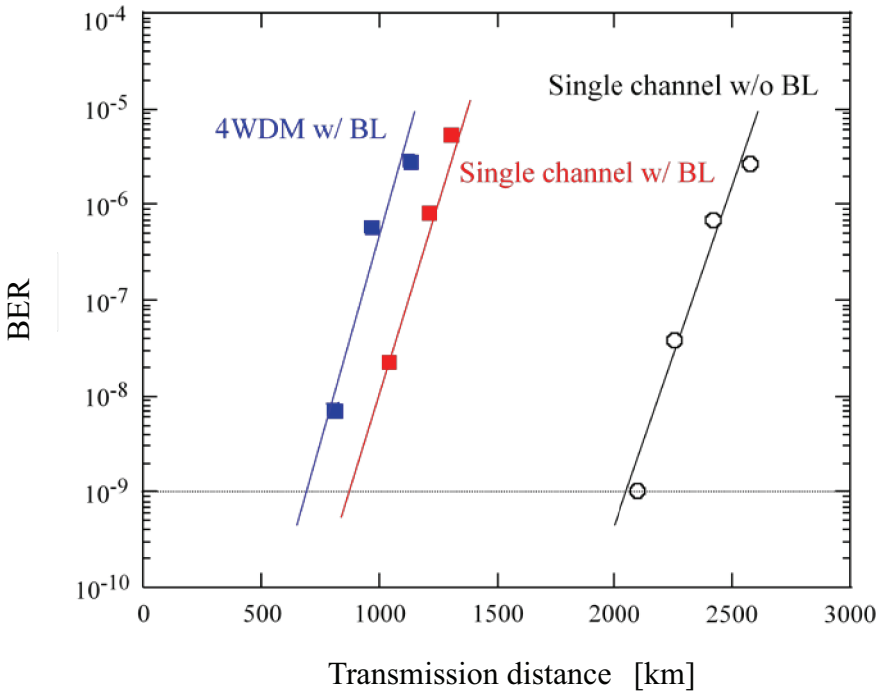

Fig. 5-17 BER performances of single channel transmissions with and without bandwidth limitation and four-WDM transmission with bandwidth limitation.

Figure 5-18 shows the BER characteristics of the demultiplexed 10 Gbit/s signals for 25 WDM channels. A BER of less than 1.0×10^{-9} was obtained for all the channels as the function of transmission distance. Figure 5-19 shows the typical waveforms of 40 Gbit/s signals and time-division-demultiplexed 10 Gbit/s signals after 640 km transmission. These waveforms were measured with a high-speed photodetector with 32 GHz bandwidth. Although the signal spectrum was trimmed significantly, the waveform was not distorted severely even after 640 km transmission.

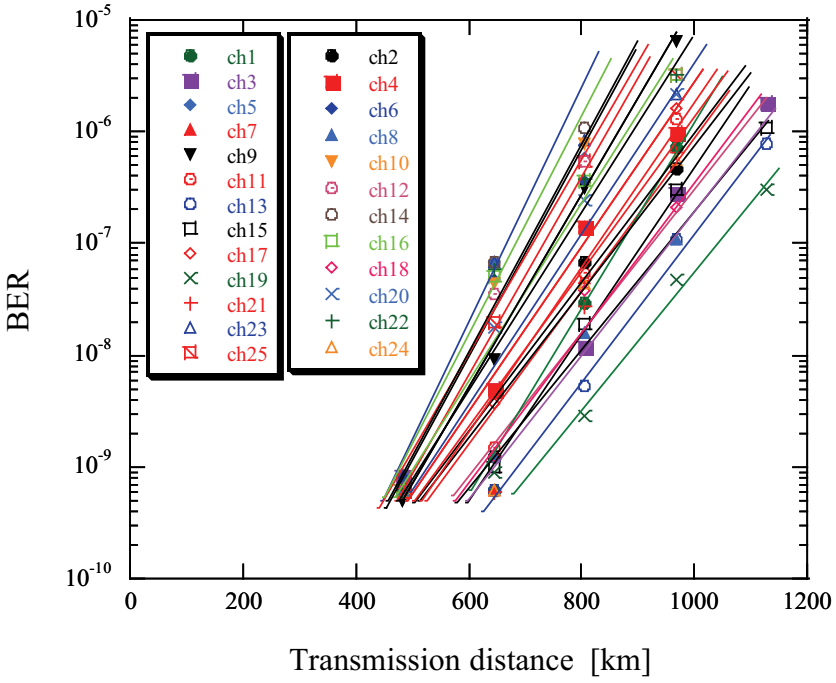

Fig. 5-18 BER performance of 25 WDM channels.

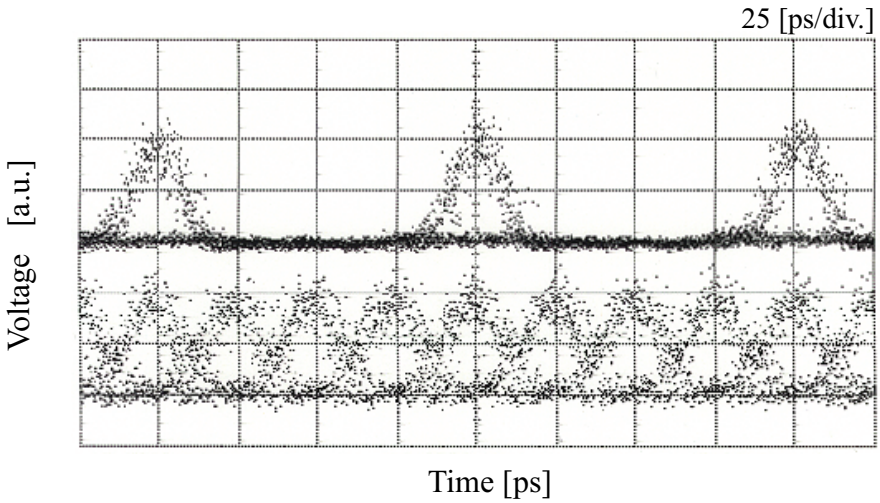

Fig. 5-19 Optical signal waveforms after 640 km transmission (upper : demultiplexed 10 Gbit/s, lower : 40 Gbit/s).

A 40 Gbit/s-based ultra-DWDM terabit-capable transmission over 480 km has been successfully demonstrated using 50 GHz-spaced bandwidth-limited RZ signals and the SMF-based dispersion-flattened transmission line without using polarization demultiplexing. The transmission distance over 480 km was more than double length of the previous report and the longest report for DWDM transmissions with the spectral efficiency of 0.8 bit/s/Hz.

It was proven that optical bandwidth limitation is quite effective for a high-density transmission and that by applying the scheme to the full bandwidth of EDFA, ultra large capacity transmission can be expected. The remaining problem for 40 Gbit/s-based transoceanic DWDM transmissions over transoceanic distances is to extend the transmissible distance. For achieving transoceanic transmissions, additional technologies are necessary in 40 Gbit/s-based systems.

5-5 Performance of optically filtered CS-RZ DPSK signal

Several kinds of RZ formats were proposed and investigated for long-haul transmissions [20]-[23], because the RZ waveform is more tolerant against fiber nonlinearities than NRZ format as explained in Appendix B. Among the RZ formats, CS-RZ is considered to be a promising format for high-speed long-haul transmissions. Regarding modulation scheme, DPSK is intensively studied instead of conventional OOK, and remarkable demonstrations of 40 Gbit/s-based DWDM transmissions have been reported. In this section, the optimum filtering condition for CS-RZ DPSK signals is numerically and experimentally investigated.

5-5.1 CS-RZ DPSK signal

Conventional RZ and CS-RZ signals have almost the same waveform in time domain, and only difference is the optical phase of the signals. In conventional optical communication systems where OOK modulation scheme is widely used, the RZ signal

has no phase difference between adjacent pulses, whereas the CS-RZ OOK signal has a phase difference of π. The optical phase is simultaneously encoded at the stage of the pulse-format generation by a Mach-Zehnder (MZ) intensity modulator. To generate a 40 Gbit/s RZ format, the MZ modulator is driven by the data-rate sinusoidal clock signal of 40 GHz with the amplitude of the half-wave voltage V_π. Since the bias is set to the middle point between the null and peak of the modulator curve, the phase between adjacent pulses does not change.

As for a 40 Gbit/s CS-RZ format, the MZ modulator is driven by the half data-rate sinusoidal clock signal of 20 GHz with the amplitude of 2 V_π. The bias is set to the null point of the modulator curve, and therefore the phase of the pulses alternate between 0 and π. This alternative phase property suppresses the carrier component and tightens the spectral bandwidth.

Figures 5-20 (a) and (b) show the signal spectra of RZ and CS-RZ formats, respectively. The carrier component of the CS-RZ signal spectrum is suppressed, and it mainly consists of two 20 GHz components.

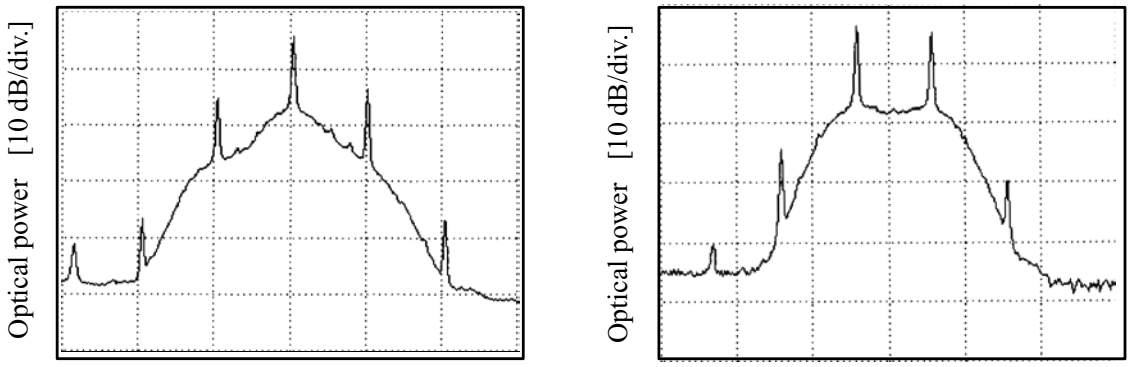

(a) RZ format (b) CS-RZ format

Fig. 5-20 Optical spectra of typical two 40 Gbit/s RZ formats.

The CS-RZ format has another advantage of a narrow spectral bandwidth relative to that of the RZ format, and it is considered to be preferable for the optical bandwidth filtering. Figures 5-21 (a) and (b) show the optical spectra and waveforms of RZ and CS-RZ signals with the 45 GHz-spectral bandwidth limitation, respectively. In the spectral bandwidth limitation, symmetric filtering was adopted to the signals. Applying the 45 GHz-filtering to the RZ signal, the 40 GHz-clock components in the optical spectrum was trimmed completely, and it made the waveform change to a NRZ-like shape. For the CS-RZ signal, the 20 GHz-clock components remained after filtering, and it kept a RZ-shaped waveform.

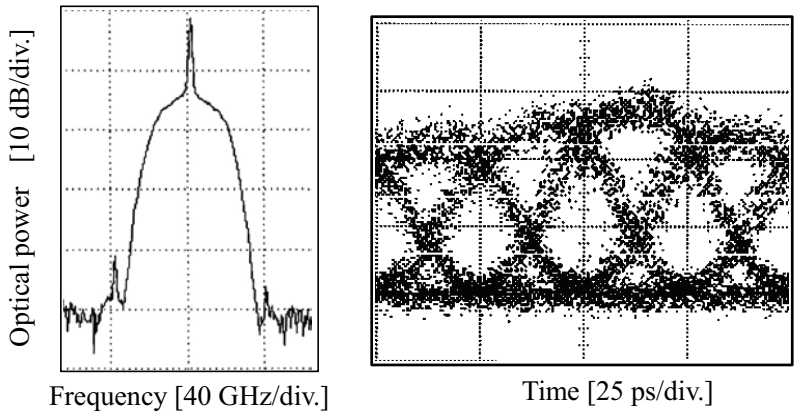

(a) RZ format

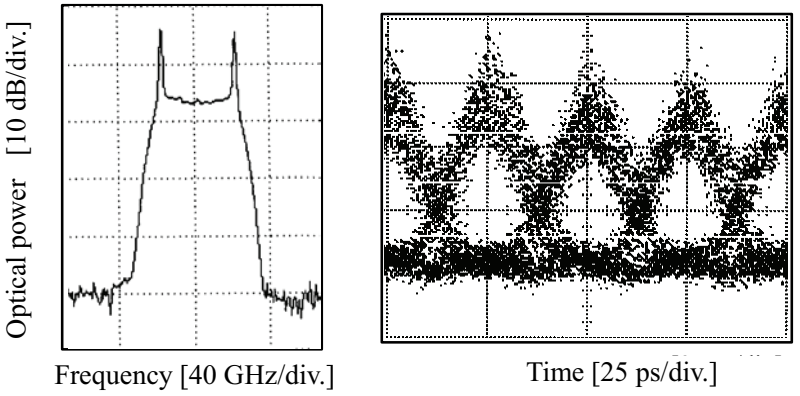

(b) CS-RZ format

Fig. 5-21 Optical spectra and waveforms of 40 Gbit/s bandwidth-limited signals.

DPSK modulation scheme has been intensively studied as an alternative to conventional OOK since it enables a 3 dB-higher receiver sensitivity and has higher tolerance against fiber nonlinearities. In particular, the high tolerance against XPM is an attractive feature in DWDM transmission systems. RZ-shaped DPSK signals convey binary digital data on its optical phase difference between adjacent pulses. The optical waveforms of RZ-shaped DPSK signals are always all-marked pattern, independently of the data pattern. It contributes the reduction of pattern-dependent XPM, whereas a random binary data pattern induces a relatively large penalties associated with XPM in OOK systems.

5-5.2 Back-to-back performance

As is described in the previous sections, the signal bandwidth limitation by optical filtering before transmission is a promising solution to achieve a high spectral efficiency. The transmission performance is severely affected by the optical filtering conditions for the bandwidth limitation in OOK systems, such as the offset of the center frequency and the bandwidth of the optical filter as shown in Fig. 5-22.

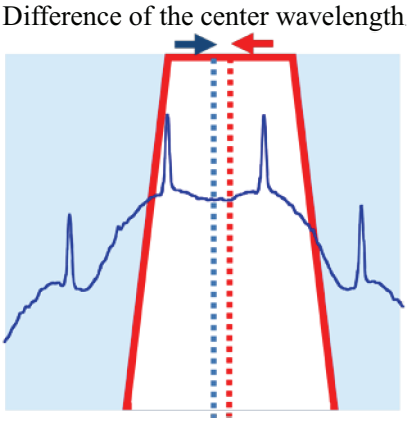

Fig. 5-22 Key parameters of optical spectral filtering.

In the DWDM systems where a narrow-bandwidth optical filter is used for the CS-RZ signal bandwidth limitation, an asymmetric filtering scheme is more beneficial in terms of the transmission performance, and the detailed studies on the asymmetric filtering have been reported for CS-RZ OOK signals. Regarding CS-RZ DPSK signals, however, similar study has not been reported yet.

In this section, the optimum filtering condition for CS-RZ DPSK signal is numerically and experimentally investigated. Firstly, the impact of optical filtering on the CS-RZ signal was evaluated for the back-to-back conditions.

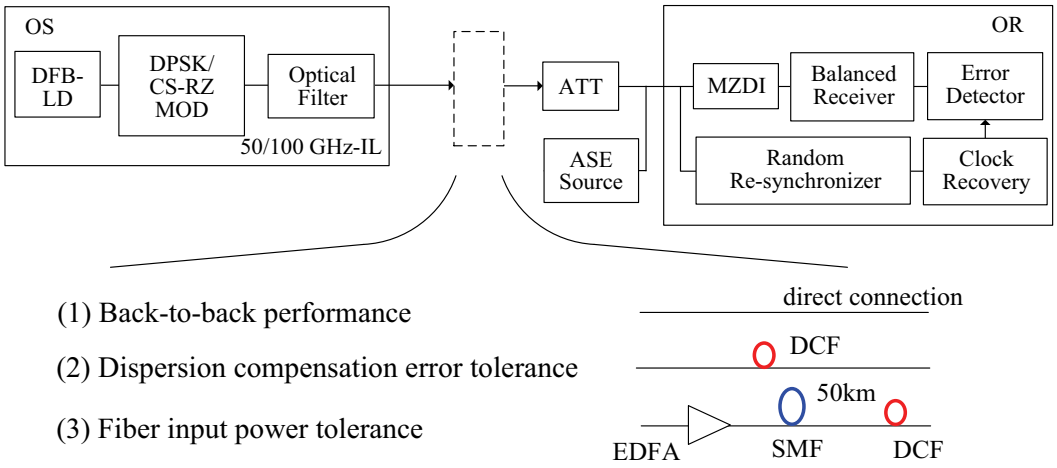

Fig. 5-23 Experimental setup for the evaluation of filter detuning characteristics, dispersion tolerance, and nonlinear tolerance.

Figure 5-23 shows the schematic experimental setup employed for the evaluations. In the transmitter, a DFB laser source and two $LiNbO_3$ modulators were used; one is for 42.7 Gbit/s data coding of the optical phase of the signal in NRZ format with a true 2^{31}-1 pseudo-random binary sequence, and the other is for bit-synchronous CS-RZ formatting. Then, the 42.7 Gbit/s CS-RZ DPSK signal was optically bandwidth-limited by using a 50/100 GHz interleaving device with a 3 dB/20 dB bandwidth of 45 GHz/68 GHz. Here, an ultra-dense WDM system with a spectral efficiency of 80 % was assumed. In the receiver, the DPSK signal was demodulated using a Mach-Zehnder delayed interferometer (MZDI) and detected by a balanced

receiver. The received 42.7 Gbit/s electrical signal was demultiplexed to 10.7 Gbit/s. To evaluate the signal performance, a BER averaged over the four tributary 10 Gbit/s data streams were measured using a random re-synchronization technique [11], and the corresponding Q-factor was calculated.

In the evaluation of the optimal pre-filtering condition, the transmitter and receiver were directly connected, and the back-to-back performance was measured by detuning the center frequency of the optical filter for the bandwidth limitation. Figure 5-24 shows the obtained Q-factor penalty due to optical bandwidth limitation for the 42.7 Gbit/s CS-RZ DPSK signal as a function of the filter detuning defined as the difference between the signal carrier frequency and the center frequency of the optical filter for bandwidth limitation. The nominal Q-factor of the unfiltered signal was set to 14.8 dB by adding the amplified spontaneous emission noise to simulate a long-distance transmission condition.

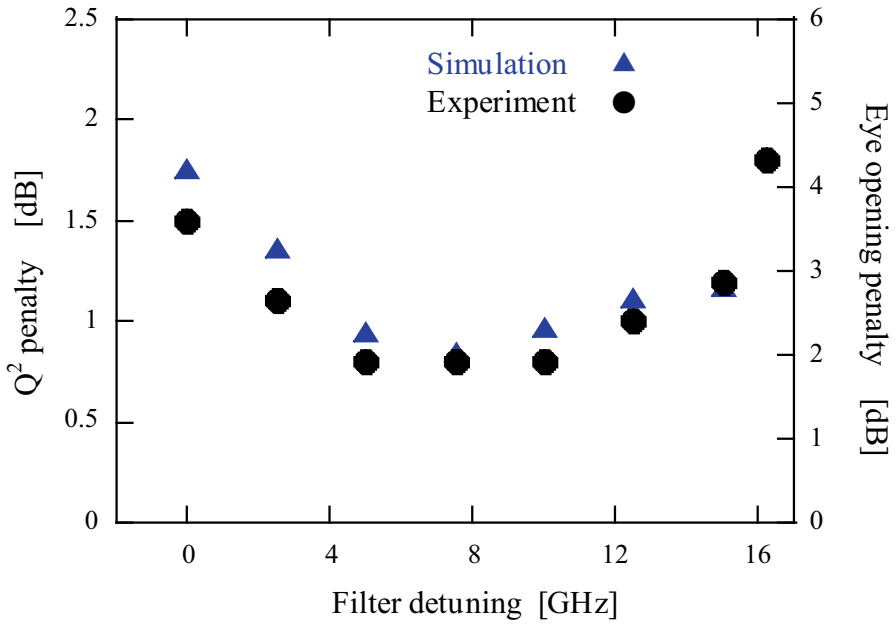

Fig. 5-24 Q-factor penalty due to bandwidth limitation as a function of filter detuning.

As shown in Fig. 5-24, the Q-factor penalty of the asymmetrically filtered signal due to the bandwidth limitation was distinctively lower than that of the symmetrically filtered signal, and the penalty was less than 1 dB. The penalties of less than 1 dB were observed in the filter tuning range of 7.5 +/- 2.5 GHz. It indicates that the asymmetrically filtered CS-RZ DPSK signal was robust against the center frequency fluctuations of the optical filter for the bandwidth limitation.

Next, in order to evaluate the characteristics of bandwidth-limited CS-RZ DPSK signals furthermore, numerical simulations were conducted in the same conditions illustrated in Fig. 5-23. The optical filter for the bandwidth limitation was assumed to be a 4^{th}-order Gaussian shape with a 3-dB bandwidth of 45 GHz, and the performance was estimated by eye-opening penalty.

The obtained results are indicated in Fig. 5-24 by closed triangles. As shown in Fig. 5-24, the simulation results agree well with the experimental results, and the asymmetric filtering showed a better performance than the symmetric one. In order to investigate the reason why the asymmetric filtering is advantageous over the symmetric one, the signal waveforms after the bandwidth limitation was observed. The bit-sequence waveforms of the symmetric and asymmetric filtering are shown in Fig. 5-25 (a) and (b), respectively. The amplitude of the mark pulses was largely fluctuated in symmetrically filtered signal, whereas it was a moderate level in asymmetrically filtered signal. From these results, it was considered that the additional Q-factor penalty of the symmetrically filtered signal was attributed to the fluctuation of the mark signal power level.

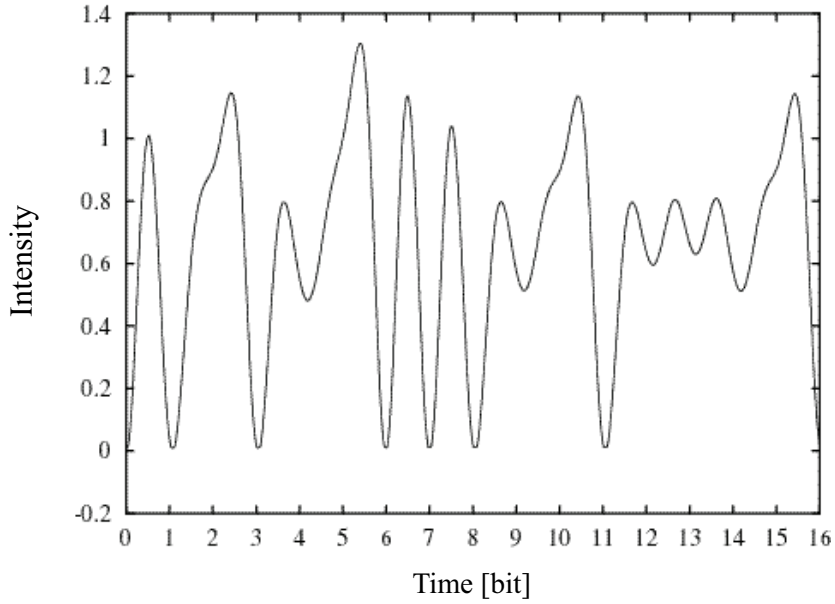

(a) symmetrically filtered signal

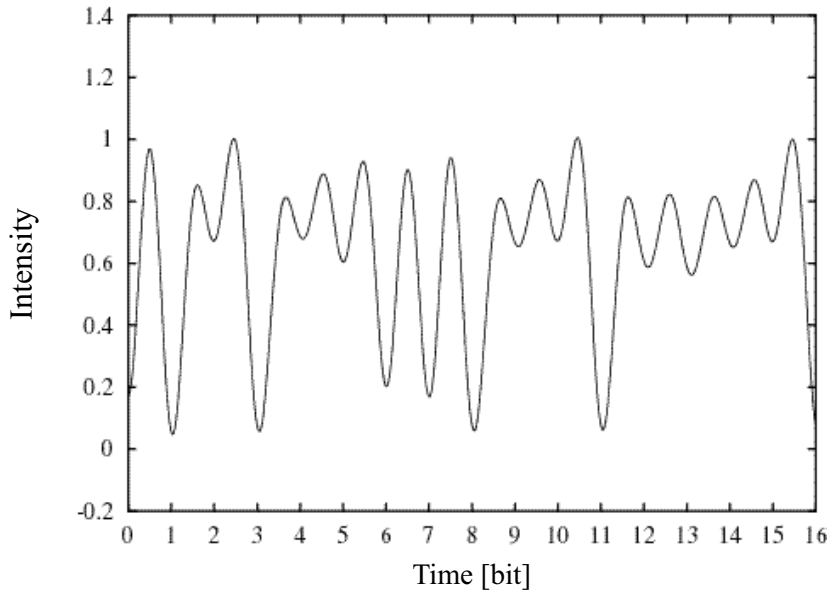

(b) asymmetrically filtered signal with 7.5 GHz detuning

Fig. 5-25. Waveforms of optically filtered 42.7 Gbit/s CS-RZ DPSK signals.

5-5.3 Dispersion and nonlinear tolerances

Next, the dispersion and nonlinear tolerances were respectively evaluated by measuring the penalties due to the mismatch of dispersion compensation at the receiver and the launch power increase to the transmission span for unfiltered, symmetrically filtered and asymmetrically filtered CS-RZ DPSK signals. The filter detuning for the asymmetric filtering was set to 7.5 GHz. In the evaluation of the dispersion tolerance, the signal from a transmitter was directly fed into DCFs. In the evaluation of the nonlinear tolerance, the transmission line consisting of a 50 km-long SMF followed by a DCF was used, in which the accumulated dispersion of the SMF was fully compensated for by the DCF.

Figures 5-26 (a) and (b) show the Q-factor penalty measured as a function of the dispersion compensation error and the fiber input power, respectively. The circles, triangles, and squares show the Q-factor penalties obtained by the experiments, and the solid, dot-dashed, and dashed lines show the eye opening penalties obtained by the numerical simulations for unfiltered, symmetrically, and asymmetrically filtered signals, respectively.

The acceptable dispersion compensation error for 1-dB Q-factor penalty was found to be 50 ps/nm for the unfiltered and asymmetrically filtered signals and 140 ps/nm for the symmetrically filtered signal. Note that this large dispersion error tolerance of symmetrically filtered CS-RZ-DPSK signal was not observed for the CS-RZ OOK signal [15], and it is a specific feature of optically pre-filtered CS-RZ DPSK signal.

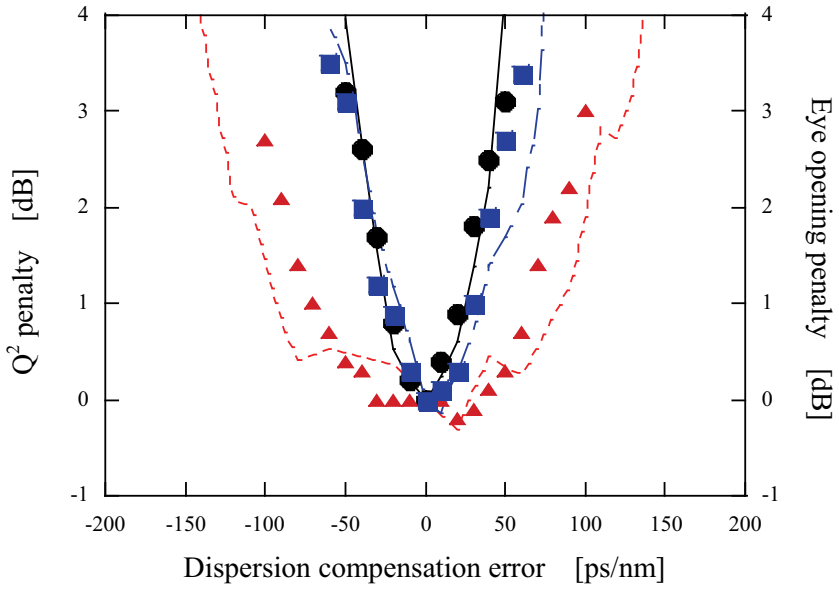

(a) dispersion tolerance

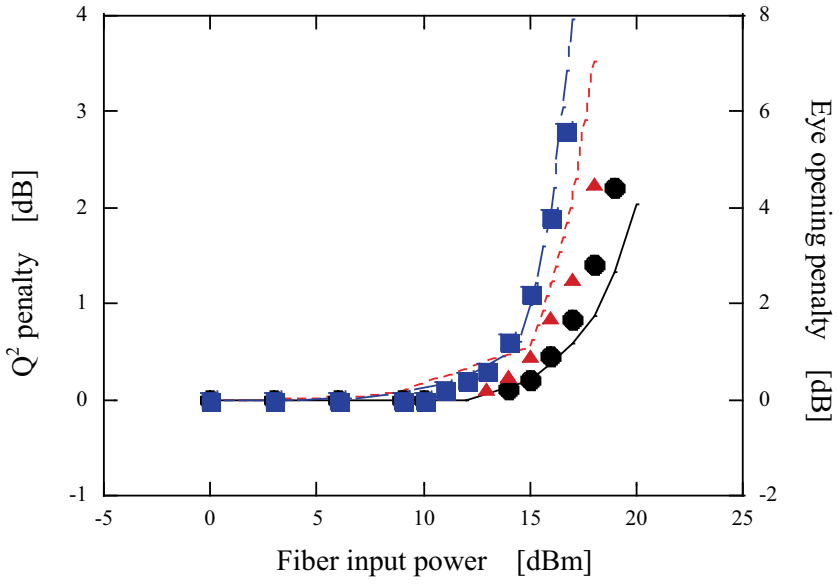

(b) nonlinear tolerance

Fig. 5-26 Tolerance of unfiltered (circles and solid lines), asymmetrically filtered (7.5 GHz detuning, squares and dot-dashed lines), and symmetrically filtered (triangles and dashed lines) 42.7 Gbit/s CS-RZ DPSK signals.

Regarding the nonlinear tolerance, for all the filtering conditions, almost no performance degradation was observed up to the fiber input power of 10 dBm. However, when the fiber input power exceeded 10 dBm, distinct penalty appeared in the order of asymmetrically, symmetrically filtered, and unfiltered signals. These were the same phenomena as the cases of CS-RZ OOK signals [15]. In both CS-RZ OOK and DPSK systems, the asymmetrically filtered signal showed a more vulnerable characteristic against fiber nonlinearities, while the back-to-back performance of them was better than symmetrically filtered ones [14], [15]. The asymmetric filtering broke the alternative phase balance between adjacent pulses of CS-RZ signals, and it induced an additional nonlinear chirping resulting in a vulnerable tolerance against the fiber input power.

5-5.4 WDM transmission experiments

Finally, in order to evaluate long-haul transmission performances of symmetrically and asymmetrically pre-filtered CS-RZ DPSK signals, a 50 GHz-spaced 64 x 42.7 Gbit/s transmission experiment up to 9,000 km was conducted. Figure 5-27 shows the experimental setup. In the transmitter, sixty-four DFB-LDs were employed and the wavelengths were equally spaced by 50 GHz between 1539.8 nm and 1565.1 nm. Even and odd channels were combined separately and fed into two cascaded $LiNbO_3$ modulators. The first modulator was driven by a 2^{31}-1 pseudo-random binary sequence for data coding in NRZ format, and the second one was driven by a 21.3 GHz sinusoidal wave for CS-RZ pulse formatting. Then, the even and odd channels were optically bandwidth-limited by using a 50/100 GHz interleaving devices with a 3-dB bandwidth of 45 GHz, and orthogonally polarization-multiplexed by using a polarization beam splitter (PBS). A 5 ns-time delay was used to de-correlate the even and add channels. At the last stage of the transmitter, all the channels were low-speed polarization-scrambled at 20 kHz to let the signal experience all the possible polarization dependence in the transmission line by using a polarization scrambler (PSCR).

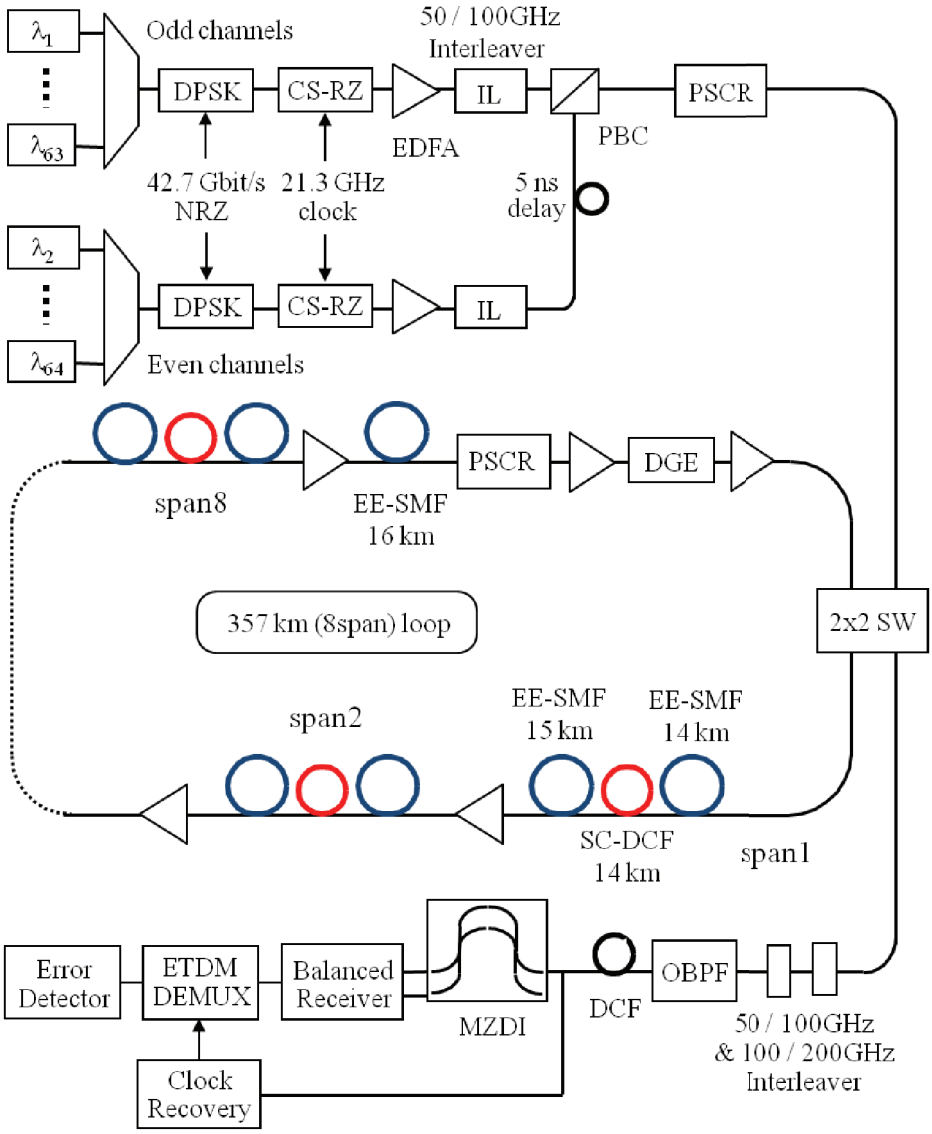

Fig. 5-27 Experimental setup.

The 357 km-long recirculating loop consisted of eight 43 km-long SMF-based spans and ten 980 nm-pumped EDFAs. The 43 km-long fiber span consisted of two EE-PDF interleaved with a SC-DCF. The dispersion, dispersion slope, and A_{eff} of the EE-PDF were around 20 ps/nm/km, +0.06 ps/nm^2/km, and larger than 110 μm^2, respectively. The dispersion characteristics of the SC-DCF were twice those of the EE-PDF with an A_{eff} of around 30 μm^2. The system dispersion of the loop was adjusted to +0.03 ps/nm/km at 1550 nm by inserting a 16 km-long EE-PDF. The

repeater output power was set to +13 dBm. In order to emulate various kinds of conceivable polarization state of the transmission line during the evaluation, a low-speed PSCR operating at 10 kHz was inserted in the loop.

In the receiver, the measured channel was selected with optical filters and the dispersion was equalized. Then, the selected signal was demodulated by a Mach-Zehnder delayed interferometer (MZDI) and detected by a balanced receiver. The received 42.7 Gbit/s signal was electrically-demultiplexed to 10.7 Gbit/s. The transmission performance was evaluated by measuring a BER averaged over the four 10 Gbit/s data streams.

Figure 5-28 shows the transmission performance of symmetrically and asymmetrically 3.8 GHz-detuning filtered signals for the repeater output power of -5 dBm/channel and -6 dBm/channel, respectively, to clarify the performance differences in terms of fiber nonlinearities. The solid and dashed lines show the results for repeater output powers of -6 dBm/channel and -5 dBm/channel, respectively. The circles and triangles show the results of symmetrically and asymmetrically filtered signals, respectively.

From Fig. 5-28, it was found that the performance of symmetric filtering was superior to that of asymmetric one up to 7,000 km transmission, while asymmetric filtering become more effective than symmetric one at distances longer than 7,000 km. For 6,000 km transmission with a higher repeater output power of –5 dBm/channel, the Q-factor calculated from the obtained BER was 11.1 dB and 11.7 dB for asymmetrically 7.5 GHz- and 3.8 GHz-detuning filtered signals, and 12 dB for symmetrically filtered signal. On the other hand, for 9,000 km transmission with –6 dBm/channel repeater output, the Q-factor calculated from the obtained BER was 9.6 dB and 9.7 dB for asymmetrically 7.5 GHz- and 3.8 GHz-detuning filtered signal, 9.3 dB for symmetrically filtered signal. In order to obtain a better performance over 7,000 km, the repeater output power had to be decreased from -5 dBm/channel to -6 dBm/channel for mitigating fiber nonlinearities. In this situation, the asymmetric filtering was found to be more beneficial than the symmetric filtering mainly owing to the advantage of the back-to-back performance.

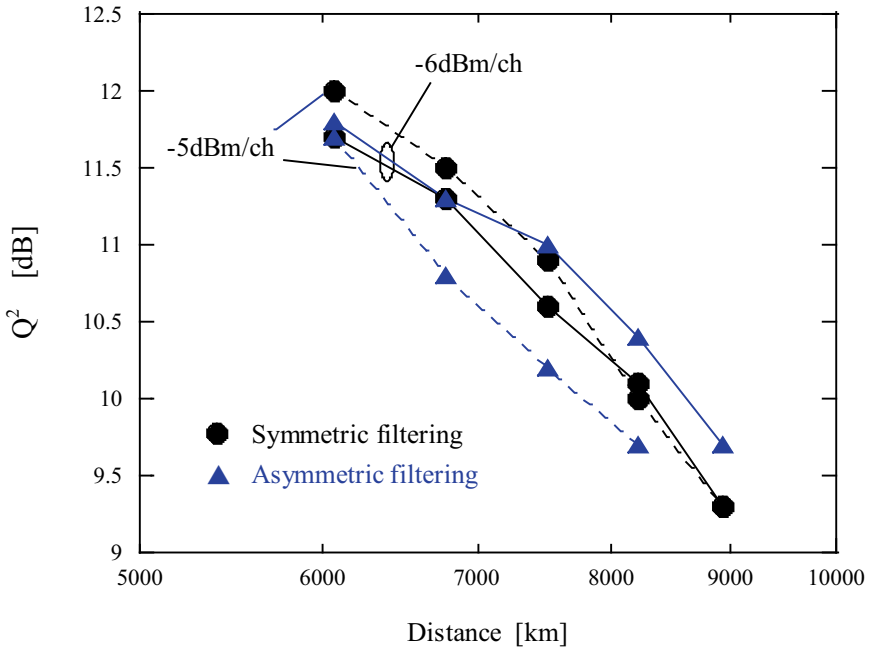

Fig. 5-28 Long-haul transmission performance of 42.7 Gbit/s symmetrically and asymmetrically 3.8-GHz detuning filtered CS-RZ DPSK WDM signals.

Several schemes have been studied to extend the transmissible distance of 50 GHz-spaced 40 Gbit/s-DWDM transmission systems, such as the adoption of the optical spectral bandwidth limitation, CS-RZ format, and DPSK modulation. Thought the numerical and experimental studies, it was found that even by using the advanced modulation schemes for mitigating fiber nonlinearities, the optical SNR has to be decreased to suppress the nonlinearities which severely degrade the performance at transpacific distances. Additional technologies are necessary to achieve a 40 Gbit/s-based high-density WDM transmission over a transpacific distance.

The advance of LSI technologies enables us to use sophisticated FEC codes, which was considered to be inapplicable to commercial systems due to its complexity and large latency characteristics. They have an advantage of high FEC gains compared with conventional RS (255, 239) code. For example, by concatenating two FEC codes of RS (255, 247) and RS (247, 239), an additional FEC gain of 6.5 dB is expected, while both FEC codes have the same FEC overhead of 7 % which is included in channel

bit rate of 42.7 Gbit/s. By using this concatenated FEC code of RS (255, 247) and RS (247, 239) with four iterations, the input Q-factor of 9.1 dB is enough for obtaining a bit-error free transmission after the decoding [23]. This indicates that a 40 Gbit/s-based transoceanic transmission is feasible with a spectral efficiency of 0.8 bit/s/Hz by using the advanced FEC.

5-6 Conclusion

The feasibility of a 40 Gbit/s-based DWDM transoceanic transmission was investigated through numerical and experimental studies. Firstly, the impact of nonlinear crosstalk in SMF-based transmission lines was evaluated, and it was found that the transmission performance is not so sensitive to the increase of WDM channel number, and the penalty due to nonlinear crosstalk was as small as less than 1 dB up to 16 channel counts. Owing to the small inter-channel interactions in the SMF-based systems, a 40 Gbit/s-based ultra-DWDM terabit-capacity transmission over 480 km was successfully demonstrated using 50 GHz-spaced spectral bandwidth-limited RZ signals which dramatically reduce the overlapping of WDM signal spectrum between adjacent channels. The transmission distance over 480 km was the longest ever reported for DWDM transmission in the spectral efficiency of 0.8 bit/s/Hz without using polarization demultiplexing. The dispersion map was numerically and experimentally optimized for 40 Gbit/s WDM transmission systems, and the transmissible distance was extended to larger than 2,000 km by adopting the dispersion map reducing intra-channel interactions.

The system configurations using CS-RZ format, DPSK modulation, and advance FEC technology were confirmed to be beneficial to enhance the transmission performance. The impact of optical spectral bandwidth limitation for 42.7 Gbit/s CS-RZ DPSK signals was experimentally and numerically investigated. By detuning the center wavelength of the optical filter for the signal-bandwidth limitation, the back-to-back performance was distinctively improved, which is corresponding to asymmetrically filtered signal condition. In contrast, it was observed that the

asymmetrically filtered signal showed slightly less tolerable characteristic against fiber nonlinearities in the evaluation using a single fiber span, because the asymmetric filtering deteriorates the optical phase conditions between adjacent pulses which convey the information signals. Through the transmission experiments to reveal the trade-offs among the back-to-back performance, dispersion, and nonlinear tolerances in total, the asymmetrically pre-filtering was found to be more effective in quasi-linear DPSK DWDM systems where fiber nonlinearities were not induced so much to deteriorate the advantageous back-to-back performance. In addition, it was demonstrated that a 40 Gbit/s-based transoceanic transmission was feasible with a spectral efficiency of 0.8 bit/s/Hz by adopting the concatenated FEC code of RS (255, 247) and RS (247, 239) with four iterations.

References

[1] I. Morita, K. Tanaka, N. Edagawa, S. Yamamoto, and M. Suzuki, “40 Gbit/s single-channel soliton transmission over 8600 km using periodic dispersion compensation”, Electron. Lett., vol. 34, pp. 1863-1865, 1998.

[2] I. Morita, K. Tanaka, N. Edagawa, and M. Suzuki, “40 Gbit/s single-channel soliton transmission over transoceanic distances by reducing Gordon-Haus timing jitter and soliton-soliton interaction”, IEEE/OSA J. Lightwave Techol., vol. 17, pp. 2506-2511, 1999.

[3] I. Morita, K. Tanaka, N. Edagawa, and M. Suzuki, “40 Gbit/s single-channel soliton transmission over 10,200 km without active inline transmission control”, ECOC’98, vol.3 pp. 47-51, 1998.

[4] T. Tsuritani, A. Agata, K. Imai, I. Morita, K. Tanaka, T. Miyazawa, N. Edagawa, and M. Suzuki, “35 GHz-spaced-20 Gbps × 100 WDM RZ transmission over 2700 km using SMF-based dispersion flattened fiber span”, ECOC2000, PD1.5, 2000.

[5] S. Bigo, A. Bertaina, Y. Frignac, S. Borne, L. Lorcy, D. Hamoir, D. Bayart, J. Hamaide, W. Idler, E. Lach, B. Franz, G. Veith, P. Sillard, L. Fleury, P. Guenot, and P. Nouchi, ”5.12 Tbit/s (128 x 40 Gbit/s WDM) transmission over 3 x 100 km of Teralight fibre”, ECOC2000, PD.1.2, 2000.

[6] W. Idler, S. Bigo, Y. Frignac, B. Franz, and G. Veith, “Vestigial side band demultiplexing for ultra high capacity (0.64 bit/s/Hz) transmission of 128 x 40 Gb/s channels”, OFC2001, MM3, 2001.

[7] G. Charlet, W. Idler, R. Dischler, J.-C. Antona, P. Tran, and S. Bigo, “3.2 Tbit/s (80 x 42.7 Gb/s) C-band transmission over 9 x 100 km of TeraLight fiber with 50 GHz channel spacing”, OAA2002, PDP1, 2002.

[8] J. -X. Cai, M. Nissov, C. Davidson, Y. Cai, A. Pilipetskii, H. Li, M. Mills, R. -M. Mu, U. Feiste, L. Xu, A. Lucero, D. Foursa, and N. Bergano, “Transmission of thirty-eight 40 Gb/s channels (> 1.5 Tb/s) over transoceanic distance”, OFC2002, PD-FC4, 2002.

[9] T. Tsuritani, I. Morita, N. Yoshikane, K. Imai, and N. Edagawa, “40 GHz-spaced 21.4 Gbit/s x 82 WDM VSB-RZ transmission over 8260 km using Raman/EDFA

hybrid repeaters and symmetrically dispersion-managed fibre", ECOC2002, 9.1.4, 2002.

[10] G. Charlet, J.-C. Antona, S. Lanne, P. Tran, W. Idler, M. Gorlier, S. Borne, A. Klekamp, C. Simonneau, L. Pierre, Y. Frignac, M. Molina, F. Beaumont, J.-P. Hamaide, and S.Bigo, "6.4 Tb/s (159 x 42.7 Gb/s) capacity over 21 x 100 km using bandwidth-limited phase-shaped binary transmission", ECOC2002, PD4.1, 2002.

[11] I. Morita, T. Tsuritani, N. Yoshikane, A. Agata, K. Imai, and N. Edagawa, "100 % spectral-efficient 25 x 42.7 Gbit/s transmission using asymmetrically filtered CS-RZ signal and a novel crosstalk suppressor", ECOC2002, PD4.7, 2002.

[12] A. Agarwal, S. Banerjee, D. Grosz, A. Kung, D. Maywar, A. Gurevich, and T. Wood, "Ultra-high-capacity long-haul 40-Gb/s WDM transmission with 0.8-b/s/Hz spectral efficiency by means of strong optical filtering", IEEE Photon. Technol. Lett., vol.15, pp.470-472, 2003.

[13] G. Charlet, J. Antona, S. Lanne, and S. Bigo, "From 2100 km to 2700 km distance using phase-shaped binary transmission at 6.3 Tbit/s capacity", OFC2003, WE3, 2003.

[14] T. Tsuritani, I. Morita, A. Agata, and N. Edagawa, "Study on optimum optical pre-filtering condition for highly spectral-efficient ultralong-haul transmission using 40Gbit/s CS-RZ signal and all-Raman repeaters", OFC2003, FE4, 2003.

[15] A. Agata, I. Morita, T. Tsuritani, and N. Edagawa, "Characteristics of asymmetrically filtered 40Gbit/s CS-RZ signals", OFC2003, MF78, 2003.

[16] A. H. Gnauck, G. Raybon, S. Chandrasekhar, J. Leuthold, C. Doerr, L. Stulz, and E. Burrows, "25 x 40-Gb/s co-polarized DPSK transmission over 12 x 100-km NZDF with 50-GHz channel spacing", IEEE Photon. Technol. Lett., vol.15, pp.467-469, 2003.

[17] B. Zhu, L. E. Nelson, S. Stulz, S. Gnauck, C. Doerr, J. Leuthold, L. Gruner-Nielsen, M. O. Pedersen, J. Kim, R. Lingle, Y. Emori, Y. Ohki, N. Tsukiji, A. Oguri, and S. Namiki, "6.4-Tb/s (160 x 42.7 Gb/s) transmission with 0.8 bit/s/Hz spectral efficiency over 32 x 100 km of fiber using CSRZ-DPSK format", OFC2003, PD19, 2003.

[18] T. Tsuritani, K. Ishida, A. Agata, K. Shimomura, I. Morita, T. Tokura, H. Taga, T. Muzouchi, and N. Edagawa, “70 GHz-spaced 40 x 42.7 Gbit/s transmission over 8700 km using CS-RZ DPSK signal, all-Raman repeaters and symmetrically dispersion fiber span”, OFC2003, PD23, 2003.

[19] T. Ito, K. Fukuchi, K. Sekiya, D. Ogasawara, R. Ohhira, and T. Ono, “6.4 Tb/s (160 x 40 Gb/s) WDM transmission experiment with 0.8 bit/s/Hz spectral efficiency”, ECOC2000, PD1.1, 2000.

[20] Y. Miyamato, A. Hirano, K. Yonenaga, A. Sano, H. Toba, K. Murata, and O. Mitomi, “320 Gbit/s (8 x 40 Gbit/s) WDM transmission over 367 km with 120 km repeater spacing using carrier-suppressed return-to-zero format”, Electron. Lett., vol. 23, pp.2041-2042, 1999.

[21] R. Ohhira, D. Ogasawara, and T. Ono, “Novel RZ signal format with alternate-chirp for suppression of nonlinear degradation in 40 Gb/s based WDM”, OFC2001, WM2, 2001.

[22] Y. Miyamato, A. Yonenaga, A. Hirano, H. Toba, K. Murata, and H. Miyazawa, “Duobinary carrier-suppressed return-to-zero format and its application to 100 GHz-spaced 8 x 43-Gbit/s DWDM unrepeatered transmission over 163 km”, OFC2001, TuU4, 2001.

[23] T. Tsuritani, A. Agata, I. Morita, and N. Edagawa, “21.4 Gbit/s x 56 WDM 9170 km transmission using symmetrically dispersion-managed fibre span”, ECOC2001, PD. M1.6, 2001.

Chapter 6

Capacity upgrade of JIH system using 40 Gbit/s-based WDM transmission technologies

6-1 Introduction

The transmissible capacity of optical submarine system has increased more than 1,000-fold and has reached more than terabit even over transoceanic distances at the research stage [1]-[4]. Such a rapid progress has greatly shortened the effective life time of the existing systems. Submarine cable systems are designed with a 25-year life expectancy. New technologies emerged in the life expectancy makes the systems an out-of-date ones in several years. In order to extend the system life time and recoup the investment, the capacity upgrade of the existing systems has been a crucial issue for the system owners.

Although there are many key parameters in designing the systems such as the repeater spacing, the launch power, and the dispersion management of the repeatered line, the only way to enlarge the system capacity of the existing submarine cable systems is to increase spectral efficiency (i.e. bandwidth efficiency) by using advanced terminal technologies. In practical, the installed undersea transmission line and equipments cannot be replaced.

Two approaches can be considered for the system upgrade. The first approach is to increase of the WDM channel count by using the same channel bit rate. As the EDFA bandwidth is the order of 20 nm, the channel spacing must be narrower. For example, for 8-fold capacity upgrade, 100 GHz-channel spacing has to be narrowed to 12.5 GHz, and the number of WDM channels to be supervised becomes 8 fold.

The use of higher channel bit rate is another approach for upgrading the system capacity. This approach can sidestep the problems of increasing the WDM channel number, and be considered to be preferable from practical viewpoints of lower terminal cost, less power consumption, and smaller footprint. In particular, the capacity

upgrade of DSF-based transmission systems using NRZ format has been an upcoming problem, because these were widely deployed for gigabit-capable submarine cable systems. However, for higher channel bit rate WDM systems using a DSF-based transmission line, the nonlinear impairments are the concerns for the system design, and the technologies to alleviate fiber nonlinearities are necessary.

The candidates are advanced signal format, modulation scheme, and FEC [5]-[11]. The trade-offs in the selection of the upgrade technologies are cost and performance, and it is important to design the upgrade system in order to satisfy the required performance quality with the minimum cost on the provided conditions.

In this chapter, the possibility of more than 16-fold capacity upgrade of Japan Information Highway (JIH) submarine cable system was studied for targeting terabit-capacity transmissions. JIH has the aggregate per-fiber capacity of around 50 Gbit/s using 2.5 Gbit/s-based WDM technologies with 100 GHz-spaced NRZ signals [12]. To achieve more than 16-fold capacity upgrade to terabit capacity in JIH system, various technical issues and practical aspects must be deliberated on the condition that the transmission fiber is non-slope-matched NZ-DSF and the repeater is a 1.48 μm-pumped EDFA with the output power of +8 dBm. In the following sections, the upgradability of the longest and typical segments of JIH system was numerically and experimentally investigated by applying the terminal technologies of FEC and signal formats. Through these studies, the feasibility of a 100 GHz-spaced 25 x 42.7 Gbit/s transmission is demonstrated for both segments by using proper FEC technology and signal formats.

6-2 JIH submarine cable system

JIH consists of 10,300 km-long cables with seventeen landing stations and links all the main islands of the Japanese archipelago as shown in Fig. 6-1. In addition to domestic large-capacity traffics, the JIH carries transit traffics among international submarine cables.

The cable consists of three fiber pairs and supports 2.5 Gbit/s-based fourteen WDM

channels with the total capacity of more than 100 Gbit/s. High system reliability is also provided by using double-landing and double-branching schemes with a self-healing function.

To evaluate the potential of the capacity upgrade of JIH system, two typical segments of Segment (A) and (B) in Fig. 6-1 are focused. The 1,500 km-long Segment (A) connecting Sendai and Naoetsu cities is the longest one in the system, and two sets of in-line dispersion compensation fiber are inserted. The 600 km-long Segment (B) connecting Chikura and Shima cities is a typical one, and the residual dispersion in this segment becomes larger than that of Segment (A) because no in-line dispersion compensation is adopted.

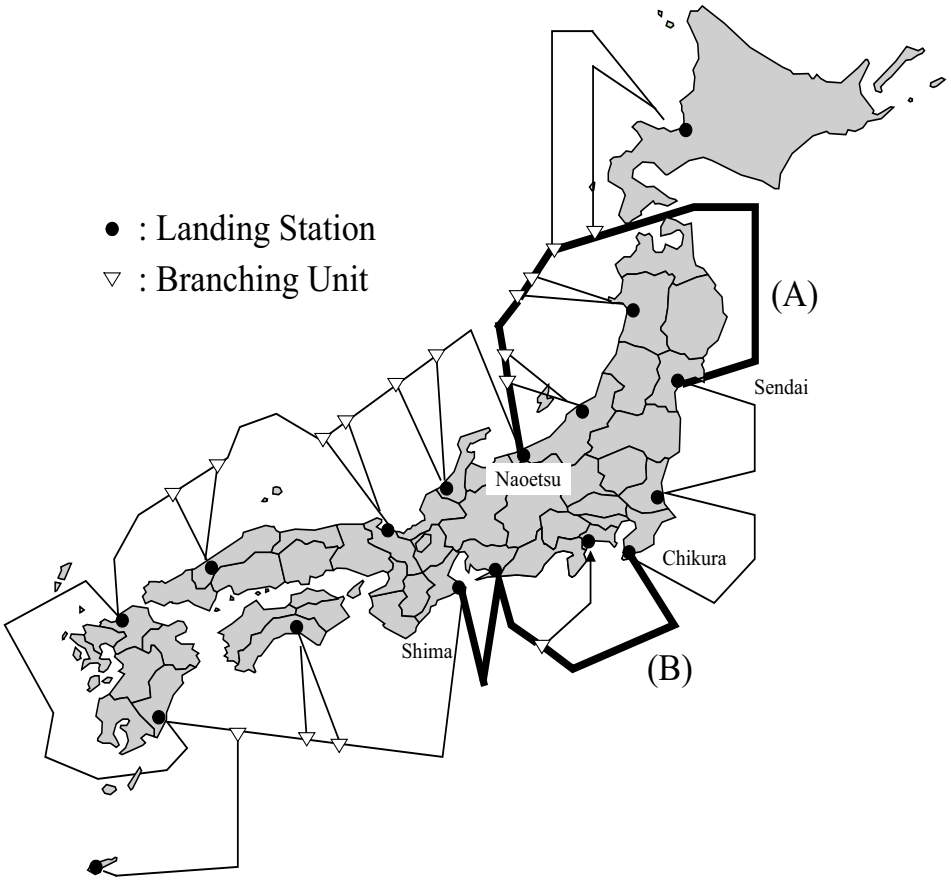

Fig. 6-1 JIH submarine cable system.

6-3 Upgrade methodology

Two methodologies are considered in upgrading the capacity of existing cable systems as shown in Fig. 6-2. One is to increase the number of WDM channel by narrowing the channel spacing, and the other is to increase the channel bit rate. For upgrading 2.5 Gbit/s-based WDM systems with a total capacity of 1 Tbit/s, the former method requires 400 WDM channels. In contrast, the method to use 40 Gbit/s-based WDM signals by increasing the channel bit rate is more practical in terms of the terminal cost, footprint, and power consumption.

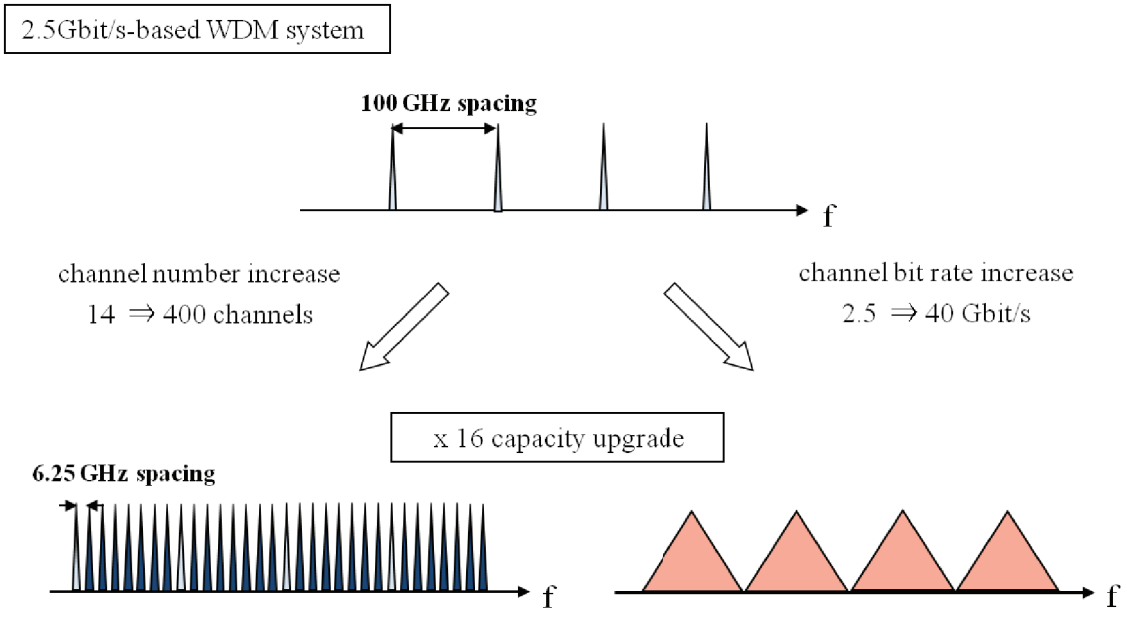

Fig. 6-2 Two upgrade methodologies: increasing the channel count and bit rate.

For achieving a 40 Gbit/s-based terabit-capacity WDM transmission on the condition that the transmission line and repeater output power cannot be changed, a suitable choice of terminal technologies are necessary to enhance the transmission performance. In this study, the adoptions of proper FEC and signal format are considered for 40 Gbit/s-based WDM transmissions in JIH system. The FEC is a proven and reliable

technology to enhance transmission performances and has already been employed in commercial submarine applications with redundancies range from 7 % to 23 % [13]-[15]. The redundancy and sort of the FEC are to be considered system design parameters. A large redundancy can achieve a higher FEC gain, although it induces a larger transmission penalty due to the increase of the bit rate.

The use of proper signal format is also important since 40 Gbit/s signals are much more vulnerable to nonlinearities and chromatic dispersion of the transmission fiber than 2.5 Gbit/s signals. As the candidates of signal formats, chirped RZ and CS-RZ are investigated in addition to NRZ [5], [6], because these are commercially available and not so sophisticated and affordable signal formats.

6-4 Numerical simulations of 1 Tbit/s transmission system for capacity upgrade

In this section, the possibility of the capacity upgrade to 1 Tbit/s is numerically investigated by using a proper signal format and FEC code for 40 Gbit/s-based WDM transmission systems.

6-4.1 Simulation model

Figure 6-3 shows a schematic diagram of the WDM system model assumed in the numerical simulations.

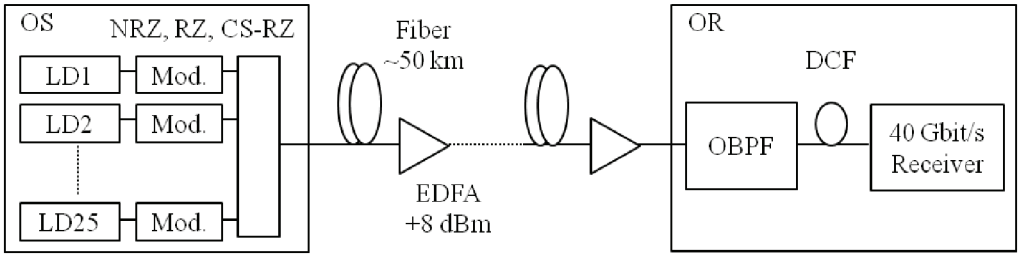

Fig. 6-3 Simulation model.

At the transmitter, each 100 GHz-spaced 42.7 Gbit/s signal with NRZ, RZ, or CS-RZ format was multiplexed in the same state of polarization between adjacent channels, which was supposed to be the worst case scenario in terms of transmission performance. The duty ratio of RZ and CS-RZ signals were assumed to be 0.4 and 0.66 respectively, and the word length was 128 for all the formats. At the receiver, the WDM signals were demultiplexed by using an optical bandpass filter whose spectral profile was 4^{th}-order super Gaussian shape with a 3 dB-bandwidth of 75 GHz. Regarding FEC, a typical RS (255, 239), which is standardized in ITU-T G. 975 and has 7 % overhead, was assumed. For the 1,500 km-long Segment (A) transmission, the required Q-factor after FEC decoding is estimated to be about 17 dB including the end of life margin on the condition that the Q-factor must satisfy ten times as high quality as the Q-factor described in ITU-T G. 826. Figure 6-4 shows the decoded Q-factor as a function of the input Q-factor for RS codes with a code rate of 93.7%, 87.5%, and 81.2% [16]. A code rate of 93.7 % indicates RS (255, 239) code. The difference between the dashed straight line and each curve in the figure represents the expected FEC gain for input Q-factors.

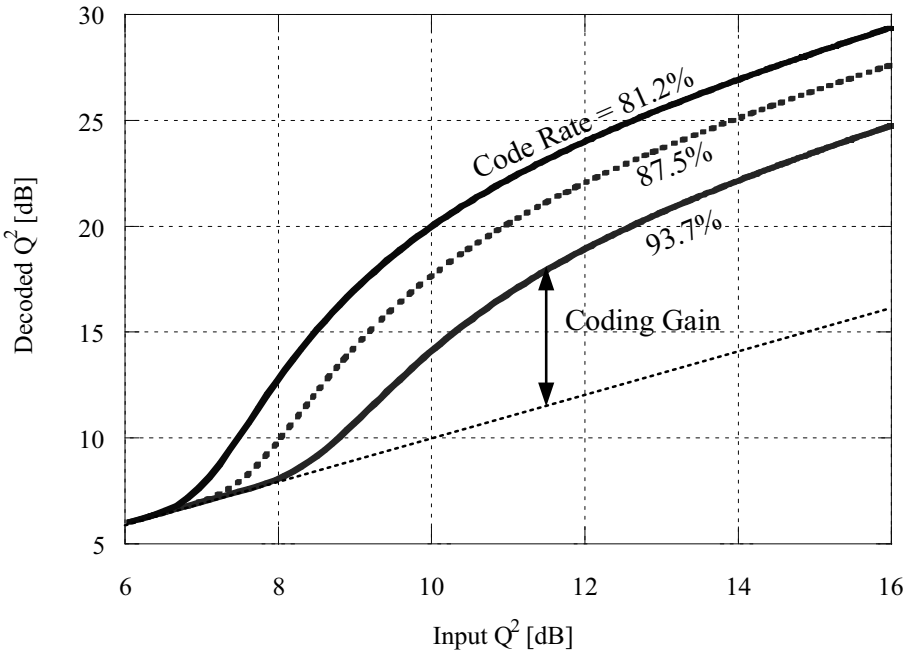

Fig. 6-4 Coding gain of RS codes.

From Fig. 6-4, a Q-factor of more than 11 dB before FEC decoding is required to satisfy the decoded Q-factor of 17 dB by using a code rate of 93.7%. For the 600 km-long Segment (B) transmission, the required Q-factor before FEC decoding will be less than 11 dB. Note that these thresholds are expected to be reduced when advanced FEC codes can be applied [17].

The transmission line consists of 50 km-long NZ-DSF spans and 1.48 μm-pumped EDFAs. The average transmission loss, dispersion, dispersion slope, and effective core area of the NZ-DSF are 0.21 dB/km, -2 ps/nm/km, +0.1 ps/nm^2/km, and 55 μm^2 at 1558.5 nm, respectively. The output power of EDFA is +8 dBm with flat gain profile, and its noise figure is 6.0 dB. Segment (A) contains two standard SMF sections placed near both edges of the transmission line so as the system dispersion at the center channel to be set to zero. In contrast, in the Segment (B), the accumulated dispersion linearly increases with distance since Segment (B) consists of only NZ-DSFs. The dispersion maps of Segment (A) and (B) are shown in Fig. 6-5 (a) and (b), respectively. The solid, dashed, and dotted lines indicate the dispersion map of ch 1, ch 13 and ch 25, respectively.

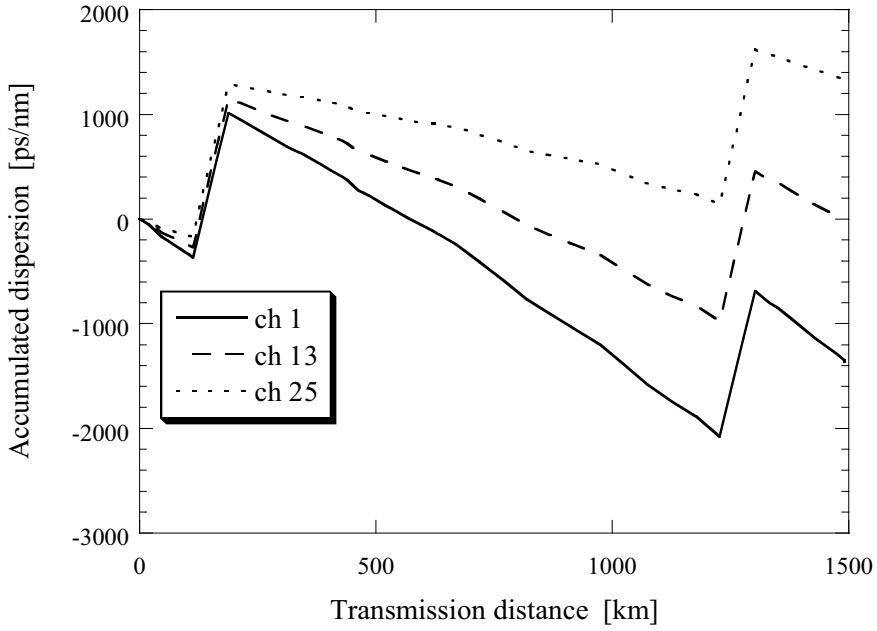

(a) Segment (A)

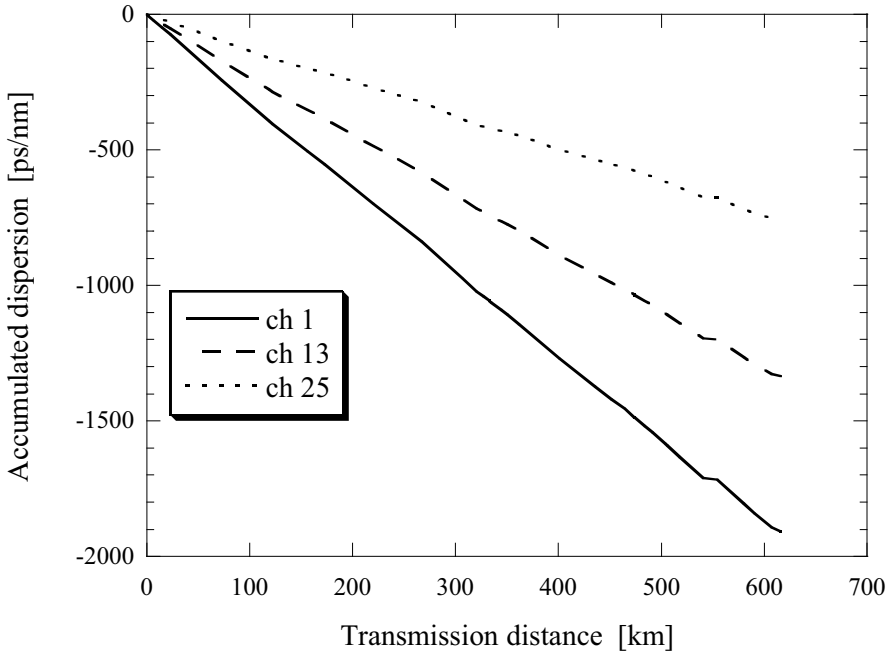

(b) Segment (B)

Fig. 6-5 Dispersion maps of the longest segment (A) and a typical segment (B) in numerical simulations.

6-4.2 Results and discussion

Figures 6-6 (a) and (b) show the Q-factor for all the 25 channels after 600 km and 1500 km transmissions. The closed circles, open circles, and triangles indicated the results of RZ, CS-RZ, and NRZ formats, respectively. From Fig. 6-6, it was found that CS-RZ and RZ signals show better transmission performance than NRZ signal, and that a Q-factor of more than 11 dB was achieved for all the formats after both 600 km and 1,500 km transmission. Regarding the channel (wavelength) dependency on transmission performance, a flat performance over all the channels was attained after 600 km transmission. On the other hand, after 1,500 km transmission, a slight performance degradation of the edge channels was observed, which was attributed to the interactions between nonlinear effects and largely accumulated dispersion. The average Q-factor of CS-RZ, RZ, and NRZ formats after 600 km were 15.7 dB, 15.2 dB, and 14.4 dB, and the minimum Q-factor after 1,500 km transmission were 13.0 dB, 12.3 dB, and 11.3 dB, respectively.

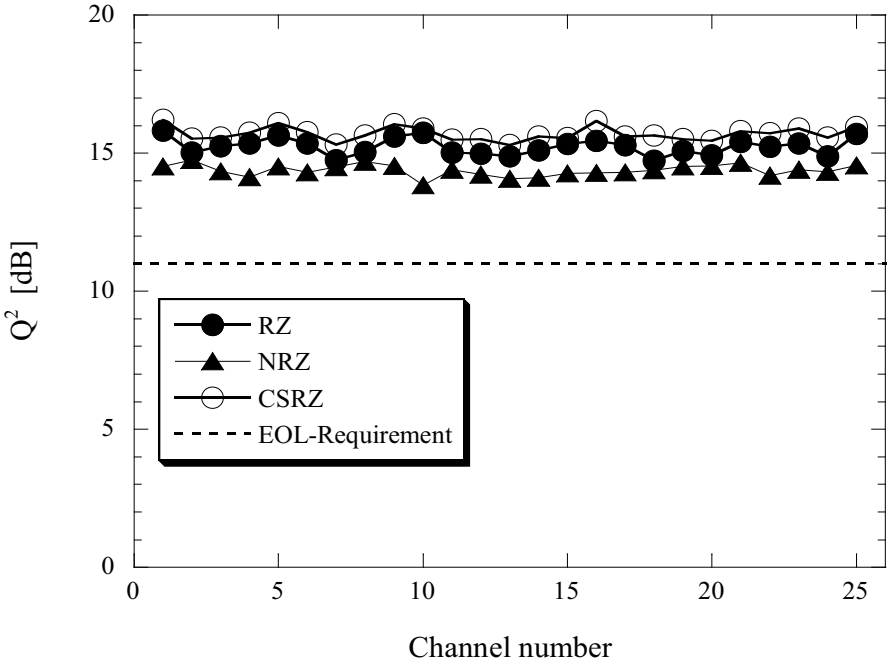

(a) 600 km transmission

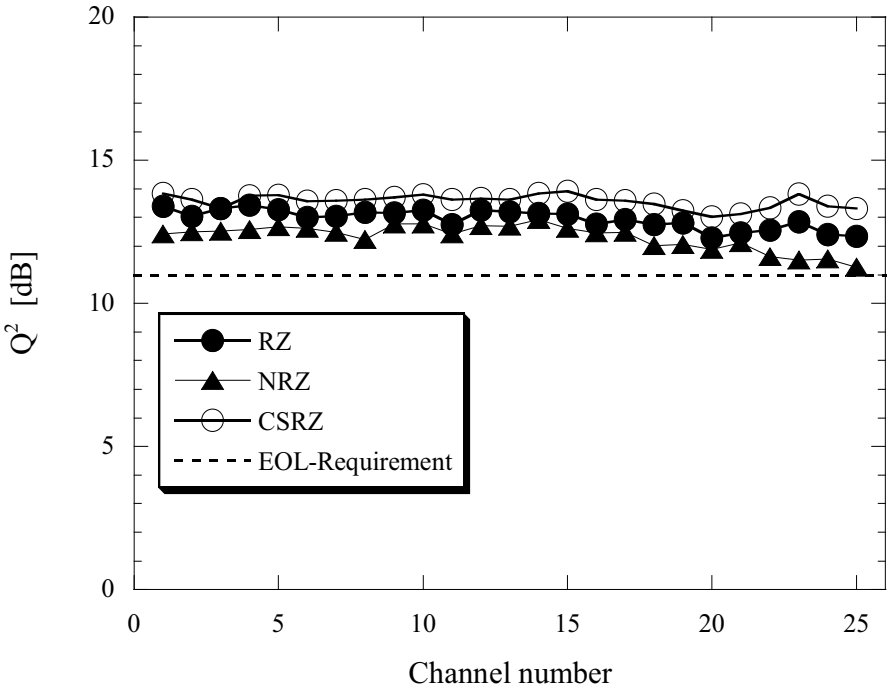

(b) 1,500 km transmission

Fig. 6-6 Obtained Q-factors in numerical simulations.

6-5 Experiments on 1 Tbit/s transmission system for capacity upgrade

In this section, the results of transmission experiments are described to confirm the results of numerical simulations. The effects of the pre- and post-dispersion compensation ratio and the state of polarization between adjacent channels were also investigated.

6-5.1 Experimental setup

Figure 6-7 shows the experimental setup. In the transmitter, twenty five DFB-LDs were employed and the wavelengths of which were equally spaced by 100 GHz between 1545.3 nm and 1564.6 nm. To generate 42.7 Gbit/s RZ and CS-RZ signals for even and odd channels independently, two $LiNbO_3$ modulator chains were used. In each modulator chain, the first modulator was driven by a 2^{31}-1 pseudo-random binary sequence for data coding, and the second modulator was driven by a 21.3 GHz sinusoidal wave biased at the maximum or null transmission points for RZ and CS-RZ formatting, respectively. For the generation of NRZ format, the second modulator was bypassed, which contributes to the cost and space reduction of the terminal equipments. At the last stage of the transmitter, the even and odd channels were combined by using a polarizing beam splitter and were launched into the transmission line.

The transmission line for the 1500 km-long Segment (A) consisted of three sections: a straight line with four spans of NZ-DSF and two spans of SMF, five loops of the 200 km-long NZ-DSF spans, and a straight line with two spans of SMF and two spans of NZ-DSF. For the 600 km-long Segment (B) transmission experiment, only three loops of the 200 km-long NZ-DSF spans were used. The zero-dispersion wavelength of the Segment (A) and (B) were 1550.8 nm and 1579.7 nm, respectively. Figures 6-8 (a) and (b) show the dispersion maps of Segment (A) and (B) employed in the experiment, which are almost the same ones in the numerical simulations.

In the receiver, after splitting the even and odd channels by using a 100/200 GHz interleaver, the measured channel was selected by an optical bandpass filter. Then, 40 Gbit/s signals were optically time-division-demultiplexed to 10 Gbit/s signals with a two-stage optical gate using sinusoidally-driven polarization insensitive EA modulators. The signal performance was evaluated with a BER averaged over four 10 Gbit/s demultiplexed channels.

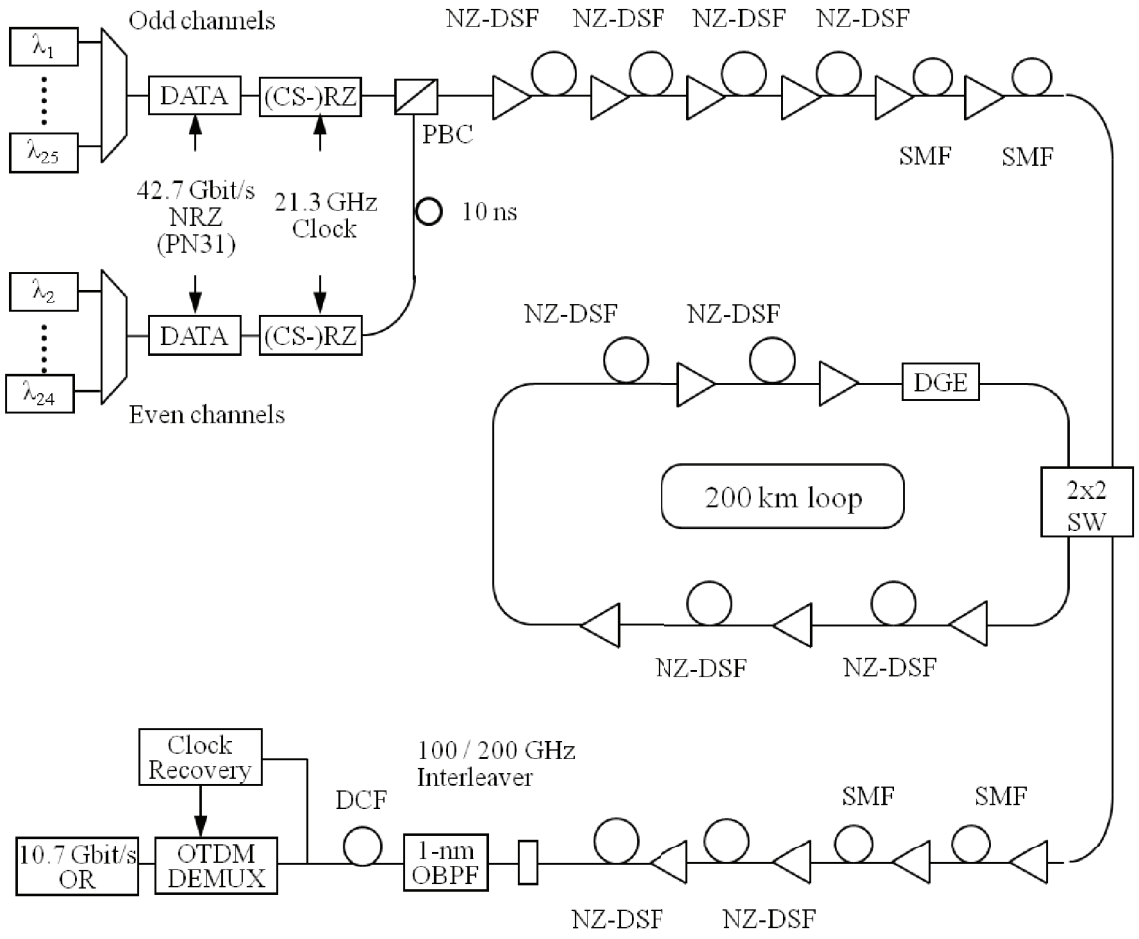

Fig. 6-7 Experimental setup for 100 GHz-spaced 25 x 42.7 Gbit/s transmissions.

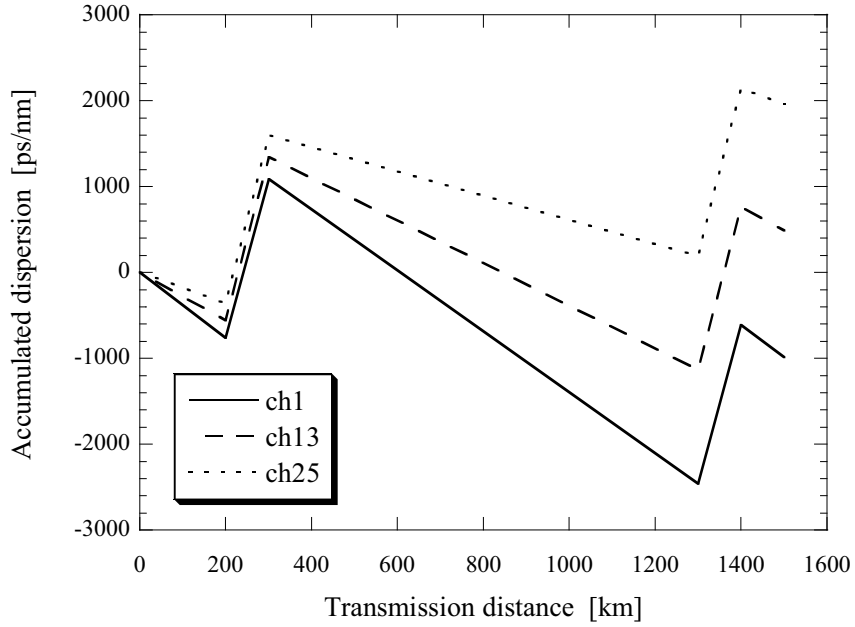

(a) Segment (A)

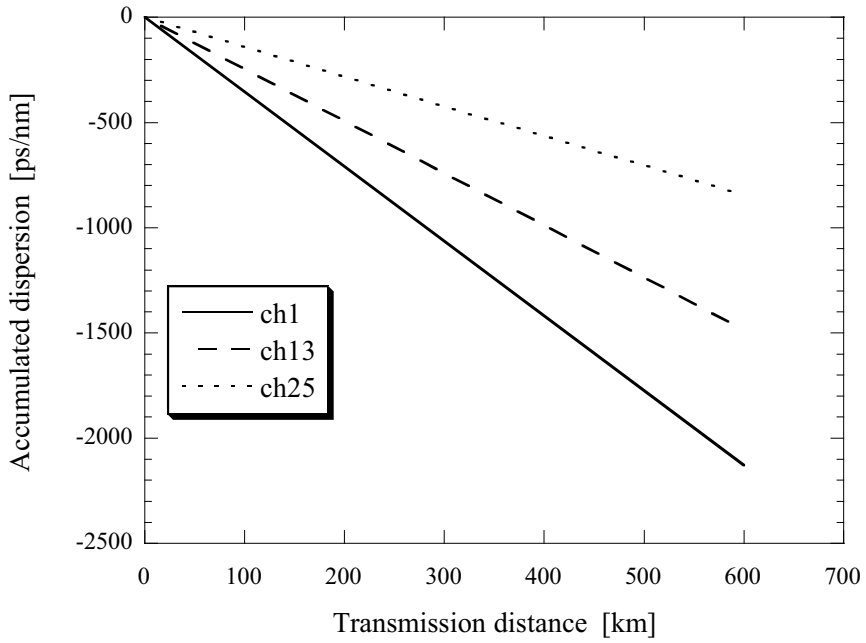

(b) Segment (B)

Fig. 6-8 Dispersion maps of the longest segment (A) and a typical segment (B) in transmission experiments.

6-5.2 Results and discussion

Figures 6-9 (a) and (b) show the Q-factors calculated from the BER of ch 1, 7, 13, 19, and 25 after 600 km and 1,500 km transmissions, respectively. The closed circles, open circles, and triangles indicate the results of RZ, CS-RZ, and NRZ format, respectively. By comparing the results shown in Figs.6-6 and 6-9, it was found that the experimental results show a good agreement with the numerical simulation results; a Q-factor of more than 11 dB was achieved for all the measured channels after both 600 km and 1,500 km transmissions, and there was almost no channel dependency on 600 km transmission performance. The slightly large channel dependency on 1,500 km transmission performance relative to the numerical simulation results was attributed to the optical SNR variation.

For the longest segment transmission over 1,500km, as the performance of NRZ signal was very close to the required Q-factor limit in both experiment and simulation, the use of RZ signal format is desirable in practical situations to earn at least 1-dB system margin. In addition, a further wide system margin can be expected by using advanced FEC technologies, if required.

Figures 6-10 (a) and (b) show the optical spectra after 600 km and 1,500 km transmissions. As is shown in Fig.6-10 (b), almost the same optical SNR was obtained up to 600 km transmission by adopting a dynamic gain equalizer (DGE) in the loop and pre-emphasis scheme for channel 25, whereas the optical SNR of both edge channels after 1,500 km transmission were degraded due to the profile mismatch between the EDF and the gain equalization filter embedded in each EDFA employed in the experiment. The quantities of pre-emphasis for channels 25 were 1 dB and 2 dB for 600 km and 1,500 km transmissions, respectively. Although the ASE noise from 1.48μm-pumped EDFAs additionally accumulated at the transmission distance of 1,500 km from 600 km, a sufficient SNR of more than 18 dB at a resolution of 0.1 nm was obtained even in 25 WDM transmission systems. Note that the optical SNR of the signal is the same among three modulation formats.

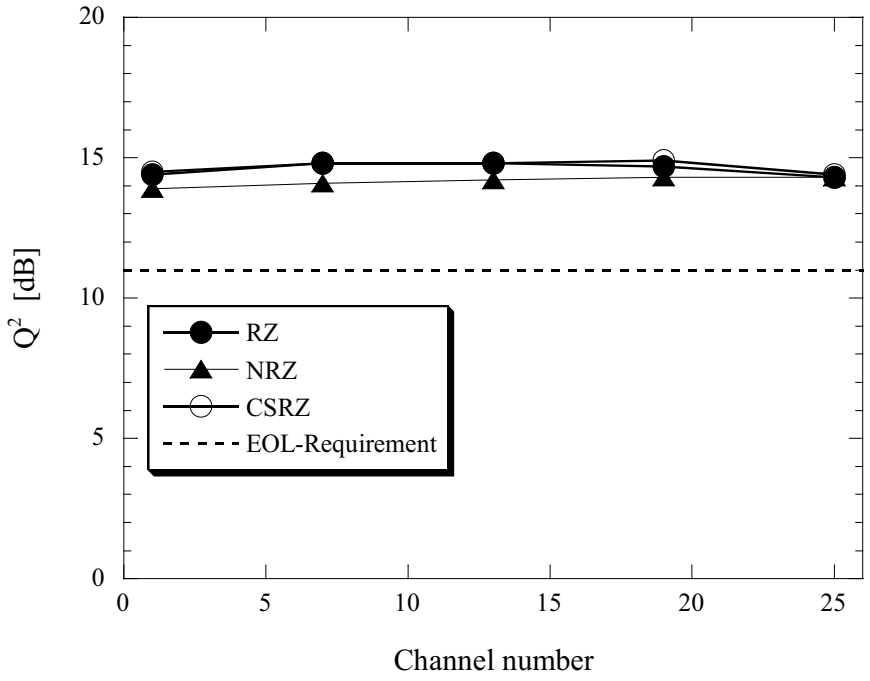

(a) 600 km transmission

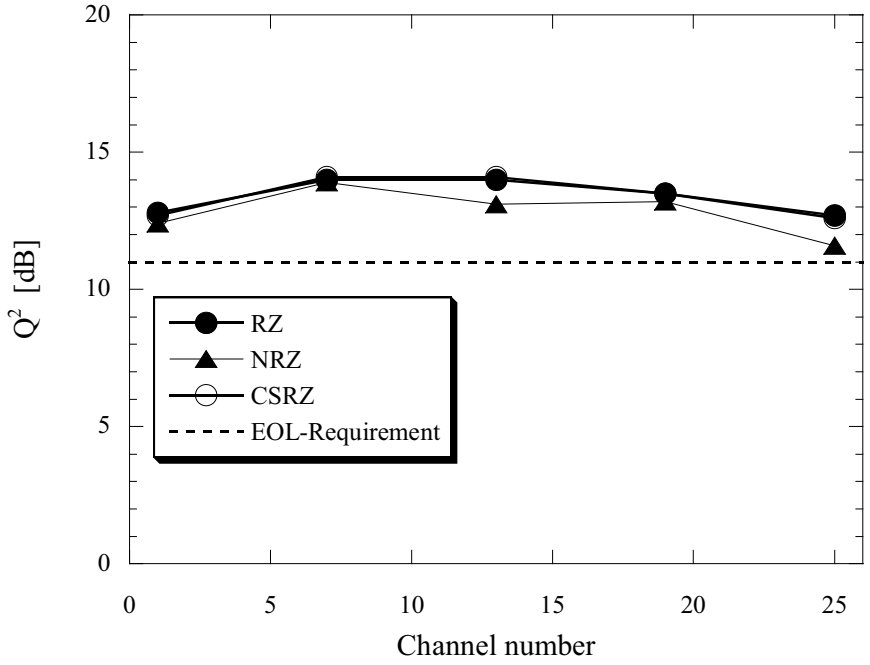

(b) 1,500 km transmission

Fig. 6-9 Obtained Q-factors in experiments.

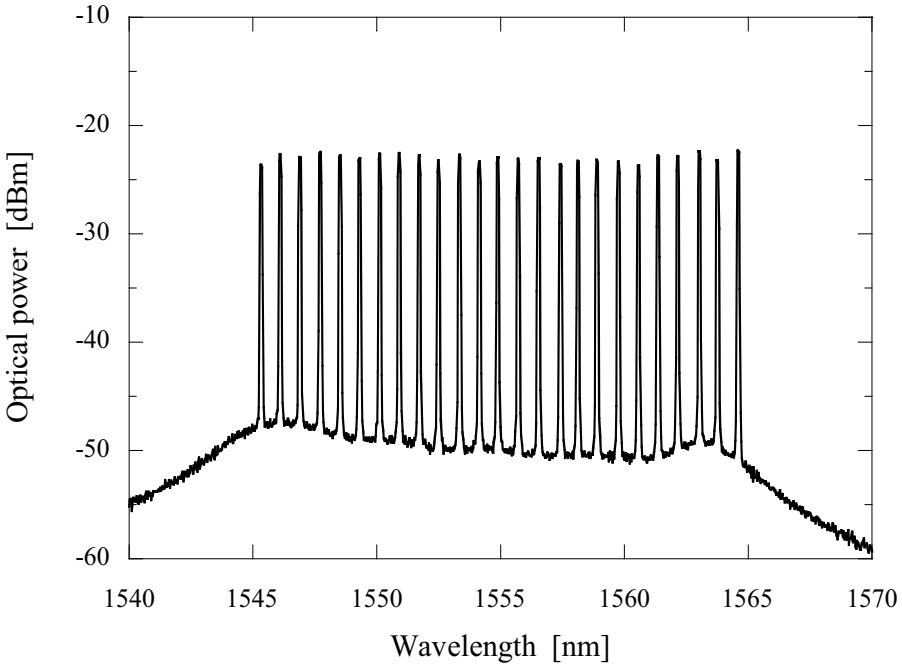

(a) 600 km transmission

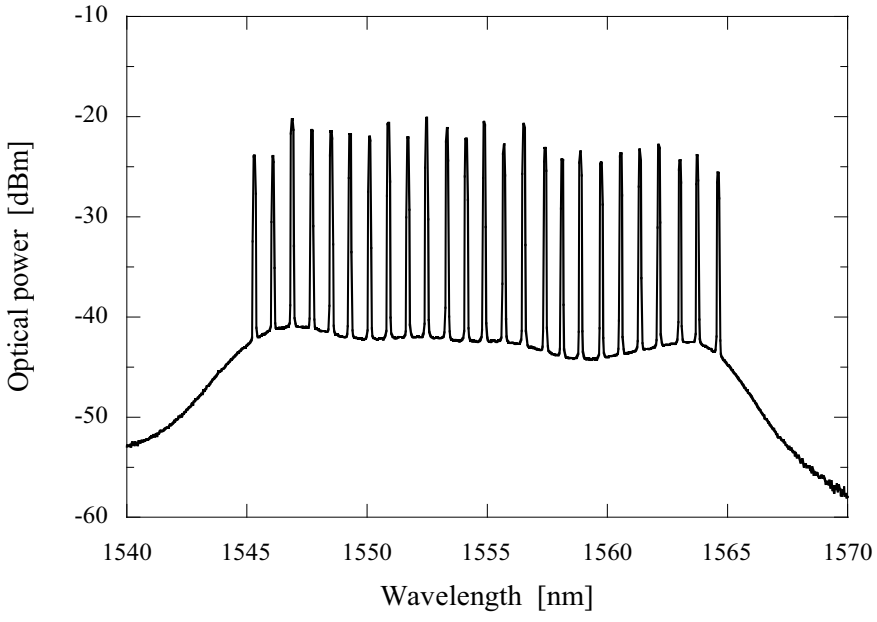

(b) 1,500 km transmission

Fig. 6-10 Optical spectra in experiments (Res.= 0.1 nm).

Figures 6-11 (a), (b), and (c) show the waveforms of channel 13 before transmission and after 600 km, and 1,500 km transmissions, respectively. NRZ, RZ, and CS-RZ signals are indicated at the top, middle, and bottom in the figures. As is shown in Fig. 6-11, the obtained waveforms after transmission were clearer in the order corresponding to the CS-RZ, RZ, and NRZ formats. The order indicates the nonlinear tolerance of the signal formats, and the NRZ is the most vulnerable due to its high bit-pattern dependence.

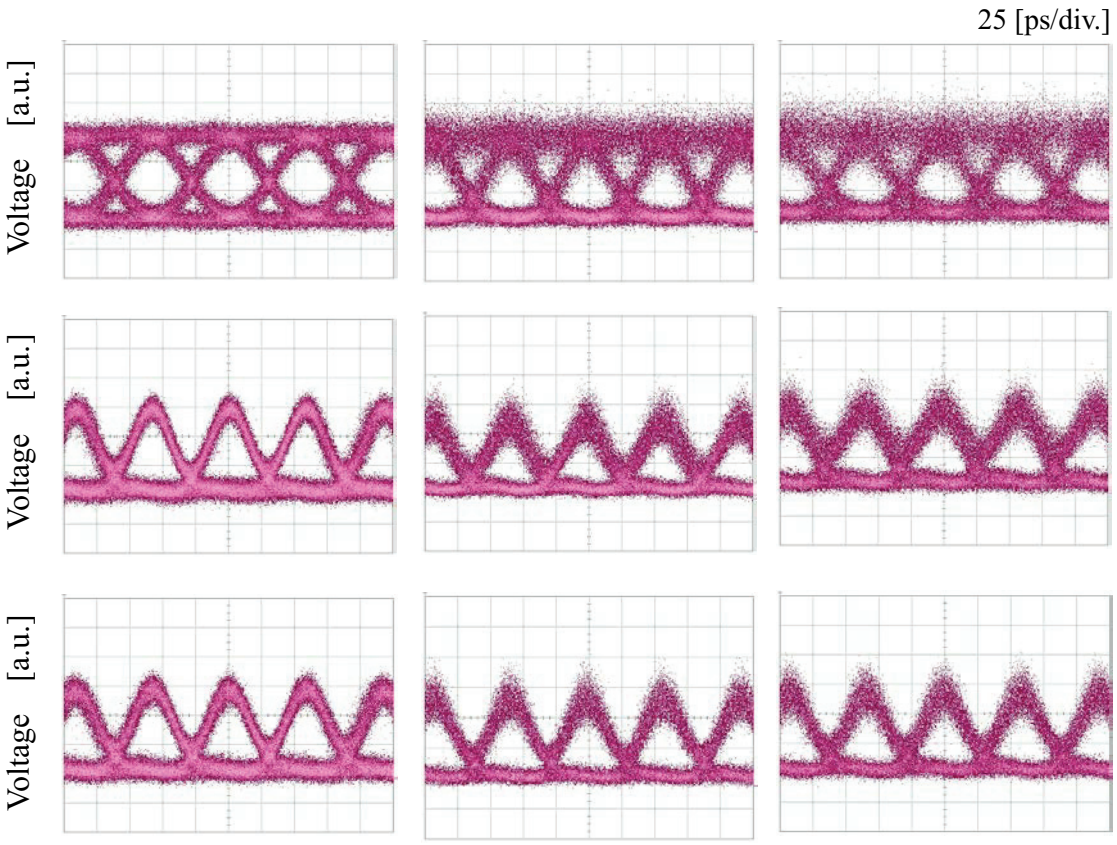

(a) back-to-back condition (b) 600 km transmission (c) 1500 km transmission

Fig. 6-11 Optical waveforms of ch13 for NRZ (top), RZ (middle), and CS-RZ (bottom) formats in experiments.

As the other terminal technologies to enhance the transmission performance, two technologies are worth considering: the optimization of the dispersion compensation at both optical transmitter and receiver terminals and the adoption of polarization multiplexing of the adjacent WDM channels [18]. Next, the system impact of these two technologies on the performance was investigated by using RZ signals because it shows the moderate performance among three signal formats.

The residual accumulated dispersion in the transmission line is compensated for at terminals. The ratio of the dispersion compensation at the optical transmitter and receiver was evaluated to optimize the dispersion compensation ratio at both terminals. Here, the compensation at the optical transmitter and receiver are described as pre- and post-dispersion compensation, respectively. Figure 6-12 shows the Q-factors of channel 1, 13, and 25 after 1,500 km transmission as a function of the pre-dispersion compensation ratio against the total quantity of dispersion compensation. A ratio of 0 % and 100 % means that the accumulated dispersion of the transmission line was compensated for by only pre- and post-dispersion compensation fibers, respectively.

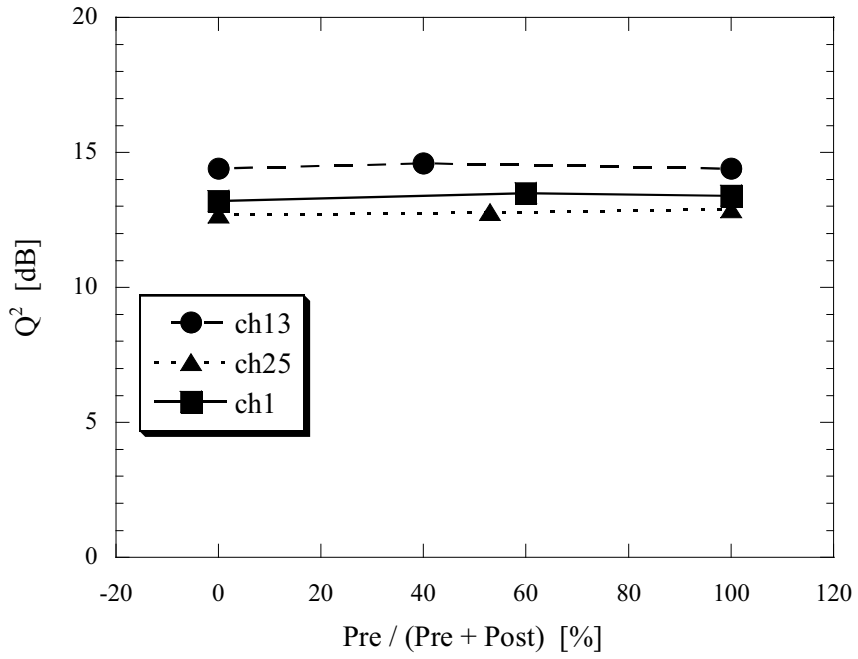

Fig. 6-12 Obtained Q-factors at various pre/post-dispersion compensation ratio.

From Fig. 6-12, it was observed that the transmission performance is independent of the dispersion compensation ratio of terminals as far as the sum of the quantity of pre- and post-dispersion compensation keeps constant.

The effect of the polarization multiplexing was also investigated by changing the signal state of polarization between adjacent channels from the parallel states to orthogonal ones. This scheme is considered to be beneficial to alleviate the nonlinear interactions between adjacent channels such as XPM and FWM.

Figure 6-13 shows the Q-factors of channel 1, 13, and 25 after 1,500 km transmission with parallel or orthogonal polarized adjacent channels. In addition, nonlinear penalty from adjacent channels was evaluated by measuring the Q-factor without adjacent channels. As is shown in Fig. 6-13, the superiority of the orthogonal state of polarization against the parallel state of polarization was as small as 0.5 dB.

The results on the optimization of terminal dispersion compensation and the impact of polarization multiplexing indicated that the nonlinear impairments was relatively small even in 40 Gbit/s-based WDM transmissions, and the system was considered to be in the linear transmission regime.

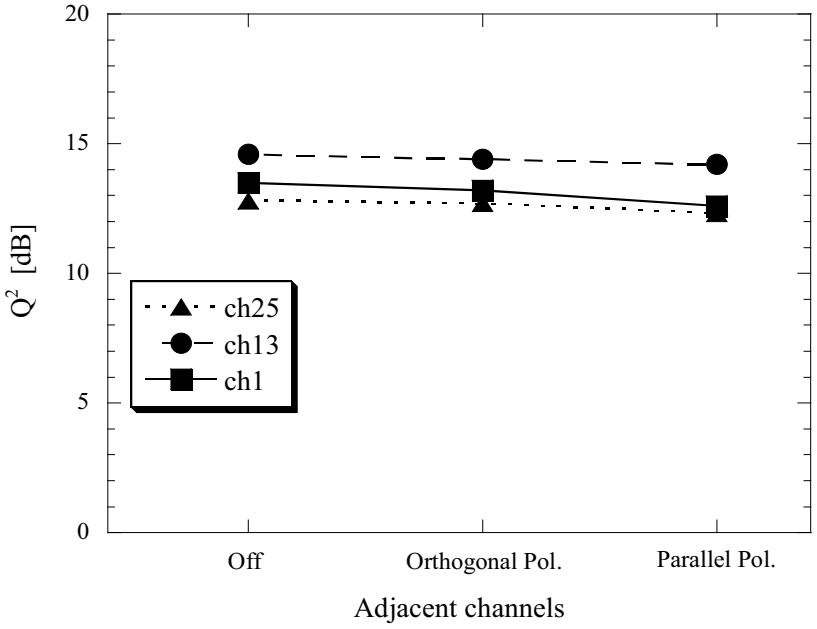

Fig. 6-13 Obtained Q-factors in orthogonal and parallel states of polarization between adjacent channels.

6-6 Conclusion

The upgradability to a 40 Gbit/s-based WDM transmission of JIH submarine system whose dispersion map was designed for a 2.5 Gbit/s-based WDM transmission has been numerically and experimentally investigated in the longest and typical length segments by adopting advanced terminal technologies. Through the studies, it was confirmed that the 40 Gbit/s-based WDM transmission with a total capacity of 1 Tbit/s can be attainable even in the transmission line designed for a 2.5 Gbit/s-based WDM transmission system.

For a typical segment of 600 km, it was confirmed that NRZ signal format and a standard FEC of RS (255, 239) can be applicable to achieve a 100 GHz-spaced 25 x 42.7 Gbit/s transmission without controlling the polarization state of adjacent channels. Regarding the capacity upgrade of the longest segment of 1,500 km, 100 GHz-spaced 42.7 Gbit/s RZ signal formats are necessary to satisfy the requirements for the system performance. Furthermore, by using advanced FEC and the channel multiplexing in the orthogonal state of polarization, additional margins of more than 2 dB and 0.5 dB can be expected respectively, while these technologies impose the terminal cost increase.

References

[1] T. Tsuritani, K. Ishida, A. Agata, K. Shimomura, I. Morita, T. Tokura, H. Taga, T. Mizouchi, and N. Edagawa, "70 GHz-spaced 40 x 42.7 Gbit/s transmission over 8700 km using CS-RZ DPSK signal, all-Raman repeaters and symmetrically dispersion fiber span", OFC2003, PD23, 2003.

[2] J. -X. Cai, D. G. Foursa, C. R. Davidson, Y. Cai, G. Domagala, L. Li, L. Liu, W. W. Patterson, A. N. Pilipetskii, M. Nissov, and N. S. Bergano, "A DWDM demonstration of 3.73 Tb/s over 11,000 km using 373 RZ-DPSK channels at 10 Gb/s", OFC2003, PD22, 2003.

[3] C. Rasmussen, T. Fjelde, J. Bennike, F. Liu, S. Dey, B. Mikkelsen, P. Mamyshev, P. Serbe, P. van der Wagt, Y. Akasaka, D. Harris, D. Gapontsev, V. Ivshin, and P. Reeves-Hall, "DWDM 40 G transmission over trans-Pacific distance (10,000 km) using CS-RZ-DPSK, enhanced FEC and all-Raman 100 km UltraWave^{TM} fiber spans", OFC2003, PD18, 2003.

[4] G. Vareille, L. Becouarn, P. Pecci, P. Tran, and J. F. Marcerou, "8370 km with 22 dB spans ULH transmission of 185*10.709 Gbit/s RZ-DPSK channels", OFC2003, PD20-1, 2003.

[5] N. S. Bergano, C. R. Davidson, M. Ma, A. Pilipetskii, S. G. Evangelides, H. D. Kidorf, J. M. Darcie, E. Golovchenko, K. Rottwitt, P. C. Corbett, R. Menges, M. A. Mills, B. Pedersen, D. Peckham, A. A. Abramov, and A. M. Vengsarkar, "320 Gb/s WDM transmission (64 x 5 Gb/s) over 7,200 km using large mode fiber spans and chirped return-to-zero signals", OFC1998, PD12, 1998.

[6] Y. Miyamato, A. Hirano, K. Yonenaga, A. Sano, H. Toba, K. Murata, and O. Mitomi, "320 Gbit/s (8 x 40 Gbit/s) WDM transmission over 367 km with 120 km repeater spacing using carrier-suppressed return-to-zero format", Electron. Lett., vol. 23, pp.2041-2042, 1999.

[7] R. Ohhira, D. Ogasawara, and T. Ono, "Novel RZ signal format with alternate-chirp for suppression of nonlinear degradation in 40 Gb/s based WDM", OFC2001, WM2, 2001.

[8] Y. Miyamato, A. Yonenaga, A. Hirano, H. Toba, K. Murata, and H. Miyazawa,

"Duobinary carrier-suppressed return-to-zero format and its application to 100 GHz-spaced 8 x 43-Gbit/s DWDM unrepeatered transmission over 163 km", OFC2001, TuU4, 2001.

[9] A. H. Gnauck, G. Raybon, S. Chandrasekhar, J. Leuthold, C. Doerr, L. Stulz, and E. Burrows, "25 x 40-Gb/s co-polarized DPSK transmission over 12 x 100-km NZDF with 50-GHz channel spacing", IEEE Photon. Tech. Lett., vol. 15, pp. 467-469, 2003.

[10] W. Idler, S. Bigo, Y. Frignac, B. Franz, and G. Veith, "Vestigial side band demultiplexing for ultra high capacity (0.64 bit/s/Hz) transmission of 128 x 40 Gb/s channels", OFC2001, MM3, 2001.

[11] B. Zhu, L. E. Nelson, S. Stulz, S. Gnauck, C. Doerr, J. Leuthold, L. Gruner-Nielsen, M. O. Pedersen, J. Kim, R. Lingle, Y. Emori, Y. Ohki, N. Tsukiji, A. Oguri, and S. Namiki, "6.4-Tb/s (160 x 42.7 Gb/s) transmission with 0.8 bit/s/Hz spectral efficiency over 32 x 100 km of fiber using CSRZ-DPSK format", OFC2003, PD19, 2003.

[12] H. Yamamoto, H. Tanaka, and K. Goto, "Japan Information Highway – wideband WDM technology –", OECC'98, 15D1-6, 1998.

[13] S. Yamamoto, H. Takahira, and M. Tanaka, "5 Gbit/s optical transmission terminal equipment using forward error correction code and optical amplifier", Electron. Lett., vol. 30, pp. 254-255, 1994.

[14] H. Kidorf, N. Ramanujam, I. Hayee, M. Nissov, J. -X. Cai, B. Pedersen, A. Puc, and C. Rivers, "Performance improvement in high capacity, ultra-long distance, WDM systems using forward error correction codes", OFC2000, ThS3, 2000.

[15] H. Taga, H. Yamauchi, T. Inoue, and K. Goto, "Performance improvement of highly nonlinear long-distance optical fiber transmission system using novel high gain forward error correction code", OFC2001, TuF3, 2001.

[16] A. Agata, K. Tanaka, and N. Edagawa, "Study on optimum Reed-Solomon code for 40 Gbit/s-based ultra long-distance WDM transmission", OECC2001, pp. 181-182, 2001.

[17] T. Mizuochi, K. Ouchi, T. Kobayashi, Y. Miyata, K. Kuno, H. Tagami, K. Kubo, H. Yoshida, M. Akita, and K. Motoshima, "Experimental demonstration of net coding gain of 10.1 dB using 12.4 Gb/s block turbo code with 3-bit soft decision",

OFC2003, PD21, 2003.

[18] I. Morita, K. Tanaka, N. Edagawa, and M. Suzuki, “40 Gbit/s single-channel soliton transmission over transoceanic distances by reducing Gordon-Haus timing jitter and soliton-soliton interaction”, IEEE/OSA J. Lightwave Technol., vol. 17, pp. 2506-2511, 1999.

Chapter 7

Conclusion

The dispersion management technologies for targeting terabit-capacity submarine cable systems have been numerically and experimentally studied in this thesis. SMF-based span configuration with dispersion-flattened property has been proven to be effective for high-speed WDM transmissions and is considered the most promising solution for terabit-capacity transoceanic cable systems. For unrepeatered transmission systems, the dispersion management scheme to extend the transmissible distance has been investigated in a 40 Gbit/s-based WDM system. The terminal technologies for increasing the spectral efficiency and upgrading the existing submarine cable system have been also studied. The conclusions of this thesis work are summarized as follows:

1. The performance difference between DSF-based and SMF-based span configurations was investigated in 32 x 10 Gbit/s WDM transmission over transoceanic distances. The SMF-based span configuration essentially achieving flat dispersion characteristics was found to be suitable for beyond 160 Gbit/s-capacity transmissions, and a 320 Gbit/s transmission over 7,280 km was successfully demonstrated. In addition, the potential of DFF-based systems was revealed, and a 400 Gbit/s soliton WDM transmission over 2,000 km was presented. Through the numerical and experimental studies, it was confirmed that SMF-based span configuration is the most promising solution for high-speed transoceanic WDM systems targeting terabit capacity.

2. The transmission line configuration was optimized for unrepeatered 40 Gbit/s-based WDM transmission systems. By allocating ultra-large-A_{eff} SMF allowing a high pump-power input for Raman amplification and a remote EDFA properly, unrepeatered 40 Gbit/s-based terabit-capacity WDM transmission over 306 km was successfully demonstrated for the first time.

3. The impact of nonlinear crosstalk and optical spectrum filtering on the transmission performance was investigated in SMF-based transmission systems. It was revealed that the transmission performance was not so sensitive to the increase of WDM channel number, and that owing to its small inter-channel interactions, a 40 Gbit/s-based ultra-DWDM terabit-capacity transmission over 480 km was successfully demonstrated using 50 GHz-spaced spectral-bandwidth limited RZ signals which dramatically reduce the overlapping of WDM signal spectrum between adjacent channels. The transmission distance over 480 km was the longest ever reported for DWDM transmissions in the spectral efficiency of 0.8 bit/s/Hz without using polarization demultiplexing.

4. The optimum pre-filtering conditions for 42.7 Gbit/s CS-RZ DPSK signals were numerically and experimentally evaluated in SMF-based transmission systems. Through the transmission experiments to reveal the trade-offs among the back-to-back performance, dispersion, and nonlinear tolerances in total, the asymmetrically pre-filtering was found to be more effective for CS-RZ DPSK signals in quasi-linear DWDM transmission systems because fiber nonlinearities were not induced so much to deteriorate its advantage of the back-to-back performance. The demonstration was revealed that the feasibility of terabit-capacity transoceanic transmission with a spectral efficiency of 0.8 bit/s/Hz by using an advanced FEC.

5. The upgradability to a 40 Gbit/s-based WDM transmission of JIH submarine system whose dispersion map was designed for a 2.5 Gbit/s-based WDM transmission was numerically and experimentally investigated in the longest and the typical segments by adopting advanced terminal technologies. Through these studies, it was confirmed that a 100 GHz-spaced 25 x 42.7 Gbit/s transmission with the total capacity of 1 Tbit/s can be attainable even in the transmission line designed for a 2.5 Gbit/s-based WDM system.

Appendix A

Fundamental equation describing optical signal propagation in a dispersive nonlinear fiber

A-1 Derivation of fundamental equation

The propagation of optical fields in fibers is governed by Maxwell's equations. In the absence of neither free electric charge nor electric current in a medium such as optical fibers, these equations are

$$\nabla \times \boldsymbol{E} = -\mu_0 \frac{\partial \boldsymbol{H}}{\partial t}, \tag{A.1}$$

$$\nabla \times \boldsymbol{H} = -\frac{\partial \boldsymbol{D}}{\partial t}, \tag{A.2}$$

$$\nabla \cdot \boldsymbol{D} = 0, \tag{A.3}$$

$$\nabla \cdot \mu_0 \boldsymbol{H} = 0, \tag{A.4}$$

where $\boldsymbol{E}(\boldsymbol{r}, t)$ and $\boldsymbol{H}(\boldsymbol{r}, t)$ are electric and magnetic field vectors, respectively, $\boldsymbol{D}(\boldsymbol{r}, t)$ is corresponding to electric flux densities, μ_0 is the permeability in vacuum. Spatial and time coordinates are represented by $\boldsymbol{r}$ and t, respectively.

The wave equation describing light propagation in optical fibers can be derived from Maxwell's equations. Taking the curl of Eq.(A.1) and substituting Eq.(A.2), we obtain

$$\nabla \times \left(\nabla \times \boldsymbol{E}\right) = -\mu_0 \frac{\partial^2 \boldsymbol{D}}{\partial t^2}. \tag{A.5}$$

Here, we define the Fourier transform of the field vectors $\boldsymbol{E}$ and $\boldsymbol{D}$ as

$$\widetilde{\boldsymbol{E}}(\boldsymbol{r}, \omega) = \int_{-\infty}^{\infty} \boldsymbol{E}(\boldsymbol{r}, t) e^{i\omega t} dt, \tag{A.6}$$

$$\widetilde{\boldsymbol{D}}(\boldsymbol{r},\omega)=\int_{-\infty}^{\infty}\boldsymbol{D}(\boldsymbol{r},t)e^{i\omega t}dt\,, \tag{A.7}$$

respectively, and with these transformations, Eq. (A.5) takes the form,

$$\nabla\times\left(\nabla\times\widetilde{\boldsymbol{E}}\right)=\omega^2\mu_0\widetilde{\boldsymbol{D}}\,. \tag{A.8}$$

Hereafter, the electric field of a lightwave signal is considered to be linearly polarized in the transverse dimensions *x* and *y*, perpendicular to the propagation direction *z*. By averaging the field over the fiber cross section, Eq. (A.8) can be written as

$$\frac{\partial^2\widetilde{\boldsymbol{E}}}{\partial z^2}+\omega^2\mu_0\widetilde{\boldsymbol{D}}=0\,. \tag{A.9}$$

In the Fourier domain, electric flux density $\widetilde{\boldsymbol{D}}$ is expressed as

$$\widetilde{\boldsymbol{D}}=\varepsilon_0 n^2\widetilde{\boldsymbol{E}}\,, \tag{A.10}$$

where ε_0 is the permittivity in vacuum and $n(\omega)$ is the effective refractive index of the fiber. By making the use of Eq. (A.10), Eq. (A.9) is given by

$$\frac{\partial^2\widetilde{\boldsymbol{E}}}{\partial z^2}+k^2\widetilde{\boldsymbol{E}}=0\,, \tag{A.11}$$

where $k=n\omega/c$ represents the wave number, and $c=1/\sqrt{\varepsilon_0\mu_0}$ is the speed of the light in vacuum.

Let the lightwave signal be represented by

$$\boldsymbol{E}(\boldsymbol{r},t)=\boldsymbol{i}_x f(x,y)q(z,t)\exp\left[i(k_0 z-\omega_0 t)\right]. \tag{A.12}$$

Here, $f(x,y)$ represents transverse distribution of electric field, $q(z,t)$ is a slowly varying envelope of electric field which propagates to *z* direction so long as the frequency does not stray too far from carrier central frequency ω_0, $\boldsymbol{i}_x$ is polarization direction of electric field, and $k_0=n_0(\omega_0)\omega_0/c$ is the wave number in the vacuum. In this case, the envelope $q(z,t)$ satisfies

$$\left|\frac{\partial q}{\partial z}\right|\ll k_0|q|\,, \tag{A.13}$$

$$\left|\frac{\partial q}{\partial t}\right| \ll \omega_0 |q| . \tag{A.14}$$

By substituting the Fourier transform $\widetilde{E}(z,\omega-\omega_0)$ for frequencies near the center frequency ω_0 defined by

$$\widetilde{E}(z,\omega-\omega_0) = \int_{-\infty}^{\infty} E(z,t)\exp[i(\omega-\omega_0)t]dt$$

$$= \widetilde{q}(z,\omega-\omega_0)\exp(ik_0 z) \tag{A.15}$$

into Eq.(A.11), and using Eqs. (A.13) and (A.14), the wave equation can be written as

$$i\frac{\partial \widetilde{q}}{\partial z} + (k-k_0)\widetilde{q} = 0 . \tag{A.16}$$

In the derivation of Eq. (A.16), the approximation of

$$k^2 - k_0^2 = (k+k_0)(k-k_0) \approx 2k_0(k-k_0) \tag{A.17}$$

is used for $|k-k_0| \ll 1$.

We consider lightwave propagation in a fiber that exhibits both group velocity dispersion and nonlinearity. Because of the relatively small value of fiber nonlinearity which is proportional to the intensity of the electric field $|\boldsymbol{E}|^2$, the effective refractive index *n* can be expressed as

$$n(\omega,|\boldsymbol{E}|^2) = n_L(\omega) + n_{NL}|\boldsymbol{E}|^2 , \tag{A.18}$$

where n_L and n_{NL} are linear and nonlinear refractive indexes, respectively. For frequencies near the central frequency ω_0, the wave number $k = n\omega/c$ can be expanded, by using a Taylor series and Eq. (A.18), to the approximate form

$$k(\omega,|q|^2) = \frac{\omega}{c} n(\omega,|q|^2)$$

$$= \frac{\omega}{c}\left\{\mathrm{Re}[n_L(\omega)] + i\,\mathrm{Im}[n_L(\omega)] + n_{NL}|q|^2\right\}$$

$$= k_0 + k'(\omega-\omega_0)+\frac{1}{2}k''(\omega-\omega_0)^2+\frac{1}{6}k'''(\omega-\omega_0)^3+\gamma|q|^2+i\alpha\,. \qquad \text{(A.19)}$$

Here, the constants k_0, k', k'' and k''' are defined by

$$k_0 = \frac{\omega_0}{c}\mathrm{Re}[n_L(\omega_0)], \qquad \text{(A.20)}$$

$$k' = \frac{d}{d\omega}\left\{\frac{\omega}{c}\mathrm{Re}[n_L(\omega)]\right\}\Big|_{\omega=\omega_0}$$

$$= \frac{1}{c}\left\{\mathrm{Re}[n_L(\omega_0)]+\omega_0\frac{d}{d\omega}\{\mathrm{Re}[n_L(\omega)]\}\Big|_{\omega=\omega_0}\right\}, \qquad \text{(A.21)}$$

$$k'' = \frac{d^2}{d\omega^2}\left\{\frac{\omega}{c}\mathrm{Re}[n_L(\omega)]\right\}\Big|_{\omega=\omega_0}$$

$$= \frac{1}{c}\left\{2\frac{d}{d\omega}\{\mathrm{Re}[n_L(\omega)]\}\Big|_{\omega=\omega_0}+\omega_0\frac{d^2}{d\omega^2}\left\{\frac{\omega}{c}\mathrm{Re}[n_L(\omega)]\right\}\Big|_{\omega=\omega_0}\right\}, \qquad \text{(A.22)}$$

$$k''' = \frac{d^3}{d\omega^3}\left\{\frac{\omega}{c}\mathrm{Re}[n_L(\omega)]\right\}\Big|_{\omega=\omega_0}$$

$$= \frac{1}{c}\left\{3\frac{d}{d\omega}\{\mathrm{Re}[n_L(\omega)]\}\Big|_{\omega=\omega_0}+\omega_0\frac{d^3}{d\omega^3}\left\{\frac{\omega}{c}\mathrm{Re}[n_L(\omega)]\right\}\Big|_{\omega=\omega_0}\right\}. \qquad \text{(A.23)}$$

The nonlinear coefficient γ can be written as

$$\gamma = \frac{\omega}{c}\mathrm{Re}[n_{NL}(\omega)]\Big|_{\omega=\omega_0} = \frac{\omega_0 n_2}{cA_{eff}}, \qquad \text{(A.24)}$$

where n_2 is Kerr coefficient that depends on the intensity and has a value of about 2.6 x 10^{-20} m^2/W, and A_{eff} is effective core area of the fiber. Loss coefficient α can be expressed as

$$\alpha = \frac{\omega_0}{c}\mathrm{Im}[n_L(\omega_0)]. \qquad \text{(A.25)}$$

Higher order terms can be adequately treated as perturbations for pulse widths of wider than 10 ps, so that they can be neglected.

The wave equation Eq. (A.16) for q is led to

$$i\frac{\partial \tilde{q}}{\partial z}+\left\{k'(\omega-\omega_0)+\frac{1}{2}k''(\omega-\omega_0)^2+\frac{1}{6}k'''(\omega-\omega_0)^3+\gamma|u|^2+i\alpha\right\}\tilde{q}=0\,, \quad \text{(A.26)}$$

by substituting Eq. (A.19) into Eq. (A.16). In the inverse Fourier-transform operation, $\omega-\omega_0$ is replaced by the differential operator with respect to time $i\frac{\partial}{\partial t}$, and Eq. (A.26) becomes

$$i\left(\frac{\partial q}{\partial z}+k'\frac{\partial q}{\partial t}\right)-\frac{1}{2}k''\frac{\partial^2 q}{\partial t^2}-\frac{i}{6}k'''\frac{\partial^3 q}{\partial t^3}+\gamma|q|^2 q+i\alpha q=0\,, \quad \text{(A.27)}$$

This is the nonlinear Schrödinger (NLS) equation which describes the optical pulse behavior in fibers.

It is useful to change the variable of time in order to simplify Eq. (A.27). The appropriate new variable is

$$t'=t-k'z\,, \quad \text{(A.28)}$$

which represents the retarded time frame moving at the group velocity k'^{-1}. By applying the transformation and omitting the prime on *t*, the propagation equation Eq. (A.27) can be simplified to

$$i\frac{\partial q}{\partial z}-\frac{1}{2}k''\frac{\partial^2 q}{\partial t^2}-\frac{i}{6}k'''\frac{\partial^3 q}{\partial t^3}+\gamma|q|^2 q+i\alpha q=0\,. \quad \text{(A.29)}$$

This is used as the fundamental equation for analytical and numerical studies in the thesis.

A-2 Key parameters describing a dispersive fiber

The problem of lightwave propagation in a fiber under the influence of group velocity dispersion (GVD) can be solved by considering the dependence of the wave number on the angular frequency. In the absence of fiber nonlinearities and fiber loss, the wave number $k(\omega)$ for frequencies near the central frequency ω_0, can be expanded up to the third order as

$$k(\omega) = k_0 + k'(\omega - \omega_0) + \frac{1}{2}k''(\omega - \omega_0)^2 + \frac{1}{6}k'''(\omega - \omega_0)^3 . \tag{A.30}$$

The group velocity $v_g(\omega)$, which represents the speed of pulse propagation, is described by

$$v_g(\omega)^{-1} = \left.\frac{\partial k}{\partial \omega}\right|_{\omega=\omega_0} = k' + k''(\omega - \omega_0). \tag{A.31}$$

The expression identifies k' as the reciprocal group velocity at frequency ω_0 and k'' as its group velocity dispersion constant at ω_0. Chromatic dispersion, or more precisely group-velocity dispersion, in lightwave systems is caused by a variation in the group velocity in a fiber with changes in optical frequency. The pulse envelope will tend to move with its average group velocity, but if the group velocity varies with frequency due to group velocity dispersion, various frequency components of the pulse separate in time. Thus, the pulse will spread as it propagates, which degrades the system performance.

The dispersion parameter D is widely used in optical fiber communication systems to represent chromatic dispersion, in units of ps/nm/km. It indicates the amount of the arrival time difference that would occur in optical waves with a wavelength difference of 1 nm while propagating through 1 km of optical fiber. The dispersion parameter D is the wavelength derivation of v_g^{-1}, and is related to k'' by

$$D = \frac{d}{d\lambda}\left(v_g^{-1}\right) = -\frac{2\pi c}{\lambda^2}k'', \tag{A.32}$$

where λ and c are the wavelength and speed of light in vacuum, respectively.

The dispersion of optical fiber also has a wavelength dependency and varies over the WDM signal wavelength bandwidth. This dispersion slope D_λ in units of ps/nm^2/km is related to k'' and k''' by

$$D_\lambda = \frac{dD}{d\lambda} = \frac{4\pi c}{\lambda^3}\left[k'' - \frac{\pi c}{\lambda}k'''\right]. \tag{A.33}$$

Appendix B

Modulation formats for optical fiber communications

B-1 Typical waveforms in IM-DD systems

Most of digital binary transmission systems use a simple modulation scheme of intensity-modulation direct-detection (IM-DD) where the intensity of an optical source is directly modulated by RF signal and demodulated through direct detection with a photo-detector. The modulation formats in IM-DD systems are simple, and they are mainly classified into two formats: non-return-to-zero (NRZ) and return-to-zero (RZ). The NRZ format keeps its intensity level to a constant value when consecutive mark signals are sent. In contrast, the RZ format does not occupy the whole bit-slot for consecutive mark signals. Soliton is a kind of RZ format with a hyperbolic secant-squared pulse shape. Figure B-1 shows typical waveforms of NRZ, RZ, and soliton for a bit-sequence of "101110001".

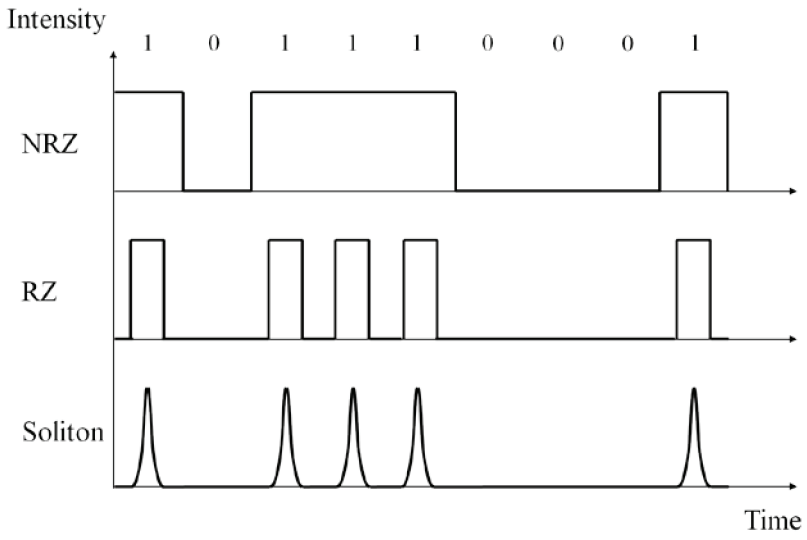

Fig. B-1 Waveforms of NRZ, RZ, and soliton formats.

B-2 Benefit of RZ format against nonlinear impairments

Nonlinear effects in optical fibers impose a severe limit on the performance of digital transmission systems. Signal distortion resulting from the interactions between nonlinear effects and chromatic dispersion is one of the crucial problems in long-haul transmission systems.

RZ formats are known to be more tolerable against nonlinear effects than NRZ. The waveform of NRZ format differs depending on the pattern of bit sequence, while RZ format does not change its waveform. The waveform characteristics of the NRZ format causes a pattern-dependent distortion due to the interactions between SPM-induced nonlinear chirp and chromatic dispersion of optical fibers. The pattern-dependent distortion of the NRZ occurs remarkably in WDM transmission systems because the overlap of consecutive mark signals of WDM channels induces additional high nonlinearities.

In order to investigate nonlinear tolerance of NRZ and RZ formats, the data-pattern dependency of 10 Gbit/s-based four WDM signals was numerically simulated. Waveforms of an optical bit-sequence of NRZ and RZ formats after 7,500 km transmission are shown in Fig.B-2 (a) and (b), respectively. The channel spacing was set to 0.8 nm and the power level of EDFA was set to +5 dBm. The figures show data-pattern dependency of each format on a 64 pseudo-random bit sequence. An important difference between them is the amplitude fluctuation of mark levels. The mark level of NRZ format was fluctuating especially in consecutive mark signals, whereas repetitive waveforms of mark level were obtained for RZ format. This feature was clearly observed in the corresponding optical eye-diagrams as shown in Fig. B-3. The average Q-factor of four channels for NRZ and RZ formats were 14.7 dB and 17.1 dB, respectively.

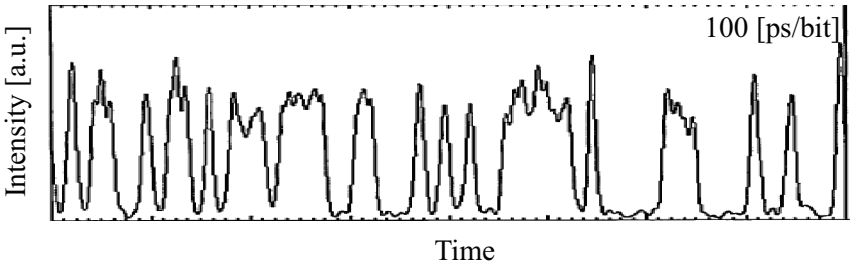

(a) NRZ format

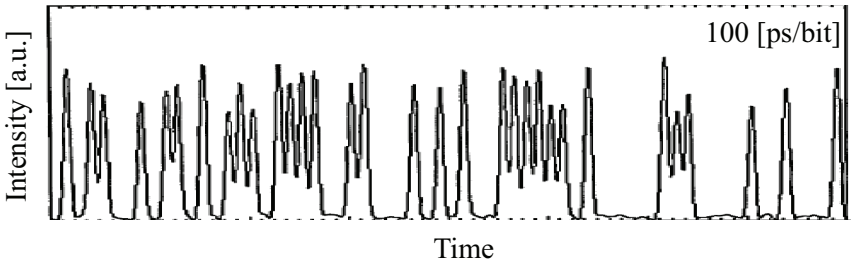

(b) RZ format

Fig. B-2 Waveforms after 7,500 km transmission of optical bit-sequence.

(a) NRZ format

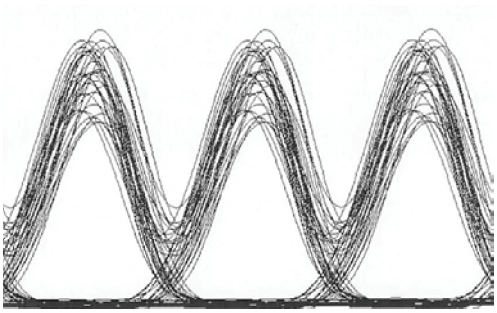

(b) RZ format

Fig. B-3 Eye-diagrams after 7,500 km transmission.

Appendix C

Forward error correction technology

Forward error correction (FEC) is one of the most important terminal technologies to enhance the system performance. FEC can be implemented simply in digital optical communication systems by encoding the information symbols into codes by means of an encoder in the electrical domain. At the receiver, a decoder can be used to recover the information bits. Figure C-1 shows the basic model of optical transmission systems by using FEC.

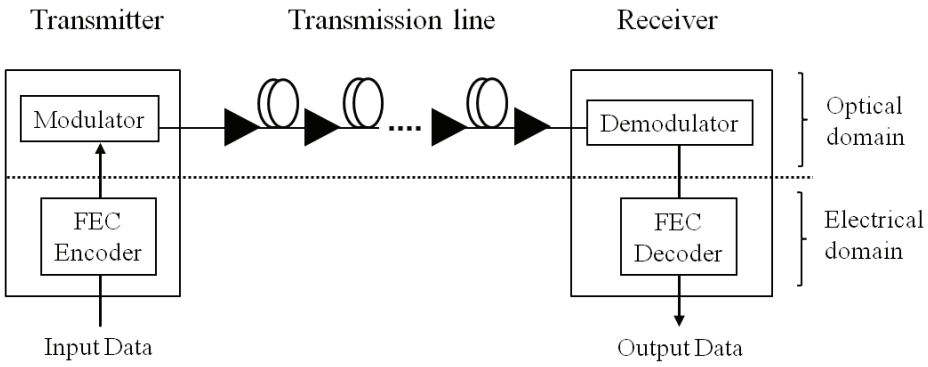

Fig. C-1 Basic model of optical transmission systems with FEC.

Among several types of FEC codes, the Reed-Solomon code with a 7 % increase in redundancy, RS (255, 239) code, is widely used in optical fiber communication systems. The error correcting performance of RS (255, 239) is illustrated in Fig. C-2. The transmission performance is improved from a BER of 4.0×10^{-4} to 1.0×10^{-9}. FEC gain is expressed as the difference between the input and output Q-factors corresponding to the BERs.

A larger redundant FEC obtains a higher FEC gain. The error correcting performance of RS (255, 223) with a 14 % increase in redundancy is also illustrated in Fig. C-2. By using RS (255, 223) instead of RS (255, 239), the required input BER to

achieve an output BER of 1.0 x 10^{-9} can be increased from 4.0 x 10^{-4} to 1.7 x 10^{-3}. In contrast, a higher FEC gain requires a higher transmission bit-rate, which may increase the transmission penalties and terminal costs due to the use of high-speed electronics. Therefore, the selection of suitable FEC code is an important system design issue.

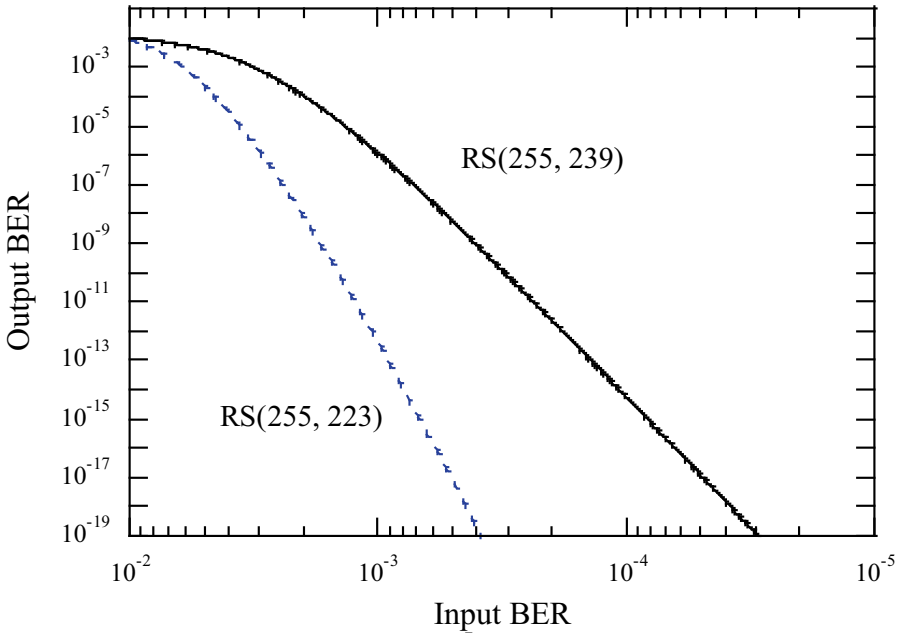

Fig. C-2 Error correcting performances of RS (255, 239) and RS (255, 223).

Acknowlegements

The author wishes to express his sincere gratitude with deep respect to Professor Katsuyuki Utaka of Waseda University for his invaluable guidance and encouragement in writing this thesis. The author would like to thank Professors Mitsuji Matsumoto, Isamu Kato, and Hirochika Nakajima of Waseda University, and Associate Professor Akihiro Maruta of Osaka University for their kind advice and suggestions.

The author is grateful to Dr. Masatoshi Suzuki, vice president of KDDI R&D laboratories Inc. for his continued support and encouragement throughout this thesis work. The author would also like to thank Prof. Yuichi Matsushima for his kind advice and warm support.

The author is deeply indebted to Drs. Noboru Edagawa and Itsuro Morita from the bottom of his heart for their invaluable advice, guidance, and encouragement throughout this research work.

The author wishes to acknowledge his sincere appreciation for kind guidance and productive technical discussions in the research work with Dr. Shigeyuki Akiba, Dr. Takehiro Tsuritani, Mr. Akira Agata, and Dr. Noboru Yoshikane of KDDI R&D laboratories Inc., and Dr. Shu Yamamoto, Dr. Yukio Horiuchi, Dr. Haruhisa Sakata, Mr. Takayuki Miyakawa, Mr. Noriyuki Takeda, Dr. Tomohiro Otani, Dr. Munefumi Tsurusawa, and Mr. Kaoru Imai of KDDI Corporation, and Dr. Hidenori Taga of National Sun Yat-Sen University.

Lastly, the author thanks his family for their patience and generous understanding for this thesis work.

List of publications by the author

1. Papers

[1] K. Tanaka, I. Morita, N. Yoshikane, and N. Edagawa, "Study on capacity upgrade of JIH (Japan Information Highway) submarine cable system using 40 Gbit/s-based WDM transmission technologies", IEICE Transactions on Communications, vol. E87-B, pp. 1463-1469, 2004.

[2] K. Tanaka, H. Sakata, T. Miyakawa, I. Morita, K. Imai, and N. Edagawa, "40 Gbit/s x 25 WDM 306 km unrepeatered transmission using 175 μm^2-Aeff fibre", IEE Proceedings on Optoelectronics, vol. 150, pp. 224-228, 2003.

2. Letters

[1] K. Tanaka, H. Sakata, T. Miyakawa, I. Morita, K. Imai, and N. Edagawa, "40 Gbit/s x 25 WDM 306 km unrepeatered transmission using 175 μm^2-A_{eff} fibre", IEE Electron. Lett., vol. 37, pp. 1354-1356, 2001.

[2] K. Tanaka, I. Morita, and N. Edagawa, "50 GHz-spaced 40 Gbit/s x 25 WDM transmission over 480 km using bandlimited RZ signals", IEE Electron. Lett., vol. 37, pp. 775-777, 2001.

[3] K. Tanaka, I. Morita, N. Edagawa, and M. Suzuki, "Impact of nonlinear crosstalk in 0.8 nm-spacing 40 Gbit/s DWDM systems", IEE Electron. Lett., vol. 36, pp. 1217-1218, 2000.

[4] K. Tanaka, T. Tsuritani, N. Edagawa, and M. Suzuki, "320 Gbit/s (32 x 10.7 Gbit/s) error-free transmission over 7280 km using dispersion flattened fibre link with standard SMF and slope compensating DCF", IEE Electron. Lett., vol. 35, pp. 1860-1862, 1999.

[5] K. Tanaka, I. Morita, M. Suzuki, N. Edagawa, and S. Yamamoto, "400 Gbit/s (20 x 20 Gbit/s) dense WDM soliton-based RZ signal transmission using dispersion flattened fibre", IEE Electron. Lett., vol. 34, pp. 2257-2258, 1998.

3. International conferences

[1] K. Tanaka, I. Morita, and N. Edagawa, “Study on optimum pre-filtering condition for 42.7 Gbit/s CS-RZ DPSK signal”, OFC2004, TuF2, 2004.

[2] K. Tanaka, and N. Edagawa, “Detuning tolerance of 50 GHz-spaced 40 Gbit/s-based DWDM system”, OECC2003, 15D1-4, 2003.

[3] K. Tanaka, I. Morita, Y. Yoshikane, and N. Edagawa, “Study on capacity upgrade of JIH(Japan Information Highway) submarine cable system using 40 Gbit/s-based WDM transmission technologies”, NFOEC2003, E2-2, 2003.

[4] K. Tanaka, “Present and future of ultralong-haul optical fiber transmission”, Nonlinear Physics: Theory and Experiment II, 2002.

[5] K. Tanaka, I. Morita, A. Agata, and N. Edagawa, “Study on the optimum signal format for long-haul 40 Gbit/s-based WDM systems”, ITCom2002, 2002.

[6] K. Tanaka, “Expected spectral efficiency by using optically pre-filtered RZ”, OFC2002, Workshop 203, 2002.

[7] T. Miyazaki, and K. Tanaka, “40 Gbit/s-based unrepeatered WDM transmission systems”, OFC2002, ThFF1, 2002.

[8] K. Tanaka, H. Sakata, T. Miyakawa, I. Morita, K. Imai, and N. Edagawa, “40 Gbit/s x 25 WDM 306 km unrepeatered transmission using 175 μm^2-A_{eff} fibre”, ECOC2001, Mo. F. 3. 6, 2001.

[9] K. Tanaka, I. Morita, and N. Edagawa, “50 GHz-spaced 40 Gbit/s x 25 WDM transmission over 480 km using bandlimited RZ signals”, OECC2001, TUE1. T, 2001.

[10] K. Tanaka, I. Morita, M. Suzuki, and N. Edagawa, “40 Gbit/s-based WDM systems with SMF-based dispersion flattened transmission line”, ROSC Symposium, 2000.

[11] K. Tanaka, I. Morita, N. Edagawa, and M. Suzuki, “Impact of nonlinear crosstalk in 0.8 nm-spacing 40 Gbit/s DWDM systems”, OECC2000, 14D4-3, 2000.

[12] K. Tanaka, I. Morita, N. Edagawa, and M. Suzuki, “320 Gbit/s (32 x 10.7 Gbit/s) error-free transmission over 7,280 km using dispersion flattened fibre link with standard SMF and slope compensating DCF”, ECOC1999, We C 4.3, 1999.

[13] K. Tanaka, I. Morita, N. Edagawa, and M. Suzuki, “400 Gb/s dense WDM soliton-based RZ Transmission using dispersion flattened fiber”, ROSC Symposium, 1998.

[14] K. Tanaka, I. Morita, M. Suzuki, N. Edagawa, and S. Yamamoto, “400 Gbit/s (20 x 20 Gbit/s) dense WDM soliton-based RZ signal transmission using dispersion flattened fibre”, ECOC1998, pp.85-86, 1998.